

Design of a wearable sensor system for neonatal seizure monitoring

Citation for published version (APA):

Chen, H. (2021). *Design of a wearable sensor system for neonatal seizure monitoring*. [Phd Thesis 1 (Research TU/e / Graduation TU/e), Industrial Design]. Eindhoven University of Technology.

Document status and date:

Published: 23/09/2021

Document Version:

Publisher's PDF, also known as Version of Record (includes final page, issue and volume numbers)

Please check the document version of this publication:

- A submitted manuscript is the version of the article upon submission and before peer-review. There can be important differences between the submitted version and the official published version of record. People interested in the research are advised to contact the author for the final version of the publication, or visit the DOI to the publisher's website.
- The final author version and the galley proof are versions of the publication after peer review.
- The final published version features the final layout of the paper including the volume, issue and page numbers.

[Link to publication](#)

General rights

Copyright and moral rights for the publications made accessible in the public portal are retained by the authors and/or other copyright owners and it is a condition of accessing publications that users recognise and abide by the legal requirements associated with these rights.

- Users may download and print one copy of any publication from the public portal for the purpose of private study or research.
- You may not further distribute the material or use it for any profit-making activity or commercial gain
- You may freely distribute the URL identifying the publication in the public portal.

If the publication is distributed under the terms of Article 25fa of the Dutch Copyright Act, indicated by the "Taverne" license above, please follow below link for the End User Agreement:

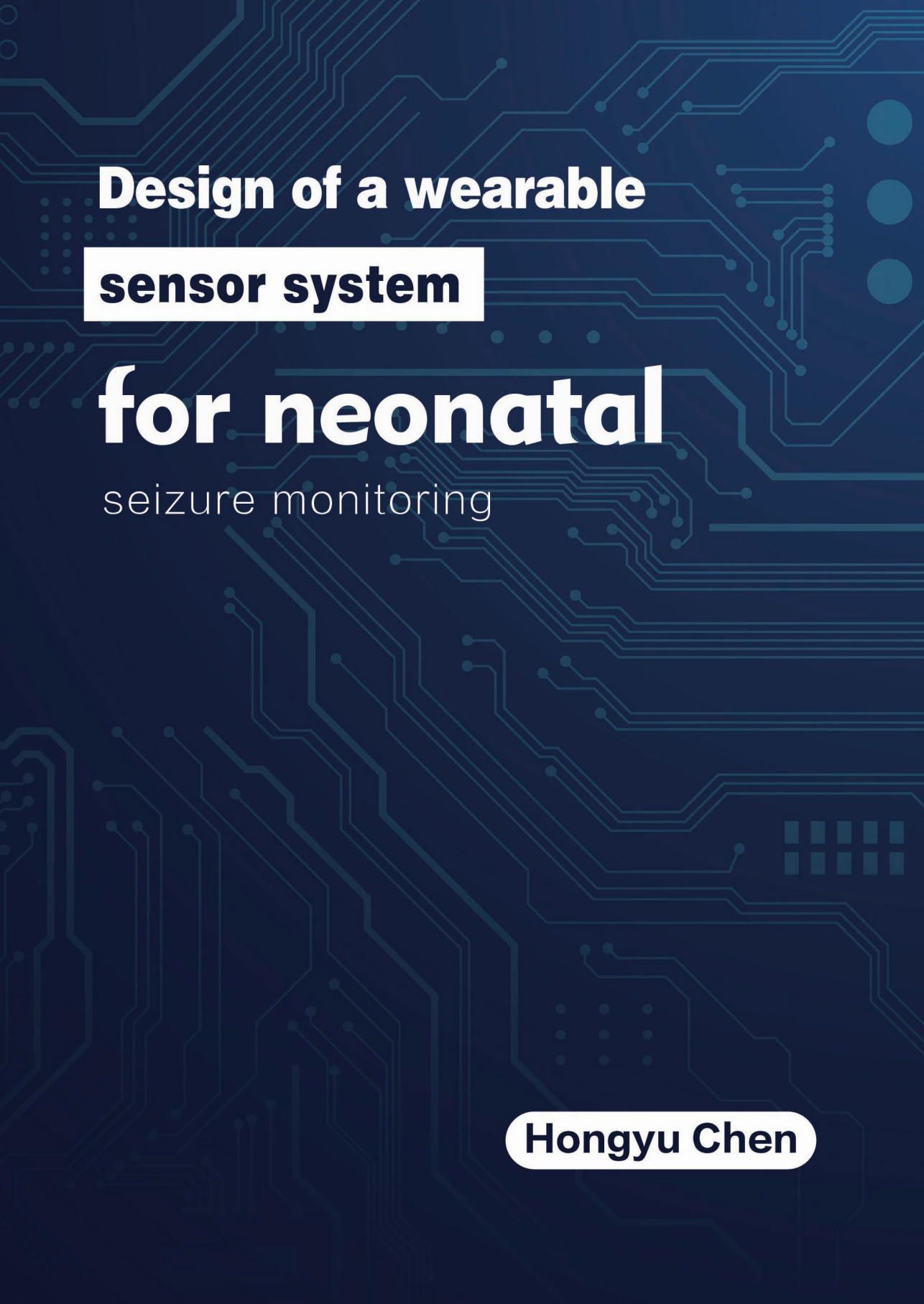
www.tue.nl/taverne

Take down policy

If you believe that this document breaches copyright please contact us at:

openaccess@tue.nl

providing details and we will investigate your claim.



Design of a wearable sensor system

for neonatal

seizure monitoring

Hongyu Chen

Design of a wearable sensor system for neonatal seizure monitoring

Hongyu Chen

A catalogue record is available from the Eindhoven University of Technology Library

ISBN: 978-90-386-5346-4

© 2021, Hongyu Chen

All rights reserved. No part of this book may be reproduced or transmitted in any form or by any means, electronic or mechanical, including photocopying, recording, or by any information storage and retrieval system without permission of the author.

Design of a wearable sensor system for neonatal seizure monitoring

THESIS

ter verkrijging van de graad van doctor aan de Technische Universiteit Eindhoven, op gezag van de rector magnificus prof.dr.ir. F.P.T. Baaijens, voor een commissie aangewezen door het College voor Promoties, in het openbaar te verdedigen op donderdag 23 september 2021 om 11:00 uur

door

Hongyu Chen

geboren te Jiangxi, China

Dit proefschrift is goedgekeurd door de promotoren en de samenstelling van de promotiecommissie is als volgt:

voorzitter prof.dr. L. Chen

1^e promotor prof.dr. S. Bambang Oetomo.

Copromotor prof.dr. W. Chen.

Promotiecommissieleden prof.dr. S. Bambang Oetomo

prof. L. Wang (Fudan University, Neonatology)

prof.dr. W. Chen (Fudan University, Department of
Electronic Engineering)

prof.dr.ir. L.M.G. Feijs

prof.dr.ir. M. Mischi

prof. J. Arends

prof.dr. A.F. Bos (University of Groningen, Neonatology)

Adviseur prof. L. Wang (Fudan University,
Neonatology)

Het onderzoek of ontwerp dat in dit thesis wordt beschreven is uitgevoerd in overeenstemming met de TU/e Gedragscode Wetenschapsbeoefening.

Abbreviations

ALTE - Apparent life threatening events
ANS - Autonomous Nervous System
ADC - analog-to-digital converter
AEEG-Amplitude-integrated electroencephalogram
BSN-Body Sensor Network
CP-Cerebral palsy
CSP-common spatial pattern
Co2-Carbon dioxide
DCNN-Deep convolutional neural network
DMA-Direct memory access
EPDM-Ethylene propylene diene monomer
EMD - Empirical mode decomposition
EEG - Electroencephalogram
ECG - electrocardiogram
EMG - Electromyography
ECoG - Electrocorticogram
FD - Fractal dimension
FWHVA - Fast weighted horizontal visibility algorithm
FSM - Finite state machine
FIR - Finite impulse response
GTCS - Generalized tonic-clonic seizure
HR - Heart rate
HRV - Heart Rate Variability
IMU - Inertial Measurement Unit
IMFs -Intrinsic mode functions
ID – Industrial Design
LED - Light Emitting Diode
LLE - Largest Lyapunov exponent
LCN - local crucial node

LF/HF - Low-frequency and high-frequency components

LDA - Linear discriminant analysis

M-PDMS-G - Mesh PDMS- Graphene

MEMS - Microelectromechanical Systems

MPE - Multiscale permutation entropy

MST - Minimal spanning tree

MPWVD - Wigner-Ville distribution

MSP - Multi-sensor platform

MRS - Magnetic resonance spectroscopy

NN - normal-to-normal

NTC - Negative temperature coefficient

NICU - Neonatal Intensive Care Unit

PANI - Polyaniline

PDMS - Poly(dimethylsiloxane)

PDMS-G - PDMS-Graphene

PCO₂ - Pressure of carbon dioxide

PO₂ - pressure of oxygen

PSG - polysomnography

PD - Photo Diode

PPG - Photoplethysmography

QRS – The Q, R and S peaks in the ECG complex

RGO - Reduced graphene oxide

RR - Respiratory rate

RIP - Respiratory-induced plethysmography

SIDS - Sudden infant death syndrome

SpO₂ - Oxygen saturation

STFT - Short time Fourier transform

SWT - Stationary wavelet transform

SPI - Serial peripheral interface

SSA - Singular spectrum analysis

SD - Standard deviation

TU/e – Eindhoven University of Technology

TFD - Time-frequency distribution

UART - Universal asynchronous receiver/transmitter

VEEG - Video electroencephalogram

xor - Exclusive OR

CONTENTS

Abstract	1
1. Introduction	3
1.1 Neonatal Seizure	4
1.2. Wearable Technologies for Neonatal Monitoring	6
1.3 Objectives of the Thesis	8
1.4. Content of Thesis	8
2. State of The Art	10
2.1 The Basis and Current Situation of Neonatal Seizure Detection	11
2.1.1. The Physiological and Pathological Basis of Neonatal Seizure	11
2.1.2. Current Practice of Seizure Detection	13
2.1.2.1. Electroencephalogram (EEG) Signal for Seizure Detection	14
2.1.2.2. Electrocardiography (ECG) Signal for Seizure Detection	14
2.1.2.3. Electromyography (EMG) Signal for Seizure Detection	16
2.1.2.4. Respiration Signal for Seizure Detection	17
2.1.2.5. Behavioral Signal for Seizure Detection	17
2.2 Research Status of Wearable Sensor System for Infant Monitoring	17
2.2.1. Related Parameters of Infant Monitoring	17
2.2.2. Wearable Sensing for Physiological Vital Signs Monitoring	19
2.2.2.1. Wearable Sensors for ECG Monitoring	19
2.2.2.2. Wearable Sensors for Respiration Monitoring	23
2.2.2.3. Wearable Sensors for Spo2 Monitoring	25
2.2.3. Wearable Sensing for Movement Monitoring	26

2.2.3.1. Method	26
2.2.3.2. Results	28
2.2.4. Acquisition System for Neonatal	35
2.3 Research Status of Signal Processing Methods for Detection and Prediction of Neonatal Seizure	37
2.3.1. Nonlinear Signal Processing	38
2.3.2. Nonlinear Dynamics	41
2.3.3. Network Science	43
3. Design of an Integrated Multi-Sensor Platform (MSP) Based on Flexible Materials for Neonatal seizure Monitoring	45
3.1 Requirement Discovery through Design Methods that Combine Technical and Medical Background	48
3.1.1. Information Retrieval	48
3.1.2. Clinical Observation	50
3.1.3. User/Expert Interviews	52
3.1.4. Requirements Summary	54
3.2 System Design of Multi-Sensor Platform	56
3.2.1. Hardware Design	58
3.2.2 Smart vest Design	66
3.2.3 Software Design	69
3.3 Signal Verification of Multi-Sensor Platform	74
3.3.1 System Signal Verification Framework	74
3.3.2 ECG Signal Verification	75
3.3.2.1 Flexible Textile Properties	75
3.3.2.2. ECG Signal Collected by MSP	80
3.3.3. Movement Signal Verification	86
3.3.4. Respiration Signal Verification	86
3.3.4.1. PDMS-G Compound Properties	86
3.3.4.2. Respiration Signal Collected by MSP	90
3.3.5. Clinical Test in Neonates	95
3.4. Neonatal Seizure Detection	98
3.4.1. Clinical Data Collection	98
3.4.2. Data Processing	101

3.4.3.	Feature Extraction	102
3.4.4.	Classifier	103
3.4.5.	Performance Evaluation	103
3.4.6.	Result	104
3.5.	Discussion	105
4.	Exploration of New sensors for Physiological Parameter Measurement	107
4.1.	Smart Textile Electrodes for ECG Monitoring	108
4.1.1.	Introduction	108
4.1.2.	Material Selected and Electrode Design	109
4.1.3.	Textile Electrodes Properties	112
4.1.4.	ECG signal Collected by Proposed System	116
4.1.5.	Conclusion	122
4.2.	Carbonized Foam Electrode for ECG Monitoring	122
4.2.1.	Introduction	122
4.2.2.	Material and Manufacturing	123
4.2.3.	Method of Evaluation	125
4.2.4.	Result	126
4.2.5.	Discussion and Conclusion	130
4.3.	Mesh PDMS-G Compound Sensor for Respiration Monitoring	132
4.3.1.	Introduction	132
4.3.2.	Material and Manufacturing of Mesh PDMS-G Compound	133
4.3.3.	Material Properties	137
4.3.4.	Respiration Signal Evaluation	140
4.3.5.	Discussion	143
5.	Conclusion	144
5.1.	Summary of Thesis	145
5.2.	Contributions	148
5.3.	Limitations	149
5.4.	Future Work	150
5.4.1.	Clinical Data Collection and Verifications for MSP	150
5.4.2.	Exploration of Sensors	150

Reference	152
Publication	174
Award	176
Acknowledgements	177
Curriculum Vitae	178

Abstract

Seizures in neonates, the most common sign of neurological dysfunction, require immediate medical attention. The continuous monitoring of neonatal seizures is critical for their optimal treatment and outcomes. The work presented in this thesis aims to solve the problems in neonatal seizure detection regarding designing a neonatal multi-parameter sensor system. The system is a combination of flexible sensor network and multi-modal signal fusion technology to achieve comfortable, continuous and efficient neonatal seizure detection.

We first reviewed the current situation of neonatal seizure detection, wearable sensor systems for infant monitoring and signal processing methods for neonatal seizure detection. The approach of the “Medical Technology Innovation Process” guided our design and development of the neonatal multi-parameter sensor platform for neonatal seizure monitoring. Experiments were conducted to systematically test the sensing-related characteristics of the proposed flexible materials and the performance of the proposed multi-sensor platform.

Furthermore, an algorithm for automatic detection of neonatal seizures based on ECG, respiration and acceleration was proposed. The proposed system was tested on 38 neonates at the Children’s Hospital affiliated to Fudan University, Shanghai, China. The algorithmic evaluation of the records of 4 patients with seizures was performed. To evaluate the utility of combining ECG, respiration and movement, we compared the performance of three seizure detectors. The first detector included features from both the ECG, respiration and acceleration recordings, the second incorporated respiratory-motion based features from respiration and acceleration recordings, and the third used ECG-based features from only the ECG recordings. The experimental results showed that the overall performance was better when multi-modal features were included.

In order to improve the comfort of the system and the stability of the signal, we further study the different flexible sensors, including textile electrodes and Carbonized Foam Electrode for ECG monitoring, and Mesh PDMS-G Compound Sensor for respiration Monitoring. The feasibility of these sensors was verified by systematic experiments.

To conclude, this thesis contributes to the design and development of the neonatal multi-

parameter sensor system aims to solve the problems in neonatal seizure detection. The system is a combination of flexible sensor network and multi-modal signal fusion technology to achieve comfortable, continuous and efficient neonatal seizure detection. The research focuses on the design and development of a non-invasive sensor system for physiological and behavioral signal measurements, signal quality tests, multi-modal physiological and motion signal fusion, and neonatal seizure detection.



Introduction

1.1 Neonatal Seizure

Neonatal seizure is an important clinical sign of brain dysfunction that occurs more commonly during infancy compared to childhood [1]. Seizures often manifest as behavioral and physiological signal changes, such as the repetitive motion of an arm, hand, leg and eye and sometimes are accompanied by the contraction of muscles at a fluctuant velocity in opposite directions [2], as well as pattern changes of electroencephalogram (EEG), electrocardiogram (ECG), respiration, etc.. An overall occurrence rate of seizure about 1~5% in neonates is reported. As for the preterm infants, it is about 6~13%, higher than the rate among normal newborns [2], [3]. Compared with children and adults, newborns are more likely to have convulsion persistence or electric seizure persistence. Although the immature brain has relatively stronger tolerance to convulsion, clinical follow-up and magnetic resonance spectroscopy (MRS) have proved that frequent and continuous convulsion damage brain development more seriously, even causing brain injury and neurological sequelae with different degrees [4], [5]. And brain dysfunction such as epilepsy, cerebral palsy, cerebral infarction, leukodystrophy etc. will appear in the later stage, with the total mortality rate reaching 30% [6].

Because newborns' brain development is immature, thus always present different clinical seizures and EEG manifestations from children and adults[7]. The clinical features of neonatal convulsions may include one kind of or all situations of the following: (1) Repeated facial movements, including sucking, chewing or eye movements. (2) Unusual leg cycling or pedal movements. (3) Continuous eye opening, eye movement or short gaze. (4) Apnea or accompanied by atypical autonomic nerve symptoms (such as the drop in heart rate and blood pressure.). (5) Spasm seizure is manifested as rhythmic twitching and may involve the face, tongue muscles, arms, legs or other positions. (6) The tonic seizure is characterized by stiffness or tightening of muscle tissue; The head or eyes may turn to one side or the fetus to bend or stretch one or both arms or one or both legs. In addition, it is difficult to distinguish the clinical symptoms of some seizures from the abnormal movement without seizures among newborns, such as sucking, chewing, stretching, shaking, postures, convulsions and cycling exercises, which also occur in normal healthy infants, so EEG is clinically used to determine whether the newborn has a seizure.

The electrophysiological characteristics of neonatal seizures are abnormal discharge

electricity of the brain. Abnormal electroencephalogram is manifested as limited small sharp wave discharge electricity, limited single rhythm attack pattern, sharp (spike) wave, sharp (spike) slow wave, multi-spike slow wave under normal or abnormal background activity like rhythm disorder, low voltage, burst inhibition, etc. [8]. EEG is the most important and reliable tool in making the diagnosis of seizures, which can also support the treatment and follow-up of neonatal seizures. The recording time of conventional electroencephalogram is short, about thirty to sixty minutes generally. Due to the great randomness of convulsion attacks, the chance of capturing convulsion attacks is limited and the probability of detecting neonatal convulsions attacks is lower. Ambulatory electroencephalogram is also called portable electroencephalogram monitoring, which can record continuously for about twenty-four hours. Therefore, it is also called twenty-four-hour electroencephalogram monitoring. Although the seizure detection rate has been improved, its error rate is high due to too much artifact interference and the absence of video recording equipment. Digital Video-EEG (VEEG) also called Video-EEG Monitoring, adding synchronous video equipment on the basis of the EEG equipment can synchronously photograph the patient's clinical seizure, display the seizure performance and EEG waveform on the same screen and monitor its clinical characteristics and EEG changes for a long time. At present, VEEG technology is widely used clinically. The seizure of newborns is diagnosed by the acquisition and analysis combining EEG and video action signals, as shown in Figure 1-1 a [8], [9].

However, in clinical practice, diagnosis based on the observation on EEG and/or video recording by experienced clinicians is time-consuming and limited by the inter-observer variability due to its subjective nature [10]. Moreover, EEG monitoring in neonates is available only in a dedicated hospital environment. Furthermore, cup surface electrodes and gel electrodes used for monitoring may cause skin lesions, as shown in Figure 1-1b. The deployment of electrodes with wires connected to monitoring devices may also interfere with the movement of infants and lead to missing detection, as shown in Figure 1-1c. Therefore, a new seizure monitoring approach is needed with the advantages of high accuracy and comfort for neonates. Considering the rapid developments in the field of sensor and wireless communication technology in recent decades, a new concept of unobtrusive monitoring of infants using a wearable sensor system has been reported[11]–[14]. Therefore, the neonatal seizure detection technology focusing on the technique of physiological signals instead of electroencephalogram has been a research emphasis in seizure monitoring for the neonate. [15], [16].

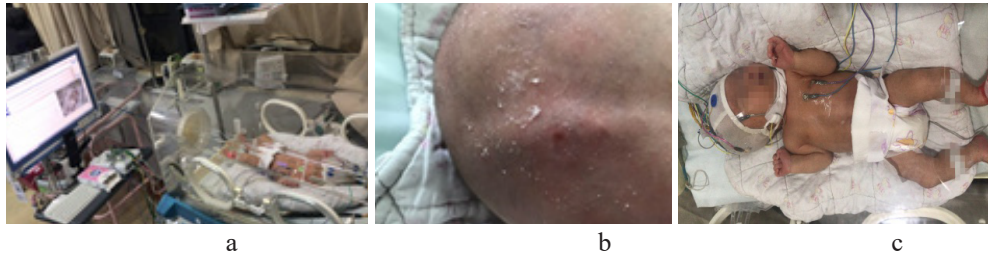


Fig. 1-1. (a) Video EEG acquisition; (b) Pressure sores; (c) Monitoring of multiple physiological parameters of infant.

To sum up, it is vital to design a new type of neonatal seizure monitoring technology with high accuracy, high efficiency and comfort as well as easy operation for clinical use and future home monitoring. It is required to develop new sensing and data analysis technologies to solve the aforementioned challenges.

1.2. Wearable Technologies for Neonatal Monitoring

In recent years, with the soaring development of wearable sensors including accelerometers, gyroscopes, smart fabrics, as well as the progress in wireless communication networks, power supplies, and data-acquisition technology for signal processing and decision support[17], various kinds of wearable sensors have emerged for many healthcare related applications [18]. For example, wearable equipment embedded with variable resistance bending sensors can be applied to human posture recognition and motion capture by detecting the bending angle of human joints[19]. A high sensitivity ultra-thin silicon stress sensor has been developed by Zhao et al, which is developed by reconfiguring a single sensor, used for the measurement of the human wrist pulse[20]. Salam et al. proposed a wearable surround sensor composed of multiple electrodes (antennas, excited at a single low frequency), which can be used to continuously measure the dielectric constant of biological tissues in the depth of the trunk, especially the lung and heart [21]. Wearable sensor systems also create a new generation of continuous health monitoring for infants. For example, Linti et al. developed a sensor baby vest, including an integrated sensor for measuring electrocardiogram (ECG), respiration, temperature and humidity (detection of excessive sweating), which can detect early potentially life-threatening events[22]. In order to improve the comfort for infants, Chen et al. used conductive textile wires instead of traditional hard wires. The sensor was integrated into a prototype tape made of a negative

temperature coefficient (NTC) sensor for temperature monitoring[23]. Sibrecht et al. developed a smart and expandable jacket for neonates to measure ECG through the textile electrode, and carried out several experiments to prove the prototype [24]. Another example is a wearable multi-parameter monitor named BBA bootee, developed to monitor infants at risk of apparent life threatening events (ALTE). The sensors, electronics and the power supply are integrated into the bootee, providing reliable pulse oximetry measurements as well as useful information about the infant's movement and position [25]. Yves Rimet et al. proposed a BBA bootee, which integrates sensors and electronics into shoes to detect the pulse oximetry, movement and position information of infants. Cao, H et al. presented an infant monitoring system using CO₂ sensors to non-invasively monitor the exhaled air from an infant to reduce the potential risks for Sudden Infant Death Syndrome (SIDS)[26]. In order to achieve safe and reliable health monitoring, a wearable sensor system needs special design and non-invasive sensor integration. Continuous monitoring of neonatal physiological and behavioral parameters is essential for clinicians and parents to understand their exact health status. In addition, various dangerous situations exist in premature or severely ill neonates' admission to hospital, including apnea, hypoglycemia, sepsis or sepsis like infection, seizure, arterial hypotonia, bradycardia, hypoxia, hypothermia, acidosis[27] and even sudden infant death syndrome (SIDS), which also need continuous monitoring. Furthermore, life-threatening accidents are prone to happen among infants aged 1-4, such as drowning in the bathroom or head injuries occurring from falls. Therefore, clinicians and parents need an inexpensive and non-invasive method to monitor infants' health status and send an alarm if terrible status appears.

Traditional infant health monitoring methods are usually carried out under the direct supervision of specialized persons such as clinicians and parents. Sometimes it is difficult for them to monitor the infants' emergencies, especially the irregular ones such as neonatal seizures. The initial purpose of the application of wearable sensor systems in infant health monitoring was to provide infants with daily monitoring, ensuring proper care or treatment can be available for the onset of complications and reducing the cost of clinical interventions in hospitalization and the burden on parents. Therefore, the health monitoring system is an early indicator reflecting the change of patients' condition, and a means to record, evaluate and control the effect of intervention and treatment[27]. These systems are usually able to monitor neonates in the Neonatal Intensive Care Unit (NICU) or at home without interfering with their daily activities (such as eating, sleeping, and natural communication with parents) and comfort. However, traditional sensors and medical

devices cannot be used for infants' daily physiological monitoring because of the difficulty and discomfort of long-time wearing[28].

In conclusion, wearable sensing technology can provide infants with comfortable monitoring environment, and help doctors or parents obtain the infants' long term physiological status. The wearable sensing technology together with advanced signal processing will provide a new exploration way for the neonatal seizure monitoring.

1.3 Objectives of the Thesis

Although some studies have focused on the development of non-EEG seizure detection systems, and the development of long-term, comfortable and stable neonatal wearable devices, less attention has been paid to the detection of neonatal seizures through wearable devices. Accuracy, comfort and stability are noteworthy factors in neonatal convulsion wearable monitoring technology.

The design and development of the neonatal multi-parameter sensor system reported in this thesis aim to solve the problems in neonatal seizure detection. The system is a combination of a flexible sensor networks and multi-modal signal fusion technology to achieve comfortable, continuous and efficient neonatal seizure detection. The research focuses on the design and development of a non-invasive sensor systems for physiological signal measurements, signal quality tests, multi-modal physiological and motion signal fusion, and neonatal seizure detection.

1.4. Content of Thesis

Chapter 1 presents the thesis outline and research questions. Chapter 2 is the literature review, mainly about the state-of-art in the field of neonatal seizure detection and wearable sensor system for infant monitoring. Chapter 3 describes the development of a multi-sensor platform (MSP) for neonatal seizures detection based on flexible materials. The development process of the platform was based on the innovative method of medical devices proposed by Meng Fei et al. [29]. The proposed system collects neonatal ECG signal, respiratory signal and motion signals by wearable motion sensors and flexible materials, and detects neonatal seizure by multi-signal fusions. Altogether this chapter introduces the collection of design requirements, the development of sensors and platforms,

and the verification of the system. In Chapter 4, we explore new wearable physiological sensors. The best textile electrode is selected by a systematic comparison of the signal quality of ECG electrodes made of different textile materials. In addition, ECG electrodes made of a new material-carbonized sponge have been developed. Finally, we explore the application of the mesh graphene sensor based on 3D printing technology in respiratory signals detection.



State of The Art

This chapter is based on:

1. Chen H, Xue M, Mei Z, et al. A review of wearable sensor systems for monitoring body movements of neonates[J]. *Sensors*, 2016, 16(12): 2134.
2. Mei Z, Zhao X, Chen H, et al. Bio-signal complexity analysis in epileptic seizure monitoring: A topic review[J]. *Sensors*, 2018, 18(6): 1720.

2.1 The Basis and Current Situation of Neonatal Seizure Detection

2.1.1. *The Physiological and Pathological Basis of Neonatal Seizure*

Neonatal seizures are the most common clinical manifestations of neonatal neurological diseases. Neonatal epileptic seizures occur from birth to the end of the neonatal period[30]–[32]. This is the most vulnerable of all the other periods of life for the development of epileptic seizures, particularly in the first 1 or 2 days from birth. The incidence among very-low-birth-weight infants is 6% to 13%, and 1‰ to 5‰ among full-term newborns [2], [3], [33]. Seizures can indicate the severity of the disease, even accompanied by hypoventilation, apnea, and circulatory insufficiency, hypoxic-ischemic brain damage if it frequently occurs; Neonatal seizures differ from those of older children and adults. They may be short-term events lasting for just a few days, but they often signify serious malfunction or damage of the immature brain, and constitute a neurological emergency that demands urgent diagnosis and management. Most neonatal seizures are acute (provoked, occasional, reactive) symptomatic seizures caused by an acute illness such as hypoxic–ischaemic encephalopathy, stroke or infection. Seizures are the most common and important sign of acute neonatal encephalopathy; they are a major risk for death or subsequent neurological disability and, by themselves, may contribute to an adverse neurodevelopmental outcome [34].

Due to no recognizable postictal state, neonatal seizures are paroxysmal, repetitive and stereotypical usually clinically subtle, inconspicuous and difficult to recognize from the normal behaviors of the interictal periods or physiological phenomena. International League Against Epilepsy (ILAE) revised the classification of neonatal seizures in 2017, as shown in the Table 1-1[35].

Table 1-1Types of clinical seizure in the infant. Adapted from ILAE, 2017

Type	Clinical manifestation
Automatisms	A more or less coordinated motor activity usually occurring when cognition is impaired. This often resembles a voluntary movement and may consist of an inappropriate continuation of preictal motor activity.
Clonic	Jerking, either symmetric or asymmetric, that is regularly repetitive and involves the same muscle groups.
Epileptic spasms	A sudden flexion, extension, or mixed extension–flexion of predominantly proximal and truncal muscles that is usually more sustained than a myoclonic movement but not as sustained as a tonic seizure. Limited forms may occur: Grimacing, head nodding, or subtle eye movements.
Myoclonic	A sudden, brief (<100 msec) involuntary single or multiple contraction(s) of muscles(s) or muscle groups of variable topography (axial, proximal limb, distal).
Tonic	A sustained increase in muscle contraction lasting a few seconds to minutes.
Autonomic	A distinct alteration of autonomic nervous system function involving cardiovascular, pupillary, gastrointestinal, sudomotor, vasomotor, and thermoregulatory functions.
Behavioral arrest	Arrest (pause) of activities, freezing, immobilization, as in behavior arrest seizure.
Sequential seizure	This term is used in the instruction manual for the ILAE 2017 operational classification of seizure types for events with a sequence of signs, symptoms, and EEG changes at different times.
Electrographiconly seizure	Subclinical, without clinical manifestation.
Unclassified seizure type	Due to inadequate information or unusual clinical features with inability to place in other categories.

In some cases, the symptoms of seizures may be overlooked when infants are unmonitored, especially when they are asleep, which increases the difficulty of diagnosis. On such occasions, a shortage of immediate medical assistance can even cause higher risks of

mortality[36].

Seizures can be recognized as repetitive movements of an arm, hand, leg and eye in general with an alternating slow and fast contraction of muscles in opposite directions. Apart from these manifestations, infants can feature subtle convulsions, including eye deviation, fixed open stare, blinking, apnea, cycling, boxing, stepping, swimming movements of the limbs, mouthing, chewing and lip smacking, or tonic and clonic seizure like stiffening, decerebrate posturing, and unifocal/multifocal repetitive jerking, or myoclonic seizure, more specifically [2], [30].

Besides, non-motion phenomena have been reported, but mistaken as an action events since they're difficult to record. These nonmotor clinical episodes in neonates include vasomotor changes, apnea, and pale skin, changes in breathing, heart rate, excessive salivation, elevated blood pressure, etc. [34].

On the other hand, clinical seizures can be accompanied by episodes of electroencephalogram (EEG) recorded by EEG - if the two are closely related, they are called "electric-clinical" events. The characteristics and clinical significance of EEG seizure activity have been reported in many literatures. However, not all neonatal seizures occur in the form of electro-clinical manifestations, because there exist changes in the relationship between EEG and clinical events, and some only have EEG seizures. These EEG episodes can be accompanied by no clinical onset, regardless of the prognosis, which depends to a large extent on the cause of primary neurological disease. Diagnostic methods based on EEG and video (VEEG) observation have been widely used clinically[34].

However, since VEEG is not convenient for continuous long-term monitoring, it may not be able to detect neonatal seizures in time. Furthermore, the diagnosis based on signal analysis is currently based on the observation on EEG and/or video recording by experienced clinicians, which is quite time-consuming and limited by the inter-observer variability in clinical practice due to its subjectivity [2], [30].

2.1.2. Current Practice of Seizure Detection

Due to the immature development of newborns' brains, neonates often manifest as clinical seizures with the EEG totally different from children and adults. VEEG is the clinical gold standard in determining whether a newborn has a seizure. In the past decade, with the rapid development of related technologies in the Body Sensor Network (BSN) [12], [37]–[42],

researchers have searched for new automatic monitoring methods different from video EEG methods for seizures in children [15], [16]. It has been studied to monitor seizures from a variety of electrophysiological and behavioral signals through diverse modern signal processing methods, including electrocardiogram, myoelectricity, electrodermal activity, respiratory, and behavioral signals. Below please find the description of different signals and their correlation to seizure monitoring.

2.1.2.1. Electroencephalogram (EEG) Signal for Seizure Detection

As the important electrophysiological feature of seizures is the abnormal synchronous discharge of brain neurons, the abnormal discharge pattern can originate from one side of the brain and spread to the entire hemisphere and even the contralateral hemisphere [2], [43]. Abnormal EEG manifests as a localized small spike discharge of normal background activity, a localized single rhythm pattern, a sharp (spine) wave, a sharp (spine) slow wave, a multi-spine slow wave, and abnormal background activity (rhythm disorder, low voltage), burst suppression) and so on. At present, the common standard for the diagnosis of seizures in clinical practice is video electroencephalography (V-EEG) [44]. By combining the EEG waveform, the simultaneously recorded video, and other clinical manifestations, medical history, etc., the clinician comprehensively confirms the seizure episode and diagnoses the epilepsy syndrome. Seizures can cause different degrees of nervous system damage to the newborn, like brain dysfunction and even death, so it is required that clinicians have strong professional knowledge and clinical experience, timely detect and promptly intervene convulsions and seizures. Therefore, exploring the automatic detection technology based on EEG signal analysis has been a hot topic [45], [46]. Amplitude-integrated electroencephalogram (AEEG) or cerebral function monitor is a simplified method which uses a fewer number of electrodes to collect EEG information compressed in time to generate a tracing that can be used for detection and evaluation of seizures, providing information in real time [47]. This modality has been adopted by neonatal units in many parts of the world [48], [49]. Although the seizure detection rate has been improved, the error rate is high due to too much artifact interference and the absence of video recording equipment.

2.1.2.2. Electrocardiography (ECG) Signal for Seizure Detection

At present, there are many researches based on ECG, mainly using heart rate (HR) signals and Heart Rate Variability (HRV) signals for seizure monitoring [50]. HRV, defined as

fluctuations in the heartbeat interval, is widely recognized as a reflection of the balance of sympathetic and vagal activity in association with the Autonomous Nervous System (ANS). The seizures are modulated by the autonomic nervous system, and accompanied by autonomic symptoms such as breathing, heart rate, blood pressure, pupil changes or salivation [44], so heart rate variability is helpful to judge and predict seizures.

Based on the automatic R wave detection algorithm, heart rate monitoring is very mature [51]. The method to quantify heart rate variability is to continuously detect the R wave in the ECG signal, calculate the interval between adjacent R waves, and obtain the respiratory rate (RR) interval sequence. For example, it is set to start at 0 and obtain the first R wave, then the second R wave is obtained at time t_1 , the third R wave at time t_2 , the fourth R wave at time t_3 , and so on. Then on the time axis, the heart rate variability signal consists of the following data points:

$$(t_1, t_1), (t_2, t_2 - t_1), (t_3, t_3 - t_2), \dots$$

The waveform of ECG and the corresponding heart rate variability signals are shown in Figure 2-1.

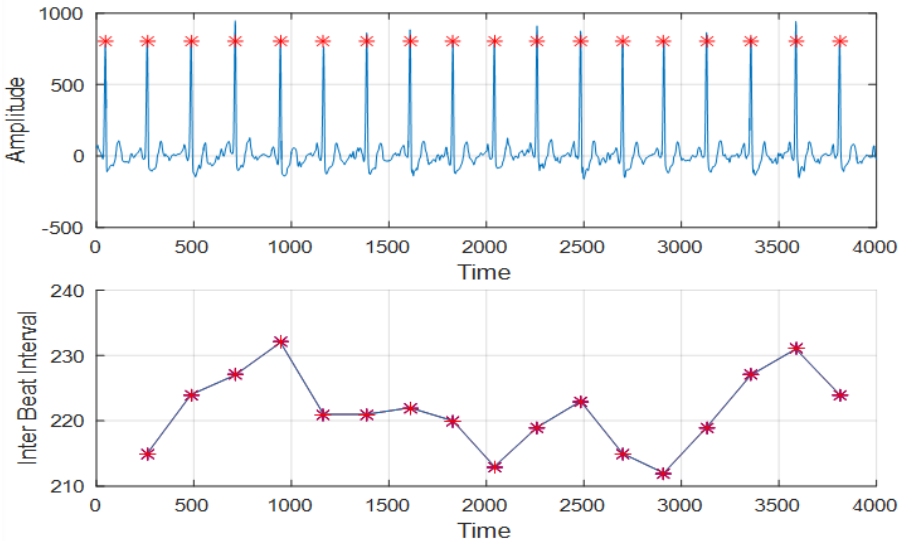


Fig. 2-1. ECG waveform and corresponding heart rate variability signal

Osorio and others [52], [53] made use of large-scale clinical data (a total of 6935 hours of cortical EEG collected from 81 patients and simultaneous acquisition of ECG, including

241 seizures) to explore heart rate in Application value for clinical seizures detection. The results indicate that heart rate, a marker reflecting the modulation of the autonomic nervous system, is valuable for convulsion detection.

Based on the researches of heart rate variability in children with refractory seizures [54], the results suggest that heart rate variability has the potential to serve as a biomarker for predicting seizures. Control studies have found that heart rate variability in children with refractory epilepsy is generally suppressed compared with healthy children. At the time of seizures, the ratio of low-frequency and high-frequency components (LF/HF) of heart rate variability increased, indicating an increase in sympathetic activity.

In addition to clinical medicine focusing on the above research results, researchers in the field of information science have also explored it.

By time-frequency signal analysis methods, researchers have found that the first-order conditional moments of low-frequency components and the variance of high-frequency components in heart rate variability are effective features. By virtue of linear discriminant analysis (LDA), a machine learning method, the researchers achieved detection of neonatal seizures with a sensitivity of 85.7% and a specificity of 84.6% [55]; In the last two years, based on the multivariate process control method, the characteristics extracted from heart rate variability have been used to predict the seizure episode, achieving a sensitivity of 91% [56].

2.1.2.3. Electromyography (EMG) Signal for Seizure Detection

The onset of certain types of seizures is likely to cause twitching of the muscles[34], so using myoelectricity to judge seizures is a direction worth exploring. Some researchers have developed a wearable wireless surface electromyography module that embeds a comprehensive spectrum analysis and zero-cross test to determine the occurrence of generalized tonic-clonic seizure (GTCS) [57]. Seizures may cause skin electrical impedance responses. In 2012, some researchers used a support vector machine to detect tonic-clonic convulsions for more than 4000 hours by a series of features extracted from skin electrical signals and acceleration signals. The sensitivity reached 94%, and the level of false positive rate was about 0.74 times per day, which explored the application of skin electricity in convulsion monitoring and prediction [58]. The main shortcomings of this research are as follows: a) only several specific types of seizures with obvious behavioral abnormalities at the time of the attack can be monitored; b) the false positive rate is higher; c) it's difficult to confirm the detected seizures one more time.

2.1.2.4. Respiration Signal for Seizure Detection

Respiration can provide important information about neonatal seizures and help identify artifacts in EEG. When neonatal seizures occur, the respiration of the neonatal slows down, accompanied by apnea occasionally. Seizures can cause neonatal ventilation disorders and a large amount of oxygen, energy consumption, further aggravating neonatal brain injury, serious life-threatening, or central nervous system sequelae. According to the American society for clinical neurophysiology's guidelines for clinical electroencephalography (EEG), neonatal non-brain electrodes should include channels for recording respiration [59]. Breathing helps identify physiological delusions, such as the apparent simplex delta activity in electroencephalography, which usually can be recognized as respiratory delusions, since babies breathe more than 100 times a minute. In addition, recording changes in breathing is more significant to diagnose neonates with convulsive asphyxia.

2.1.2.5. Behavioral Signal for Seizure Detection

Some seizures may lead to clinical observation of characteristic movements (such as tonic seizure, colonic seizure, and tonic-colonic seizure). By measuring motion-related data, information reflecting motion can be obtained to support the automatic diagnosis of seizures. Studies using behavioral signals to diagnose seizures in adults have only recently emerged, see [15], [60], [61].

2.2 Research Status of Wearable Sensor System for Infant Monitoring

2.2.1. Related Parameters of Infant Monitoring

In the NICU or at home, the vital signs of the infant are monitored to ensure their physical health. The changes of these signs represent potential changes within the body, manifested through external physical characteristics. The most frequently monitored human physiological vital signs and related sensing principles and sensors in neonatal intensive care are shown in table 1-2 [27].

Table 1-2. The main physiological vital signs and parameters monitored during neonatal intensive care, with relative sensing principles and transducers.

Parameter or Vital Sign	Sensing Principles	Transducers
ECG, EEG	Electrical, bio-potential	Skin electrodes, textile electrodes, flexible conductive electrodes
Heart rate, Pulse	Optical, pressure	Photodetector, force sensitive resistor
Non Invasive Blood Pressure	Auscultatory	Pneumatic cuff & microphone
Invasive Blood Pressure	Electrical, impedance, Optical, reflection	Strain gauge, piezoresistor, Photodetector & emitter
Temperature	Electrical, resistance Electrical, thermoelectric Optical, IR emission Optical, fluorescence	Thermistor Thermocouple IR pyroelectric detector Photodetector
Respiration	Mechanical, expansion	Strain gauge
	Electrical, impedance	Skin electrodes
SpO2	Optical, absorption	Photodetector & emitters (red and IR)
PO2	Optical, fluorescent	Photomultiplier tube
	Electrochemical, amperometric	Clark oxygen electrode
PCO2	Optical, fluorescent	Photomultiplier tube
	Electrochemical, potentiometric	Ion-sensitive electrode

Electrocardiogram (ECG), temperature, respiratory frequency and oxygen saturation [2] are the four major vital signs of standard clinical evaluation on neonates with acute diseases. As a result, these parameters regularly serve as early warning scores in pediatric assessments. Clinicians often diagnose infants in a critical state and take appropriate action based on the monitoring results. Effective monitoring protects these premature babies from various threats such as apnea, hypoglycemia, epilepsy, bradycardia, hypoxia and hypothermia. In addition to these physiological monitoring parameters, some researchers attempt to achieve health monitoring by detecting neonatal exercise parameters.

It is a recent development to study infants' movements by wearable motion sensing technology. Based on the application of micro motion sensors, the long-term monitoring of the infants' daily activities is more feasible than ever before, which is of great significance for the research on infants' movement patterns, but the clinical effects still need exploration. What's more, wearable motion sensor systems can be used in healthcare and patient monitoring for some special situations. For example, a tri-axial acceleration sensor is connected to an infant's clothes to detect whether the baby sleeps on the back, side or abdomen of the prototype [62]. Another monitoring system measures the fluctuation of the water in the bathtub to prevent infants' drowning injury at home [63].

2.2.2. Wearable Sensing for Physiological Vital Signs Monitoring

Continuously monitoring physiological parameters was only carried out in hospital settings in the past. However, with the evolvement of sensor technology, different types of sensors have been proposed to obtain physiological parameters of infants, even at home. To be effective and non-invasive, sensors for neonatal monitoring have been continuously improved in recent years. At present, most infant wearable sensors focus on the newborns' vital signs including electrocardiogram, body temperature and breathing, which are important physiological parameters in the neonatal intensive care unit. The limitations of the baby health monitoring sensor mainly include the position of the sensor on the body, its fixed clothes to reduce the influence of moving parts and motion artifacts, integration with other sensors, the interference with the external environment (such as temperature, humidity, sound, etc.), and the difficulty to be miniaturized, low-cost, low-power and unobtrusive, etc., which should be taken into consideration when designing wearable sensor systems [64]. This section briefly describes the main wearable sensors currently used to detect neonatal physiological parameters or vital signs.

2.2.2.1. Wearable Sensors for ECG Monitoring

Electrocardiogram, a widely studied biological signal describes the electrical activity of the heart, usually composed of QRS waves, P waves, and T waves [65]. The electrocardiographic electrode often transmits an electrical signal near the heart to the electrocardiograph through a lead wire, wherein the impedance, polarization, and the like of the electrocardiographic electrode greatly affect the accuracy of the electrophysiological signal. At present, electrodes for measurement of ECG signals include metal plate

electrodes, adsorption electrodes, disk electrodes, suspension electrodes, dry electrodes, and soft electrodes, which also can be divided into copper alloy silver plating electrodes, nickel silver alloy electrodes, zinc silver-copper alloy electrodes, stainless steel electrodes and silver-silver chloride electrodes according to the electrode materials. Currently, the Ag/AgCl electrodes with conductive paste are widely used, but will cause the following problems if used for long-term:

- (1) Since the electrode materials lack of breathability and moisture permeability, prolonged use will cause skin discomfort;
- (2) The conductive paste will gradually dry up after long-time use, causing significant changes in the contact resistance between the electrode and the skin and affecting the stability of ECG signals;
- (3) The conductive paste is also a factor of skin allergy and other uncomfortable reactions.

As a result, some researchers have developed other types of electrodes, such as textile electrodes, conductive polymer electrodes, capacitive electrodes and conductive ink printed electrodes.

The measurement of biological signals is more effective and user-friendly with the development of textile electrodes, including conductive fabrics, metal-coated fabrics and flexible electronics.

Textile electrodes, usually woven from conductive yarns are often used in wearable devices because of their compatibility with clothing. In terms of conductive yarns, there are several types to choose from, such as complete metal yarns and polymer-metal yarns. Complete metal yarns are made of stainless steel, copper or other alloys filaments. Polymer-metal blends made of co-spinning metal filaments with polymers, metal-filled polymer filaments, or metal-coated polymer fibers, can be coated with conductive metals like silver, and coated or mixed with conductive polymers, such as polyaniline (PANI) or poly (3, 4-ethedioxythiophene) (PEDOT) [66]. The main structure of conductive yarns is a non-conductive fiber (nylon, polyester, etc.) coated with a thin layer of silver or some other conductive materials. Different coating materials lead to different properties of textile electrodes. For example, textile electrodes coated with gold and silver can get good signals because of the low resistance of these two materials. However, compared with the silver-plated electrode, the gold-coated textile electrode is not hypoallergenic and loses its electrical conductivity after washing because gold is more chemically active than silver[37]. They may be adhesive and corrosion resistant, although textile electrodes may be very compatible with textiles. Two patches with different versions of gold and silver

textile electrodes (a) and a blanket with large silver electrodes (b) are shown in Figure 2-2. Textile electrodes typically have a knit structure in which the metal material is woven or woven into cloth by a fabric. To avoid babies' direct contact with the wires, electrical components and circuitry, replacing the conventional device and hard wire with textile electronics and conductive fabrics and integrating them reliably into the garment can make the ECG measurement on the baby convenient and comfortable. On the other hand, textile electrodes also have some disadvantages. For instance, textile electrodes with a knitted or woven structure are generally of poor quality and poor skin-to-electrode contact, requiring high sensitivity to motion artifacts[64]. Furthermore, the effect of abrasion and washing on the brittleness of the metal remains a problem in textile electrodes. As a result, it is badly needed to find a good method for fixing the textile electrode to the cloth and optimizing ECG measurement. Chen et al. integrated the textile electrodes into a smart jacket to detect a baby's ECG signal, whose quality can be increased by optimizing the electrode structure and fixing.

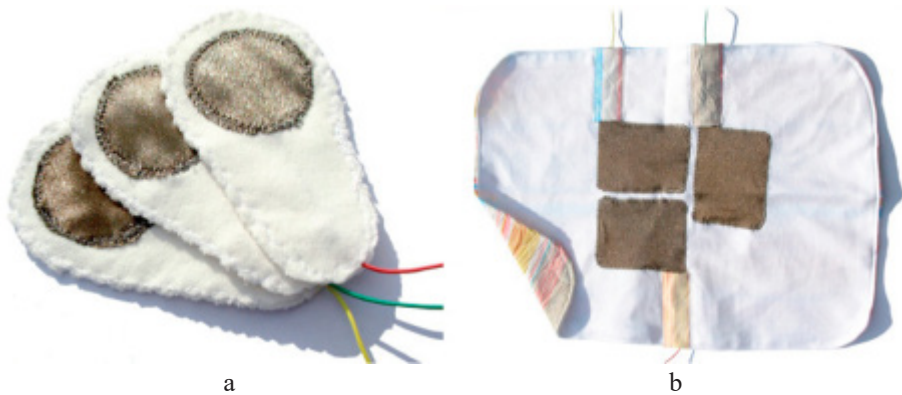


Fig. 2-2. Two types of non-contact electrodes[38]

Various conductive electrodes are conductive polymer additives in the polymer or applied polymer surface, made of a dry electrode. Typically, conductive additives such as carbon, stainless steel fibers and carbon nanotubes are combined with some flexible polymers. Chen and the team developed a conductive polymer electrode, made by mixing carbon into ethylene propylene diene monomer (EPDM) [67], as shown in Figure 2-3a. Baek and the team etched a gold pattern on titanium and deposited it on a flexible elastomeric poly(dimethylsiloxane) (PDMS) [68], as shown in Figure 2-3b. Conductive polymer electrodes are not very comfortable compared to textile electrodes, not used to monitor

newborns yet.



Fig. 2-3. (a) Conductive polymer dry electrodes based on EPDM[68]; (b) conductive polymer dry electrodes based on PDMS[69]

Figure 2-4 showed two capacitive electrodes [69], [70], most of which are used as non-contact electrodes, utilizing capacitive coupling. Peng et al. tested the non-contact electrodes and reported the ability to measure the ECG through cotton shirts without physical contact[69]. No direct contact with the skin is required, but the capacitance is very sensitive to the distance between the electrode and the skin, which makes it difficult to get stable and accurate signals. Another drawback of capacitive electrodes is the change of dielectric properties caused by sweat which may induce the erosion of the dielectric interface [71]. A silicon dioxide dielectric layer supported a foam cushioning layer, providing protection for the dielectric layer without the risk of wearing out or corrosion [72], which is shown in an example of a capacitive electrode fabricated on silicon. However, most non-contact electrodes are made of rigid material, so they are not flexible or comfortable. As a result, capacitive electrodes are considered to be a challenge for integration into textiles for long-term use.

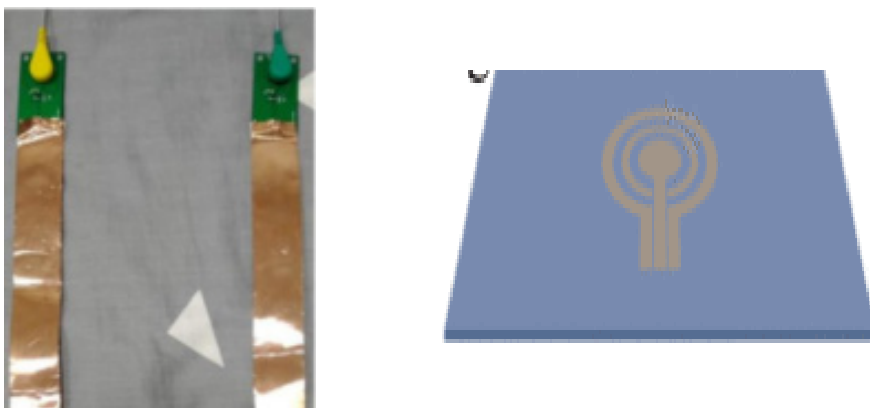


Fig. 2-4. Two types of non-contact electrodes[69], [70]

The electrodes can also be made of conductive ink. First, the conductive ink must contain a suitable highly conductive metal precursor such as silver, copper, gold, NPs, and support, most of which are water-based, that is, water is the main component of the ink, as pure as possible to limit the contaminants. These special inks can be printed on a variety of materials like textiles to create electroactive patterns. Screen printing also makes integration and planar electronics simpler than conductive yarn systems. There are several technologies for printing conductive materials on different substrates. Inkjet and screen printing based on sheetfed are best suited for low-volume, high-precision work [73]. Examples of screen-printed electrodes integrated into different substrates are presented in Figures 2-5. The combination of printed conductive elements and textiles has great potential for developing new products. The textiles for daily use are comfortable, while the printed electrodes are light, flexible and not sharp, so the functionality is added without deteriorate the comfort. The multi-layer structure is flexible and easy to implement in different designs. Improved wear resistance, abrasion resistance and wash fastness are current challenges for screen printed electrodes [72].

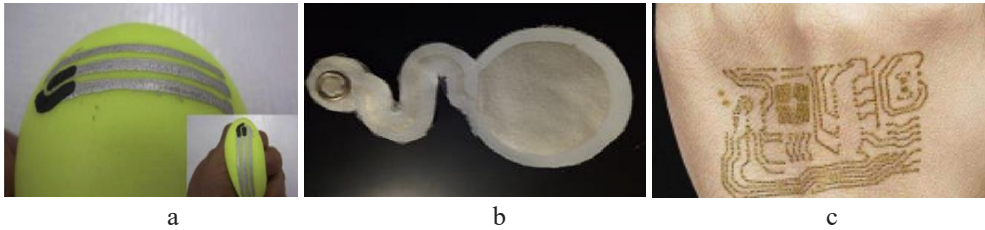


Fig. 2-5. (a) Three electrode contingent on a stress ball; (b) Screen-printed electrodes on the textile substrate; (c) Screen-printed electrodes on the epidermis.

2.2.2.2. Wearable Sensors for Respiration Monitoring

Respiratory rate is very critical in neonatal monitoring [18]. Respiratory rate, also called breathing rate, refers to the number of breaths and exhalations per unit of time. Actually, the respiration rate is usually determined by counting the number of times the diaphragm expands and contracts per minute. Respiration is usually classified as either contact or non-contact, though monitored in many ways.

Sensing devices are attached to the patients' bodies as the contact method. The commonly measured parameters by this method are breath sounds, respiratory airflow, respiratory-related chest or abdominal movements, respiratory CO₂ emissions, and oximetry probe

SpO₂ [74]. Thoracic electrical impedance is the most common method of respiratory monitoring in the clinic, which uses adhesive electrodes attached to the skin to obtain signals, but long-term attachment to the skin may cause irritation. Researchers studied the feasibility of several sensors for wearable respiratory monitoring systems, such as piezoelectric sensors or three-dimensional accelerometer signals [75], [76], both of which make the respiratory signal collected contain a large number of motion artifacts, affecting the accuracy of the respiratory rate measurement. Therefore, the respiratory-induced plethysmography (RIP) proposed by T. Chadha et al., including an inductive band that can be attached to the abdomen or chest [75]. The resistance of the strip varies with stretching. Surveillance based on respiratory flow is an effective method of respiratory monitoring due to changes in the circumference of the chest during abdominal breathing. Zhang and the team proposed a RIP-based wearable respiratory monitoring device for respiratory biofeedback training, however, the device's frequency band making method is complicated and difficult to embed in a wearable device [77].

For the non-contact method, some researchers used a CO₂ sensor placed around the crib on the railing to provide enough information about the breath [78]. There are many commercially available CO₂ sensors on the market with multiple sensing principles, such as electrochemical sensors, infrared sensors and metal oxide sensors. The electrochemical sensor has good performance but short life, and the infrared sensor has high sensitivity, large volume but high cost. Metal oxide sensors are low-cost but susceptible to temperature and humidity [26]. Hsu and Chi have proposed a thermal sensor-based respiratory rate monitoring system, another typical example of non-contact respiratory monitoring. The thermal sensor placed on the mask is sensitive to temperature changes of breathing, and the sensor data is simultaneously collected and analyzed by the personal computer and connected to the central nursery. With the thermal sensor array, the sensor mask has the ability to sense the temperature change caused by breathing, and in order to avoid undetection, an ellipsoidal mask is prepared which can be adjusted to accommodate the baby's face in different directions [79].

The main disadvantage of contact monitoring methods is the direct connection to the baby like face or abdomen, which makes many babies uncomfortable and difficult to tolerate. The advantage of the non-adhesion monitoring method is the no contact with the baby's skin, avoiding any possible skin irritation or other hazards, as compared to the respiratory

monitoring contact method. However, non-contact monitoring equipment can be more complex and susceptible to external environmental disturbances (such as temperature changes, gas flow and breathing by nurses or parents). At the current, non-contact respiratory monitoring methods have not reached the maturity level of clinical routine applications, because of the concerns about infant safety, electromagnetic interference with existing medical devices, and operational complexity[74]. These two different respiratory monitoring methods will complement each other to achieve effective and reliable respiratory monitoring with the development of technology. Respiratory sensors used in future wearable sensor systems will be miniaturized, intelligent, user-friendly, and precise, making the baby's respiratory monitoring more reliable and convenient.

2.2.2.3. Wearable Sensors for Spo2 Monitoring

Oxygen saturation is one of the important indicators for evaluating the oxygen content of hemoglobin in arterial blood. Transmission and reflection are two non-invasive techniques for pulse oximetry (SpO_2) measurement [80], [81]. Currently, in hospitals, blood oxygen saturation is monitored by a light-transmissive pulse oximeter attaching to the newborn's foot or palm[27]. The location of these sensors and the presence of all wires cause discomfort, and even when the pain is intensified, the sticky sensor should be removed [37], [82]. A reflectance oximeter that increases the flexibility of installation can avoid such problems and meet the needs of modern home healthcare, whereas the research of reflectance oximeters is still in a shortage relative to the transmittance type and there are few complete solutions for reflectance oximetry[83]–[85].

In reflectance oximetry, LED (Light Emitting Diode) and PD (Photo Diode) are placed on the same body surface side by side, and measuring the intensity of the reflected light with PD is helpful to measure photoplethysmography (PPG) signals from different parts of the body flexibly, making it more suitable for non-invasive wear.

Unlike conventional fingertip probes, a transmissive SpO_2 sensor probe that can be embedded in a finger ring is proposed in [86], and a novel optical sensor and LED distributed around the square matrix are also proposed and mounted on a flexible PCB. Experiments were carried out on ten experimental subjects whose results were in accordance with the measurements of commercial fingertip oximeters. Cai and the team[83] designed a reflectivity probe to measure the photoplethysmography (PPG) signal, which can be worn as a wristband equipped with an RF transmission module to facilitate wireless communication between the measurements system and the medical center. The experimental

results show that the system can effectively detect changes in oxygen content in the blood and can be used in non-invasive, continuous, remote monitoring systems. Chen and the team demonstrated a neonatal non-invasive oxygen saturation monitoring system[87]. The reflectance sensor is embedded in a soft fabric, suitable for wearable long-term monitoring systems. The experimental results show the measured data is in good agreement with that of the commercial monitoring system. However, there is a need to further improve the design to minimize the effects of motion artifacts which can cause erroneous readings.

2.2.3. *Wearable Sensing for Movement Monitoring*

Unlike physiological parameters, the physical condition of the neonatal can be indirectly reflected by their motor signals. Patterns of motions, a crucial step in early life, can predict and identify impairments in neuro-motor development, then further perfect therapeutic approaches to evaluate infants' physical activity patterns [88]–[90]. Cerebral palsy (CP) is a clinical diagnosis made by doctors' observation of spontaneous movements and neurological examinations. There is empirical evidence that markedly abnormal movements reflect the existence of serious brain dysfunction [91]. In addition, the clinical signs of brain dysfunction like neonatal seizures usually manifest as abnormal movements of the limbs and eyes. The occurrence and types of seizure can be appreciated by observing the nature, speed and amplitude of the movements [2], [30].

With the development of wearable sensors, research on the monitoring of newborn movement signals has become a new trend recently, but its clinical application is not mature yet. The authors used the systematic review method to search for the literature published between 2010 and 2016 in order to study the technology of infant movement monitoring based on the wearable sensor systems.

2.2.3.1. *Method*

A search on the following publication database was conducted: PubMed (MEDLINE since 1960), IEEE Xplore, SpringerLink and Science Direct, issued in Feb. 2016. Relevant articles in recent 7 years (2010-2016) were collected. To seek out related articles, we target the following three aspects: infant, movement monitoring, and wearable sensor systems. Generic search terms (according to the thesaurus of each individual database) were used for the identification of relevant studies. Due to the different formats of each database, we used slightly different expressions of our search strategy for each database. Table 1-3 displays the

search strategy for the PubMed database. The search strategies for the other three databases resemble this. Only papers in English were included in the review process.

Table 1-3. Literature search strategy (PubMed)

Infant	Infant OR Baby OR Neonatal OR Newborn
AND	
Movement	“Seizure activity OR Convulsion OR “Motor behavior OR Movement OR Position OR Motion OR Moving
AND	
Monitoring	Monitoring OR Feedback
AND	
Wearable	Wearable OR Mobile OR Ambulatory OR garment OR soft suit OR exosuit
NEAR	
Sensor	Accelerometer OR “Motion sensing OR “Activity sensing OR Gyroscope OR MEMS OR IMUs OR bend sensor OR flexible sensor

The selection procedure consists of two steps. The first selection was performed based on the title, the abstract and the identifying of exclusion criteria:

Exclusion criteria were:

- **No infant target population**
- **No wearable sensor technology**
- **No “movement” or “monitoring” in the research**
- **Reviews**
- **Books of conference proceeding;**
- **Language other than English.**

We applied such exclusion criteria for obtaining desired relevant results which were well confined within the scope we are interested in.

The second step was based on the full-text scan of the paper. Papers were included in the full-text review when they satisfied all of the following inclusion criteria.

Inclusion criteria were:

- **All studies with infants as subjects**
- **Technology: wearable motion-sensing technology.**

● **Related “body movement” or “moving” or “motor pattern” had to be reported.**

During the second step, the other two persons decided whether the article should be included in the review.

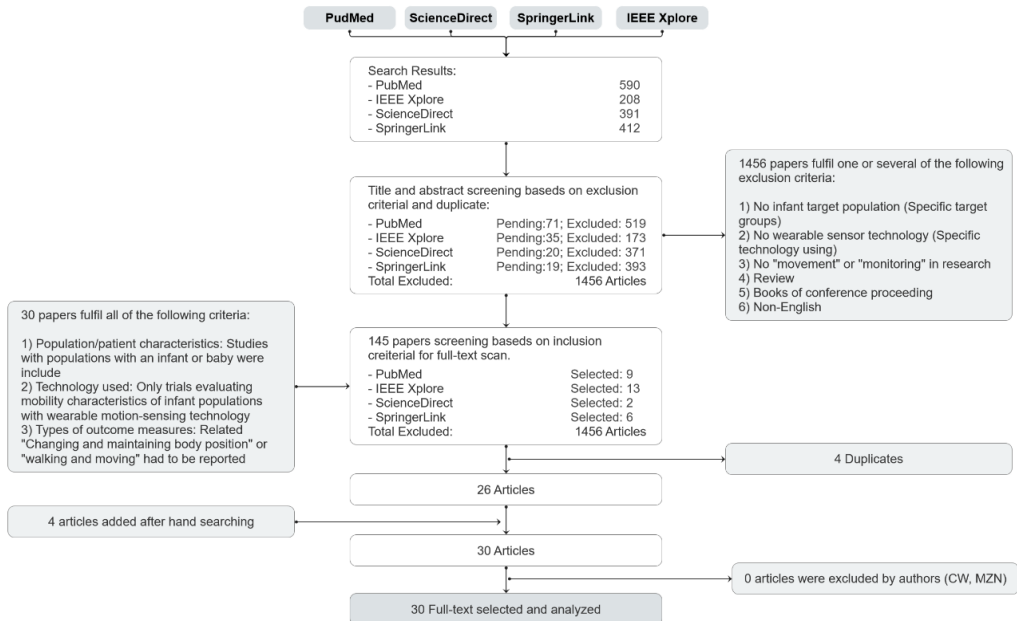


Fig. 2-6. Procedure for study selection with databases used for the literature research

Figure 2-6 shows the selection procedure and results. There are 1165 articles selected by our search strategy. After reading the titles and abstracts, we identified 145 papers based on the exclusion criteria. Two articles were excluded because they were written in languages other than English. After the application of the inclusion criteria, the number was reduced to 30. And after removing 4 duplicates, 26 papers remained for consideration. We manually searched the references for these 26 articles. Four articles were added after hand searching of references. Finally, 30 papers were taken into account in this review after two authors carried out the decision on the 30 selected papers. This resulted in 30 articles that were considered in this review.

2.2.3.2. Results

With the development of sensor technology and wireless communication technology, the research on movement monitoring with wearable sensor systems for infants has made a lot

of progress. Wearable sensor systems are becoming smaller, so many of them and more intelligent ones have been commercially available [92]. These sensor systems have been embedded in more and more diversified products such as shoes, buttons, belts, clothes etc., for movement monitoring. A typical infant movement monitoring system with the wearable sensor is commonly composed of sensors, power supplies, wireless communication modules and links, control and processing units, interface with the users (maybe for parents or doctors), software, and algorithms for signal processing, feature extraction and decision-making. Table 1-4 summarizes recent work from 2010 to 2016.

Table 1-4. Overview of the wearable sensor system to monitor infant movements

Research Work	Year	Sensor	Placement	Form	Evaluation	Purpose
Andra Rihar et al. [93]	2014	6 Wireless IMUs, 2 pressure mattresses	Trunk and arm	Silicone bracelets	Technical experiment(test baby doll) technical report user test	Infant motor pattern assessment
Fabrizio Taffoni et al.[94]	2012	2Wired magneto-inertial sensor	Wrist	N/A	Technical experiment	Study motor skill at risk for autism spectrum (ASD)
Beth A. Smith et al. [95]	2015	2 Inertial movement sensor(Opals, APDM) IMUs	Leg	Placed sensor on each leg using knee socks	Clinical test (n=12)	Quantification of daily infant legmovements
Mohan Singh et al. [96]	2010	4 Custom Accelerometer (Eco)	Wrist and ankle	N/A	Clinical test (n=10)	Predict CP
Elham Saadatian et al.[97]	2011	1 Accelerometer	N/A	Wearable hardware gadget	Technical experiment	Baby care
Franziska Heinze et al. [98]	2010	4 Accelerometer	Extremities	N/A	Clinical test (n=23)	Predict CP

Hiroataka Gima et al. [99]	2011	2 Accelerometer	Ankle	N/A	Clinical test(n=8)	Infant motor pattern assessment
Sabri Boughorbel et al. [100]	2010	4 Pressure sensitive sensor	N/A	Mat	Technical experiment, Usability Evaluation(n=1)	Infant care/ SIDS
Lee, E.[92]	2015	1 Accelerometer	Ankle	Ankle band	Commercial product	Baby safety
Mingming Fan et al. [101]	2012	4 Accelerometer	Wrists and ankles	Clothes bands	Clinical validation(n=10)	Infant motor pattern assessment / predict CP
Sandra Waldmeier et al. [102]	2013	1 Accelerometer	Hand	Fixed to the infant with a tape	Preclinical test, Usability Evaluation(n=22)	Infant motor pattern assessment
D. Gravem et al.[103]	2012	5 Accelerometer	Ankle, wrists and forehead	Cloth bands	Clinical test (n=10) Comparison Experiment	Infant motor pattern assessment/ diagnosis CP
Drew H. Abney et al. [104].	2014	4 Accelerometer	Wrist and ankle	N/A	Preclinical test, Usability Evaluation(n=2)	Characterizations of infant behavioral development
Wei Lin et al. [105]	2014	1 Accelerometer	Chest	Soft belt	Technical experiment	Prevent SIDS
Aryan Kaushtik et al. [106]	2013	1 Accelerometer	Chest	Jacket	Technical experiment	Fall protection
Gillian R. Hayes et al. [107]	2011	5 Custom Accelerometer (Eco)	Ankle, wrists and forehead	Cloth bands	Preclinical test, Usability Evaluation (n=10)	Infant motor pattern assessment/ Predict CP
Philippe Jourand et al. [108]	2010	2 Accelerometer	Abdomen	N/A	Technical experiment	Monitor SIDS
Gustavo López et al.[109]	2013	1 Accelerometer	N/A	Bear gadget	N/A	Prevent SIDS

H.DC Clercq et al. [110]	2010	2 Accelerometer	Abdomen	N/A	Technical experiment	Infant care/ SIDS
Marco Donati et al. [111]	2014	768 Pressure Sensor	N/A	Mat	Preclinical test, Usability Evaluation(n=1)	Infant motor pattern
Fernandes, Duarte[112]	2016	1 Accelerometer	Chest	Belt	Technical experiment	Monitor SIDS
Bouwstra, S et al. [12]	2011	1 Accelerometer	Right chest	Smarm Jacket	Technical experiment	Motion artifacts reduction
Leier et al[113].	2013	1 Accelerometer	Foot	Shoe	N/A	Baby safety
Farooq et al.[114]	2015	1 Jew Motion Sensor/ Flexible sensor	Jaw	N/A	Clinical validation(n=10)	Feeding Behavior
Huyen et al. [115]	2016	1 Accelerometer	Abdomen	Belt	Technical experiment	Baby safety
Rihar et al.[116]	2016	2IMU	Trunk and wrist	Bracelets and chest strap	Technical experiment	Infant motor development assessment/ early intervention treatment
Koch et al. [117]	2016	Flexible 6 × 6 sensor	Abdomen	N/A	Technical experiment	Respiratory monitoring
Galland et al. [118]	2012	1 Accelerometer	Shin	N/A	Clinical validation(n=33)	Sleepstate monitoring
Rogers et al. [119]	2015	4 Joint angle sensors/ Flexible sensor	Knees and hips	Sensing suit	Preclinical test, Usability Evaluation(n=1)	Early intervention treatment
Karch et al. [120]	2012	Electromagnetic tracking system	upper and lower limb	N/A	Preclinical test (n=75)	Predict CP

Among the 30 selected articles, a total of five types of sensors, including the accelerometer, Inertial Measurement Unit (IMU), Magneto-inertial, pressure sensor and flexible sensor

are discussed. However, only 19 of them describe the form of wearable systems, such as gadgets, bands and jackets. Ten of the researches use the form of banding, including cloth bands, belts, bracelets and so on. Two of the researches applied gadgets and another two mats. The form of shoes and shocks was also used by two researchers. But only three use the form of jacket and suit. Most of the researches place the sensors on the hands or feet. Some also combine the sensors with other parts of the body, such as the forehead. Besides, three of the researches put the sensors on the abdomen or the chest. Six passages illustrate the weight of the sensor and show the lighter sensors exert less influence upon the research results.

Regarding the purpose of sensor systems, 12 articles are about infant motor pattern assessment, 3 articles are used to predict CP and 13 are applied for baby safety. None of the 30 articles had mentioned seizures.

13 articles demonstrated the technical tests on system feasibility. 14 research works carried out clinical tests or pre-clinical tests. Most of the tests were not large trials because the movement sample capacity was below 25. Only two tests had a sample size larger than 25, one was 33, the other was 75.

Wearable sensor technologies for infant movement monitoring

Various sensors were used to monitor movements in infants, including accelerometers, gyroscopes and Magneto sensors, etc. Different types of sensors have their own advantages and disadvantages. Therefore, it is crucial to choose an appropriate one that meets the specific requirements for monitoring the movements of infants.

Microelectromechanical Systems (MEMS) is a process technology used to create tiny integrated devices or systems, which refers to the integration of mechanical elements, actuators, and electronics on a common silicon substrate through the utilization of microfabrication technology. One of the applications of MEMS technology is the MEMS-based inertial sensor.

Inertial sensors mentioned above, also known as inertial measurement units (IMUs), consisting of accelerometers and gyroscopes and/or magnetometers, are one of the most important types of silicon-based sensors. They gather movement information by measuring acceleration, angular rate and the magnetic field vector (some of them) in the three axes of their own three-dimensional local coordinate system respectively [121], [122].

MEMS-based inertial sensors have achieved significant progress recently in the aspects of satisfactory sizes, low costs and low power consumption, making the inertial sensors prevalent in physical activity monitoring [123].

Recently, inexpensive on-chip inertial sensors including gyroscopes and accelerometers have gradually found practical applications in baby motion analysis.

Fabrizio Taffoni et al [94] propose a magneto-inertial platform, composed of three sensors: two wired magneto inertial sensors that can be worn by infants on their wrists to evaluate upper limb movements. Hirotaka Gima et al. [94] proposed a low-cost system based on accelerometers to evaluate the newborn's movement.

In some studies [114], [117], [118], flexible sensors are also used to monitor infant movement, such as bend sensors, which are usually used to acquire joint angle data, the Jew motion sensor used to capture the action information of mouth mastication. Flexible sensors can acquire knowledge about the posture of static objects, which is beyond the ability of IMUs. Moreover, flexible sensors are thin and light, easy to be adopted in wearables. So, the flexible sensor is also suitable for the monitoring of infant movement, especially in quasi-static scenarios or for interests in the object's posture. On the other hand, pressure sensors are also used. They are often embedded in a non-wearable system to collect activity-related data, without affecting the baby's normal activities, such as mats [93], [100], [111].

For infant movement monitoring, various types of sensors have been used as is shown in Table 1-5. The data in table 1-5 are from literature search results from 2010 to 2016. For some flexible sensors working in the form of pressure sensing, we take them as a flexible sensor to emphasize their flexibility which is related to system design, while the sensing principal is not what we are interested in. As illustrated in the table, a majority of studies use accelerometers as their primary sensors. 50% of all the research papers have mentioned the use of accelerometers for this purpose. Motor characterization of infant general movement with inertial sensors has already given rise to several scientific contributions. For instance, Andraž Rihar et al. provided a study about the motor characterization of infant trunk posture and arm movement assessment performed in a multi-sensor measure system [93].

Table 1-5. Statistical representation of sensors selection for infant movement monitoring

Category	Discussed by papers
IMU	[93], [95], [116]
Accelerometer	[12], [92], [96]–[99], [101]–[110], [112], [113], [115], [117]
Magneto-inertial	[94], [120]
Pressure sensor	[93], [100], [111]
Flexible sensor	[114], [117], [119]

In conclusion, with the development of background technique, inertial sensors (IMU, Accelerometer, Magneto-inertial) are about to take the spotlight in the motion sensing areas. Due to its low cost, portable size and high-performance, increasing researchers are considering these sensors a good choice for movement monitoring in infants.

Tendency of utilization of wearable sensors

Among the data demonstrated above, researchers have chosen various forms of sensors to monitor infant movements. For instance, 20 of all the 30 articles use accelerometer sensors to monitor babies while 3 of them use pressure sensors.

Figure 2-7 illustrates the baby-related movement monitoring research from 2010 to 2016; The usage rate of the acceleration sensor is decreasing gradually while that of the IMU is obviously increasing. That's because IMU measurements provide data with more degrees of freedom for movement monitoring.

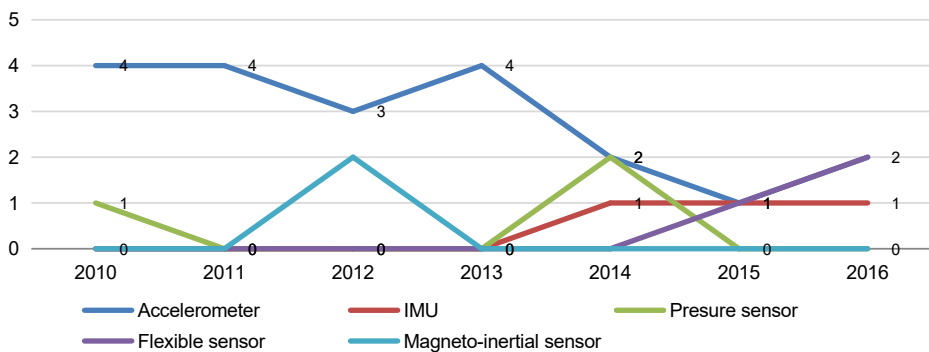


Fig. 2-7. Trends of sensor technology usage in baby-related movement monitoring research

Conclusions

So far, the wearable sensor system of infants' movement monitoring has achieved much progress, with good prospects for future applications. And new systems need to be developed and verified by more clinical trials before being promoted to a wider population. For instance, the accuracy of the results obtained from the wearable motion sensors, the preferable choice to place the sensor for data collection in various applications, the reliability and comfort index of the system and the aspects affecting the results of the wearable sensors are expected to make improvements. Moreover, the application of wearable sensor-based movement monitoring in infants has not yet reached its full

potential. The available literature does not show successful examples to detect infant seizure conditions based on the use of wearable motion sensors. Thus, there is a great development space of infant motion monitoring with wearable sensors for infant seizure detection. Another important research trend is to create a “baby care system” to achieve feedback between clinicians and infants with wearable sensors. Through the “baby care system”, monitoring infants’ daily physical activities and understanding the real-time development status are within reach. Once these issues achieve any substantial progress, it will be a great attraction for both parents and clinicians to significantly improve the care of infants.

2.2.4. Acquisition System for Neonatal

With the development of wireless communication technologies and the advancement of sensor technology and smart devices in wearable electronic devices, neonatal signal acquisition systems have also become diverse. The signal acquisition system can be divided into a multi-parameter acquisition system which provides comprehensive, safe, reliable and accurate health care for preterm infants in the NICU and a single signal acquisition system which monitors infants’ health through a key parameter, simplifying the health monitoring system with improved comfort.

Multi-parameter acquisition systems can be added with different types of sensors or wearable electronics, making the monitoring system smaller, more comfortable, and easier to maintain. For example, the BBA bootee [25] developed by Rimet and their team is based on an oximetry module and a three-axis accelerometer for multi-parameter monitoring of infants. The data connection and transmission of the sensor are managed by a single-chip transceiver via a short-wave RF link. An adjustable strap made of elastic textile ensures contact between the SpO₂ sensor and the skin and allows the boot to be mounted to the foot when the baby is from one size to another. By integrating the sensor into the bootee, it measures pulse oximetry and detects the baby's movement and prone position. The baby swaddle designed by Baker et al. [62] comfortably wraps and holds the baby with two sensor-equipped dishes. Sensors are placed on both plates to monitor temperature, moisture and pulse rate. The sensor mote contains a thermistor temperature sensor, as well as electrodes that monitor the baby's pulse rate and hydration, and the circuit unit is integrated into the glove. The sensor board is placed on the front and back sides of the child's upper body, and the upper body is the largest heat mass in the body. The wireless base station allows information exchange between the sensor dust particles and various computing

systems (such as PDAs, cell phones, and laptops), and parents or nurses can be alerted when the child's vital signs exceed a predetermined health condition. Besides, the sensor baby vest proposed by Linti et al. [22] is fully integrated, and can also monitor multiple parameters in the NICU or home environment. Parameters can include breathing, heart rate, temperature and humidity, etc., such as sweating. Using different sensors integrated, vital signs such as PPG, electrocardiogram, systolic and diastolic blood pressure, heart rate and body temperature can be monitored and collected simultaneously with the data-integrated sensor system, resulting in a whole frame of infant health, which greatly improves the efficiency of the doctor. In addition, the smart jacket proposed by Chen et al. [24] is a comprehensive platform for multi-parameter monitoring of newborns. Equipped with flexible, lightweight textile sensors and electronics for easy monitoring of ECG and breathing parameters of the jacket. A silver-plated textile electrode integrated into a smart jacket prototype. The jacket is open-chested and has an open structural fabric on the back for clinical observation. The jacket also includes a hat that protects the eyes. Six textile electrodes distributed at different positions of the jacket can effectively reduce the bad signals caused by motion artifacts. Prototype design also allows for free movement, protects the eyes, and provides an aesthetic effect that has won the appreciation of parents and clinicians. In future designs, some other sensors, such as temperature sensors, sweat pH sensors and body odor sensors, can also be integrated into the jacket.

Although multi-parameter acquisition systems have great potential for development in infant wearable sensor systems, there are still exist some limitations that need to be addressed. For example, continuous and reliable power supplies are still a big problem due to the high-power consumption of various sensors and complex data processing circuits. These obstructed wires make the baby feel uncomfortable in daily activities. In addition, the integrated platform is difficult to maintain non-invasive and small in size while providing various monitoring units. In the future, the integration platform needs to be improved with rugged and low-key, providing consistent and reliable data flow and higher-level medical algorithms to classify measurement results (such as normal, abnormal, risk, high risk and error) and transmit data through a wireless sensor network [124].

Most medical measuring instruments such as thermometers and sphygmomanometers use the principle of the single parameter method. In order to reduce the risk of SIDS in neonates (especially premature babies), the neonatal intensive care unit (NICU) requires continuous ECG monitoring of preterm infants. Coosemans and the team reported some prototypes for continuous monitoring of infant ECG using a garment embedded system [125]. All

electronic equipment, including textile electrodes and induction coils, are mounted on a flexible circuit that facilitates the integration of baby pajamas. For comfort, the baby's clothes are embroidered with electrical circuits and conductive wires. The system has only three textile electrodes for single-point ECG measurement, making the data processing circuit simple and small. This single-parameter monitoring device is characterized by usually only one sensor for measuring specific parameters, simple circuits and low power consumption. A single physiological parameter monitoring method has great potential to reduce the risk of small island developing States usually caused by cardiac arrest, and can be effectively monitored by ECG monitoring.

2.3 Research Status of Signal Processing Methods for Detection and Prediction of Neonatal Seizure

When researchers from the clinical side talk about ‘complexity’ in seizure, much more attention is likely to be paid to highly varied clinical manifestations, etiology, patterns of propagation and the evolution of epilepsy with aging, etc., while researchers from the engineering side use ‘complexity’ to refer to untapped information contained in medical images and electrophysiological recordings. Although clinicians interpret these data in their own way, usually with the aid of experience and medical knowledge, experts on the engineering side do not always place a priority on the interpretability of their methods. Instead, inspired by complexity theory, they take the human body as an extremely complex system getting input from the environment and adapting itself, while the medical images and physiological signals are just observable and measurable ‘states’ or ‘output’ of this system. Direct treatment implications and anticipation of prognosis are not necessary for them. However, exploring the complexity of these signals in a different perspective may shed new light on the analysis of these data. Different methods are utilized to tackle the complexity of physiological signals, mainly for epileptic seizure detection. Among them, three subjects as fountainheads, e.g., non-stationary signal processing, nonlinear dynamics and network science, can be roughly identified. Non-stationary signal processing is the most straightforward methodological source. And nonlinear dynamics and network science influence this field in a more heuristic and subtle manner. Methods originate from more than one of these three subjects could be adopted in the research.

2.3.1. Nonlinear Signal Processing

Since the physiological processes are confirmed to be nonlinear and non-stationary, non-stationary signal processing techniques are the most intuitive choice for such problems. Compared with traditional time-domain statistical methods and frequency-domain methods which provide averaged information, non-stationary signal processing methods such as short-time Fourier transform, time frequency analysis, wavelet transform [126] and model-based analysis has the advantages of representing and capturing transient anomalies.

Gotman was the pioneer in the exploration of an EEG-based automatic seizure detection method. To capture the transient behavior during long-term EEG monitoring, in [127], EEG signals are decomposed in time-domain into half waves, based on morphological characteristics. The half waves are then characterized in terms of its duration and amplitude compared to background activity. Typical spikes in EEG recordings, which are usually accompanied by the onset of epileptic seizures, are thus possible to be recognized using a real-time computerized algorithm. Artifacts reduction and inter-channel relations are also discussed in this work, being unsolved problems in EEG-based automatic seizure detection. The false alarm rate is high [128] because the waveforms of many different types of artifacts and non-epileptogenic EEG bursts are quite similar to the waveforms during epileptiform discharge. Short time Fourier transform (STFT) is one of the most popular techniques used for non-stationary signals. The original signal is truncated into smaller slices and windowed, and then a discrete Fourier transform is performed on it so the transient behavior could be revealed. STFT is widely used as a feature extraction technique applied to raw EEG recording [129]. Usually, the statistical metrics of the coefficients are taken as features and feed into the classifier [130]. Islam, Rastegarnia, and Yang [131] used a stationary wavelet transform (SWT), which is translationally invariant, to de-noise single-channel EEG signals. No additional assumptions about the data are needed for this method, neither over-correction would happen across channels.

In addition to noise rejection, wavelet transforms are widely used to extract features from physiological signals. A discrete wavelet transform was used to decompose EEG signals into approximate coefficients and detailed coefficients [132]. Reduced complexity was observed during the ictal period and the decomposition helped improve the overall detection accuracy. Subasi and Erçelebi [133] used a lifting scheme to speed up the computation of wavelet transforms, and logistic regression and neural networks served as a classifier with compared performances. Wavelet-based methods depict the signal under different time

scales and help discover discriminate features which could be veiled in the original signal [134].

Joint time-frequency distribution is a powerful tool to adapt to the nature of non-stationary signals. Figure 2-8 shows that the time-varying frequency components cannot be reflected by spectral analysis but are clear in a time-frequency distribution. One dimensional signals are transformed into a 2-dimensional distribution where for every time point on the x-axis, a distribution of instantaneous frequencies is estimated and plotted on the y-axis. Visual inspection or automatic detection algorithm can be performed on time-frequency distribution (TFD). Tzallas et al. [135] used different time-frequency analysis to calculate the power spectrum density of EEG signals. Energy fraction measures in the specific time-frequency window in TFD are extracted as features and feed into neural networks. High accuracy of detection is achieved. Boashash and Ouelha [136] used modified TFDs and a more comprehensive feature set consists of signal features, statistical features and image features extracted from TFD to handle multichannel EEG data recorded from neonates. A new criterion taking sensitivity into consideration was proposed for feature selection. Reduced computational cost and improved detection performance were obtained together.

Advanced techniques for time series analysis are also used for seizure detection. Celka and Colditz [137] used a computer-aided seizure detection system based on a nonparametric time series modeling method, singular spectrum analysis (SSA). By evaluating the proposed method on both real and synthesized data, a 93% detection rate was obtained and a false detection rate was less than 4%. Alam and Bhuiyan [138] transformed the raw EEG into the empirical mode decomposition (EMD) domain. Every raw time series was decomposed into nine intrinsic mode functions (IMFs) and the variance, skewness and kurtosis of each IMF are expected to be different when a seizure happens.

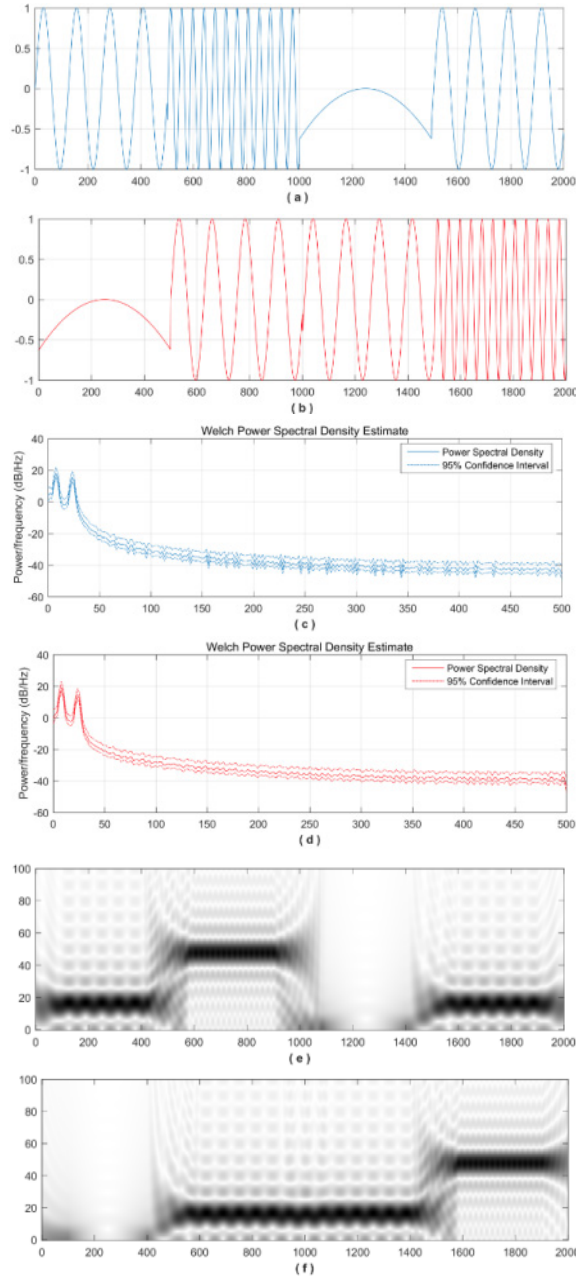


Fig. 2-8. Time-frequency Distribution of Non-stationary Signals: (a, b) Two signals with frequency components that vary with time; (c, e) Welch power spectrum density estimation and time frequency distribution of the signal in (a); (d, f) Welch power spectrum density estimation and time frequency distribution of the signal in (b).

Although EEG reflects the electrical activity on the scalp or in the brain directly, other physiological signals can serve as useful complements. Greene et al.[139] used 41 HRV-based features and linear discrimination model, and achieved considerable detection accuracy in comparison with EEG-based methods. Patient-specific models provide higher accuracy. Qaraqe et al.[140] proposed a method using fused multichannel EEG signals and single-lead ECG signals. A matching pursuit Wigner-Ville distribution (MPWVD) is used to extract features from HRV. Multichannel EEG signals are first enhanced by a common spatial pattern (CSP)-based algorithm and then decomposed by multiresolution wavelet transforms into four sub-bands. The energies of four sub-band signals are computed as features. A data fusion technique reduced the false alarm rate significantly at the expense of a slightly increased detection delay [56].

Deep learning is a revolutionary paradigm which has overwhelmed the whole machine learning community, especially in the field of computer vision and natural language processing where great success has been achieved. And the influence of deep learning has spread to epileptic seizure monitoring. Thodoroff et al. [141] developed a recurrent neural network framework taking image representation of multichannel EEG data as input for automatic seizure detection. Significant higher sensitivity and lower false alarm rates in comparison with state-of-art algorithms across all patients were obtained. It is worthy of notice that the proposed deep learning framework works more robustly under missing channel conditions than the compound of handcraft features plus SVM. Acharya et al. [142] used a 13-layers deep convolutional neural network (DCNN) to perform computer-aided seizure detection. However, the data used in this research was limited and the amount of parameters in this DCNN is much larger than the number of data, so an extreme over-parametrization was conducted. Seizure prediction leveraged by deep learning has also been reported [143]. Representation learning methods for feature learning are also investigated [144].

2.3.2. *Nonlinear Dynamics*

Various measures of the complexity of a function stem from the research about nonlinear dynamics are used to discriminate physiological processes under different pathological conditions [145]. These methods propose a different paradigm and independent information compared to that acquired by classical spectral analysis and non-stationary signal processing techniques. In classical spectral analysis, a signal is treated as a function and is correlated

with harmonics of different frequencies. Coefficients are thus employed to measure the ‘intensity’ of different frequency components in this signal. While for most of non-stationary signal processing methods, similar operations were performed on different time scales and different resolution levels. And the signal is not necessarily to be correlated with trigonometric functions. Instead, more functions with desired characteristics can be used (wavelets). Furthermore, in-situ process without the need of another function was developed [146]. For all these methods, only homogenous descriptions (a set of weighted and mutually independent feature vectors, describing homogenous properties of interest) can be expected because the trigonometric functions and ‘wavelets’ are served as the basis of $L^2(R)$ space. The internal correlations and similarities of a signal are ignored. Different from the ‘decomposition-and-superposition’ paradigm where data segments are treated, in some way, individually first, and then accumulated, correlations and similarities in a function (signal) can be reflected by such measures derived from nonlinear dynamics, so these measures of complexity can provide information sometimes unattainable by other methods.

‘Entropy’ and ‘dimension’ are widely used in this area to measure the ‘complexity’ of physiological signals, in signal level or feature level. However, different entropy measures have different meanings in terms of their theoretical roots [64,65]. Among them, sample entropy [145], approximate entropy [149], multi-scale entropy [150] and distribution entropy [151] were developed.

According to [134], EEG signals can be decomposed up to four levels and reconstructed signals approximately correspond to five EEG sub-bands. Correlation dimension and largest Lyapunov exponent (LLE) are calculated on each sub-band signal. These parameters only show differences with statistical significance in sub-band signals rather than the original signals.

Approximate entropy [149] is one of the most frequently used measures in epilepsy research. It can discern the changing complexity of a dynamic system with relatively few observations (data points). Heuristically, approximate entropy estimates the probability or tendency that patterns close to each other will remain close to each other. In [39,75], approximate entropy is calculated at the signal level and feature level as a discriminative parameter. Liang, Wang, and Chang [153] reported that the combination of approximate entropy and spectral features provides robust seizure detection. It was also found the better ability of approximate entropy to discriminate between ictal and interictal EEG recordings. Guo et al. [152] used multiwavelet transform to decompose EEG signals into sub-bands and also approximate entropy are estimated on sub band signals

respectively.

Labate et al. [154] proposed multiscale permutation entropy (MPE) and justified its ability to separate patients with epilepsy from healthy controls. Kannathal et al.[155] compared four kinds of entropies measures with respect to their ability to seizure detection, including spectral entropy, Renyi entropy, Kolmogrov-Sinal entropy and approximate entropy. All the entropy measures showed significant lower values on epileptic group compared to control group.

Polychronaki et al.[156] evaluated the accuracy and three kinds of algorithms estimating the fractal dimension (FD), Katz's algorithm, Higuchi's algorithm and k-nearest neighbor (k-NN) algorithm. Only the k-NN algorithm showed consistent changes approaching a seizure's onset.

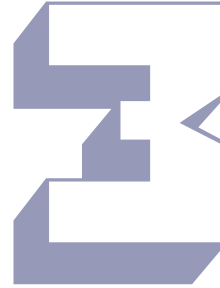
2.3.3. *Network Science*

The research on epilepsy is also inspired by network science [157]. Complex networks are graphs with huge numbers of nodes and edges connected. The connection can be direct or indirect, weighted or unweighted, and could even evolve with time. The 'nodes' and 'edges' are abstractions of 'entities' and 'relations' in the real world. With a graph, the relations between entities of interest could be modeled. However, network science not only pays attention to the topology of a graph, which is the focus of classical graph theory, but also cares about the dynamics and the equilibrium of a network and the control strategy for different purposes. The influence of network science proceeds along two theoretical approaches. Due to the anatomical basis of human's brain, a complex network is an analogy of the human brain on many important aspects. The use of mature methods developed in network science to depict the topology of an anatomical brain network may help explain the structural and functional abnormality of the brain of patients with epilepsy. Another approach is relatively suggestive. Graph and time series are two distinct kinds of mathematical objects. Heuristic transformation rules are proposed to set up a bridge between them. When physiological signals are transformed into graphs, matured methods in network science can be applied directly. For such a graph, periodicity is ill-defined. Instead, topological properties describe the physiological signal in a very different way.

Ortega, Sola, and Pastor [158] generated a minimal spanning tree (MST) from the correlation matrix whose entries are Pearson correlation coefficients between pairwise multichannel electrocorticogram (ECoG) recordings and identified the so-called local crucial node (LCN)

which has largest average correlations with its first neighbors as an indication for epileptogenic zone localization. Ponten, Bartolomei, and Stam [159] used synchronization likelihoods instead of Pearson correlation coefficients to calculate a similar square matrix and then transform it into a binary graph with adaptive thresholds. Larger clustering coefficients and higher characteristic lengths were observed on data collected from patients with temporal lobe seizures. The brain network seems to exhibit small-world properties during ictal period of seizure.

Zhang and Small [160] were the first to bridge time series to complex networks. They found pseudo periodic time series with different dynamics, when being transformed to a complex network, exhibit distinct topological structures. Lacasa et al. [161] introduced visibility algorithm constructing a graph remains invariant under affine transformations of the original time series. Zhu, Li, and Wen [162] proposed a modified algorithm, called fast weighted horizontal visibility algorithm (FWHVA). Mean length of the transformed graph as feature is efficient to distinguish seizure from healthy. Wang and Meng [163] constructed a functional brain network with MEG data. The individual nodes correspond to specific brain areas while the connections between nodes are determined by the degree of phase synchronization. Significant differences between the clustering coefficients and shortest path length of the functional brain network of patients with epilepsy and healthy control are confirmed. Diyk, Li, and Wen [164] constructed weighted undirected networks from feature vectors instead of raw data. The modularity of transferred network outperformed other network characteristics. Wang et al. [165] studied the EEG seizure patterns' influence on detection performance. A visibility graph algorithm and two derivatives are applied on EEGs recorded from epileptic patients with intellectual disability. Features based on degree distribution were found efficient in distinguishing seizure EEG from background EEG and improved the detection accuracy on intellectually disabled patients whose seizure patterns are highly varied.



Design of an Integrated Multi-Sensor Platform (MSP) Based on Flexible Materials for Neonatal seizure Monitoring

This chapter is based on:

1. Chen H, Xue M, Oetomo S B, et al. Neonatal seizure detection with wearable sensors system[M]//Intelligent Environments. Institute of Electrical and Electronics Engineers (IEEE), 2016.
2. Chen H, Gu X, Mei Z, et al. A wearable sensor system for neonatal seizure monitoring[C]//2017 IEEE 14th International Conference on Wearable and Implantable Body Sensor Networks (BSN). IEEE, 2017: 27-30.
3. Chen H, Bao S, Lu C, et al. Design of an Integrated Wearable Multi-Sensor Platform Based on Flexible Materials for Neonatal Monitoring[J]. IEEE Access, 2020.
4. Mei Z, Zhao X, Chen H, et al. A Distributed Descriptor Characterizing Structural Irregularity of EEG Time Series for Epileptic Seizure Detection[C]//2018 40th Annual International Conference of the IEEE Engineering in Medicine and Biology Society (EMBC). IEEE, 2018: 3386-3389.
5. Mei Z, Gu X, Chen H, et al. Automatic atrial fibrillation detection based on heart rate variability and spectral features[J]. IEEE Access, 2018, 6: 53566-53575.

In Chapter 2, we reviewed the methods of existing seizure detection methods and the wearable technologies and devices. Traditional neonatal seizure diagnosis is mainly judged with VEEG signals. Clinically used seizure detection methods are based on Video and/or EEG diagnosis and AEEG-based diagnosis. In clinical practice, diagnosis draws a conclusion according to the results of observations on EEG and/or video recordings experienced clinicians have made. Not only featured with considerable time consumption, but it also is confined to the inter-observer variability influenced by its subjective nature [10], [13], [166]. As a simplified method, tracing was first generated from timely compressed EEG information, used to provide information in real-time. It is a kind of detection and evaluation of seizures. Amplitude-integrated electroencephalogram (AEEG), comparatively, is to utilize a fewer number of electrodes to collect EEG information [47]. Moreover, EEG monitoring in neonates can be only conducted in a dedicated hospital environment. EEG cup surface electrodes and gel electrodes may also lead to skin lesions. In addition, the deployed electrodes with wires connected to monitoring facilities are likely to interfere with infant movement and result in missing detection.

Many researchers have begun to diagnose neonatal seizures through non-EEG signals. For example, Osorio et al. [52], [53] explored and verified the value of heart rate in the detection of clinical seizures. C. P. Panayiotopoulos et al. developed a wearable wireless surface electromyography module to determine the occurrence of the generalized tonic-clonic seizure (GTCS) [57]. In recent years, many researchers have used motion signals to detect seizures, which is not yet used in newborns currently. At the same time, researches on wearable technology for newborns are also growing rapidly. Chen et al. incorporated the textile electrodes in a smart jacket to monitor infants' ECG signal and improved the quality of the ECG signal by optimization of the electrode structure and location [57].

Researchers in the University of Southampton [167], [168] have recently worked out a silver paste. They printed the silver pastes onto non-woven textiles with which a new model of ECG monitoring device was then born in wearability. In addition, Zhang et al. have also proposed a wearable RIP based on respiratory monitoring devices. Such a type of instrument was devised deliberately for respiratory biofeedback training [77], [169]. Furthermore, it can be seen that the newborn wearable motion monitoring system has been also drawing more and more attention. Between 2010 and 2016, 20 articles on wearable newborn motion monitoring mentioned that motor signals of newborns could be obtained with the help of acceleration sensors [12], [92], [96]–[99], [101]–[110], [112], [113], [115], [117].

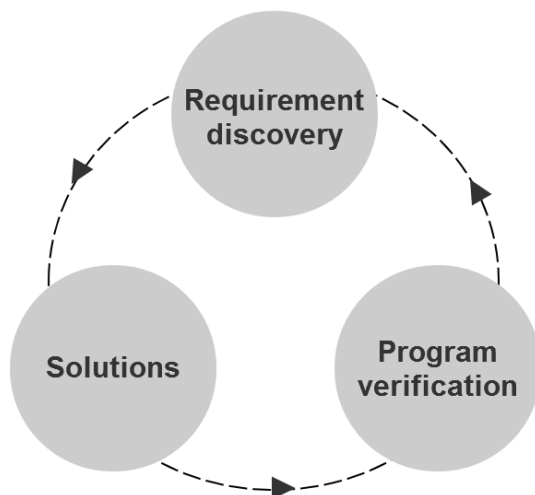


Fig. 3-1. Iterative process of system design

In this context, we propose to solve the problems occurring in neonatal seizure monitoring through a combination of a ‘flexible sensor network’ and ‘multimodal signal fusion technology’. We diagnose neonatal seizures by combining multimodal physiological parameters (electrocardiogram, respiration) and motor signals to achieve comfortable, continuous and effective neonatal seizure detection and prediction, hoping to provide new research directions and perspectives for neonatal seizure monitoring.

The whole process of this system design involves interdisciplinary efforts in the field of medical science, industrial design, user research, sensing technology, electrical engineering, clothing design and software design. In order to better realize the effectiveness and usability of the system, we designed the whole system based on “The Process of Innovating Medical Technologies”, adopting a rapid iterative method [29]. In contrast to “The Process of Innovating Medical Technologies”, we have determined the neonatal seizure diagnosis as the design scope at the beginning of the project. The iterative process of system design is shown in Figure 3-1, divided into three parts, namely requirement discovery, solutions and program verification.

The “requirement discovery” is arranged to select promising design opportunities according to clinics and related technology and collect medical needs through observation. Then in the section of “solutions”, we propose the framework concept of solutions based on the design requirements and realize the prototype implementation. Finally, the usability test and validity test are conducted in the “program verification”. The next iteration cycle will be carried out based on these test results and feedback.

3.1 Requirement Discovery through Design Methods that Combine Technical and Medical Background

There are three main steps in the requirement discovery part, namely, information retrieval, clinical observation and user interviews. The "Requirement Discovery" process starts from information retrieval, and we summarize clinical problems and the existing feasible technologies. Through the combination of various aspects of information to find out the possible design opportunity. We define the target users according to design opportunities which finds out by information retrieval. Then clinical observation and user interviews were carried out to find out the problems in the actual environment and clarify design requirements. The whole process of user interviews and clinical observation was conducted in China, so the results obtained were limited.

3.1.1. Information Retrieval

In chapter 2, we have conducted relevant information retrieval aiming at the Clinical symptoms of neonatal seizures, detection methods, the latest wearable technology and clinical issues. The summarizing of the information retrieval is shown in table 3-1.

Table 3-1. Summary of neonatal seizure-related symptoms, existing detecting techniques and related techniques.

Technology (wearable technology for neonate)	Clinical symptoms (seizure-related symptoms)	Detection of seizures (techniques already used clinically)	Issues conclusion
Wearable monitoring of electrocardiogram	Electroencephalography abnormality	Video- EEG- based judgement	Uncomfortable EEG diagnostics, possible miss detection
Wearable motion monitoring	Convulsive seizure	EEG-based judgement	EEG testing cannot be carried out for long periods of time

Wearable respiratory monitoring	Fast eye movement sleep phase	AEEG-based judgement	A large number of wires affect newborn's sleep
Wearable monitoring of myoelectric	Abnormal movement of the limbs		Video observation is too limited and inefficient
Wearable monitoring of temperature	Chewing movement		
Wearable monitoring of SPO2	Abnormal heart rate		

According to the results, the existing detection technology is mainly dominated by electroencephalography, which is expensive, specific environmental support needed, and is not suitable for long-term detection. Amplitude Integrated EEG (AEEG) is a simplified method that has been used by neonatal units in many parts of the world. Although the detection rate of epilepsy has increased, the detection rate of neonatal seizures is higher because of excessive pseudo-interference and the lack of video recording equipment. Compared with electroencephalogram testing, video observation is based on the experience of doctors and has great limitations. In addition, we found that newborn seizures displayed not only abnormal electroencephalogram, but also abnormal movements, heart rate and respiratory. In recent years, the study of convulsive detection methods based on non-brain electrical signals has been increasing and the feasibility of such methods has also been proven. On the other hand, it can be seen from the table that the wearable detection technology of non-brain electrical signals has become a feasible technical solution.

So, we found a design opportunity and proposed a hypothesis that a combination of "wearable monitoring technology" and "multimodal signal fusion technology" could be used to solve problems in neonatal seizures monitoring. Thus, enabling comfortable, continuous and efficient neonatal seizure detection. However, clinical problems in information retrieval are often incomprehensive. We need clinical observation and interviews to further clarify and refine our design requirements.

3.1.2. Clinical Observation

Clinical observation is arranged to understand users' real application scenarios and treatment methods, observe problems encountered in the actual scene, and analyze the causes of the problems. We summarize the special events in the observation process and analyze the causes of the events.

Location of observation: In the NICU Ward 2 of Children's Hospital affiliated with Fudan University.

Scene of observation: The recorded scene of a seizure in a neonate who was admitted to the hospital with a seizure. Two scenarios involved: (1) Nurses record EEG signals by wearing an EEG cap on babies; (2) Nurses observe the seizures of neonates with the eye.

Time: Five-day observation in the NICU ward and day-to-day participation in the entire work of nurses and doctors.

Results:

Table 3-2 summarizes the problems we found in the clinical observation. The problems we found were briefly summarized and analyzed.

Through clinical observation, it is found that the method to record and judge neonatal seizures mainly depends on the EEG and video. However, because of the fragile skin of infants, the detection time of EEG should not exceed 4.5 hours. As a result, many sudden seizures occur were not recorded. In addition, there are more patients and fewer nurses in China, which makes it difficult for nurses to care about the situation of all patients, especially at night. In this case, many neonatal seizures are also ignored.

Besides, it was complicated to use EEG detection equipment, which cost nurses 15-30 minutes to wear EEG caps for infants. What's more, EEG detection equipment was connected with an EEG cap and instrument through a data cable, so infants cannot move in the process of EEG detection. As a result, some tests cannot be carried out simultaneously with EEG.

Table 3-2. Summary of Clinical observation

Events in observation	Explain	Conclusion
Record and judge the seizure and brain damage by Video and EEG	Video-EEG is the golden standard for judging seizures. Expert usually diagnose seizures by means of electroencephalography (EEG). When the diagnosis is not certain, secondary confirmation via video is required.	Clinically, no other device can detect seizures except EEG device.
It takes nurses a lot of time (15-30 minutes) to wear EEG caps.	Since wearing the EEG caps requires the adjustment of the contact impedance of each electrode, it results in a long wearing time.	Operating difficulties
Long-term electroencephalogram monitoring sometimes damages the skin of the baby's head.	Because the infant's sleeping position is not fixed, and the electrodes of the EEG cap are hard, so long-term measurements can easily cause skin damage.	Uncomfortable wearing
An electroencephalogram can only be recorded for about 4 hours, resulting in four hours of electroencephalography data often not accompanied by seizures.	Due to long-term measurements can easily lead to skin damage, an electroencephalogram can only be collected for about four hours at a time. Neonatal seizures are sudden, and it is difficult to tell in advance whether seizures occur within four hours.	Lack of long-term neonatal seizure monitoring equipment.
Cleaning and disinfection of EEG caps	EEG caps are reusable and require contact with different newborns, so they need to be cleaned and disinfected after each use.	

When the neonatal seizures happened, the nurse did not discovered them.	With many patients and fewer nurses in China, it was difficult for nurses to care about the situation of all patients, especially at night.	Lack of long-term neonatal seizure monitoring and alarm equipment.
In the process of EEG detection, the infant cannot move, resulting in some tests cannot be carried out at the same time.	Because EEGs require wired connections to large devices, they are not easy to move and can only be operated in a fixed location.	The device is not portable.

3.1.3. User/Expert Interviews

Interviews, an important part of “requirement discovery” " is designed to identify the user’s essential goals, the task flow, the current use condition and opinions of the existing products. We interviewed six volunteers face-to-face, including five nurses in the NICU ward and a pediatrician, all from the Children's Hospital of Fudan University.

They need to clinically pay attention to the occurrence of neonatal seizures and to operate brain function instruments to collect the brain electrical signals of a newborn baby with seizure. In this study, the subjects mainly included doctors and nurses who had direct contact with neonatal seizures occur. The content of this interview mainly focuses on the characteristics and the current detection methods of neonatal seizure, and the corresponding problems in the detection process.

We summarize in the following table with key statements through user interviews:

Table 3-3. Summary of User/expert interviews

Key words/short sentences are obtained in interviews.
Sentence: It is difficult to detect neonatal seizures through real-time observation. Explain: There are no 24-hour continuous monitoring and seizure alarm devices in hospitals (In China), which makes neonatal seizures easily overlooked by doctors, especially at night. Conclusion: Lack of long-term neonatal seizure monitoring and alarm equipment. Source: Nurses and Doctors

<p>Sentence: Whether seizures happen or not are recorded and judged by video and EEG.</p> <p>Explain: The current gold standard for judging neonatal seizures is to combine EEG and video observations to determine whether neonatal seizures occur or not.</p> <p>Conclusion: The method of seizure detection is single.</p> <p>Source: Doctors</p>
<p>Sentence: The data is stored in the database</p> <p>Explain: The data need to be stored for secondary diagnosis, further consultation or analysis.</p> <p>Conclusion: Data needs to be stored</p> <p>Source: Doctors</p>
<p>Sentence: EEG collection equipment is troublesome to wear.</p> <p>Explain: The existing EEG equipment needs to be configured with an EEG cap to configure the position of the 8-lead, each of which needs to smear conductive paste to reduce the impedance for normal and smooth work. It is very time consuming usually taking 15-30 minutes to wear a single electric cap.</p> <p>Conclusion: Operating difficulties</p> <p>Source: Nurses</p>
<p>Sentence: The time of EEG detection cannot exceed 4 hours one time.</p> <p>Explain: Because the baby's sleeping position is not fixed and the electrode of the EEG cap is often convex or hard, prolonged compression may easily lead to skin damage.</p> <p>Conclusion: Lack of long-term neonatal seizure monitoring equipment.</p> <p>Source: Nurses and Doctors</p>
<p>Sentence: Abnormal behaviors occur during neonatal seizures.</p> <p>Explain: The occurrence of neonatal seizures was often accompanied by abnormal movements, which are medically explained and consistent with our previous findings.</p> <p>Conclusion: Seizures occur can be identified by movement monitoring</p> <p>Source: Nurses and Doctors</p>
<p>Sentence: Sudden seizures were difficult to be captured and recorded.</p> <p>Explain: Neonatal seizures were irregular sometimes and sudden usually, increasing the difficulty for the doctor to capture and record.</p> <p>Conclusion: Lack of long-term neonatal seizure monitoring and alarm equipment.</p> <p>Source: Nurses and Doctors</p>

3.1.4. Requirements Summary

Figure 3-2 shows the design criteria acquisition process. Based on information of information retrieval, clinical observation and user interview, we extracted a requirement for a neonatal seizure detection system: There was a requirement for a method to long-time and comfortable detect the neonatal seizures occur. Based on the requirements description and survey results, we have developed the design criteria.

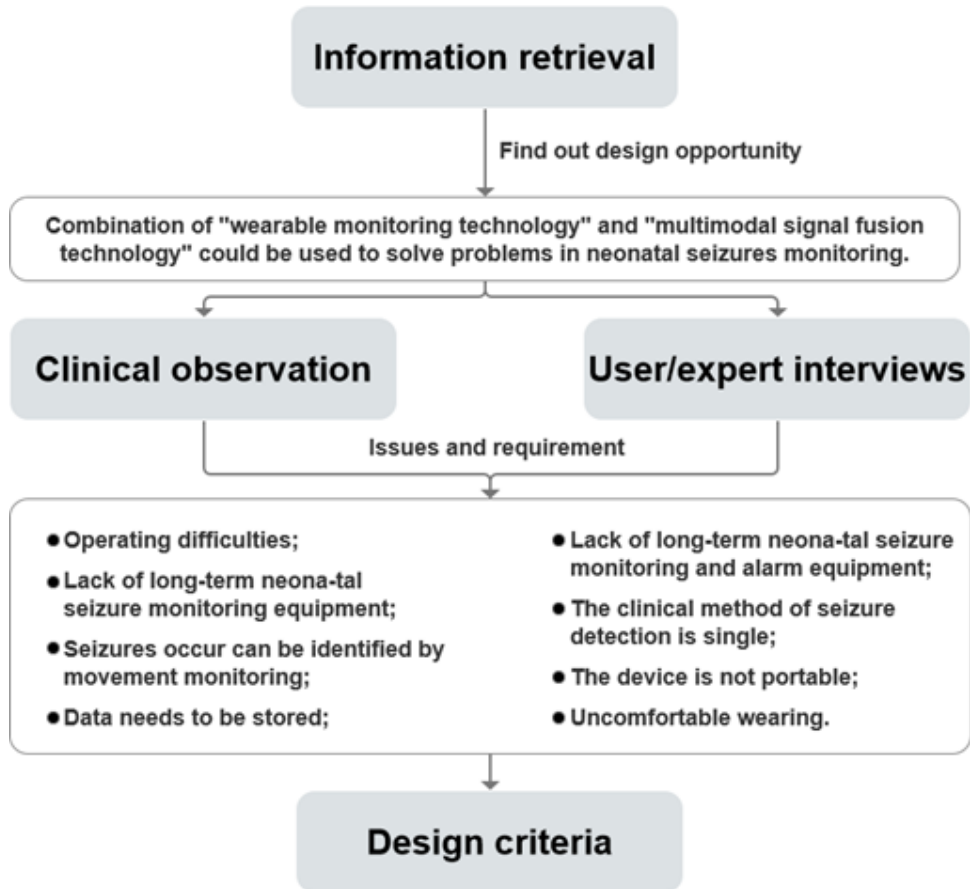


Fig. 3-2. Design criteria acquisition process

The design criteria were discussed by experts, nurses and designers, and divided into "criteria of necessary to have" and "criteria of better to have", as shown in table 3-4. The "criteria of necessary to have" must be met by the solution. This is the key to the adoption of the method. "criteria of better to have" may enhance the attractiveness of the method [29].

Table. 3-4. Requirements summary

Necessary to have	Better to have
Can detect the occurrence of neonatal seizures	Easy to wear
Can be used for long-term monitoring	Portable - wireless transmission
Does not damage newborns skin	The skin contact part can be cleaned or disinfected or disposably used
Can store data	Real-time display of signals
	Can provide alarm of neonatal seizure

According to the required standard, we put forward the conceptual framework from method, form and function, three aspects to meet the design requirement, as shown in Figure 3-3.

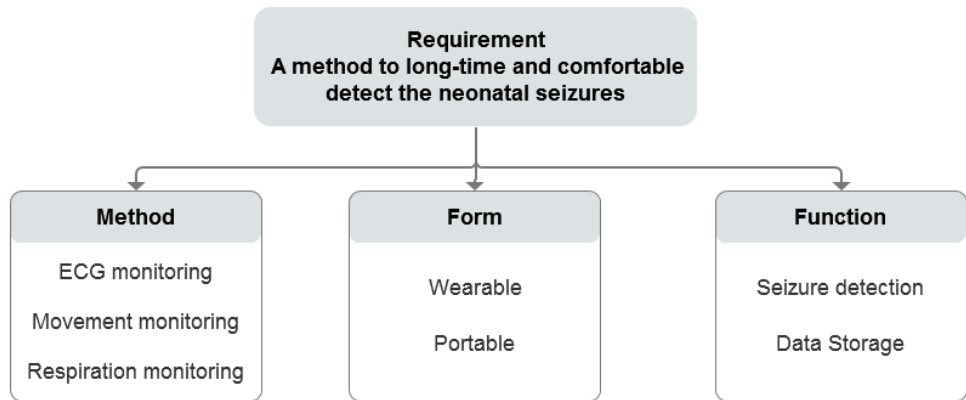


Fig. 3-3. Conceptual framework from

In order to realize the requirement, the combination of flexible sensing network and multimodal signal (electrocardiogram, respiratory and motion signals) fusion technology was provided to solve the existing problems in neonatal seizure monitoring to achieve comfortable, continuous and efficient neonatal seizure detection purposes. We have proposed the following technical routes. As shown in Figure 3-4, mainly includes multi-modal physiological and behavioral parameters acquisition, data transmission and multi-modal signal fusion analysis for neonatal seizure detection. The specific research methods and technical routes are introduced in the following 3.2 -3.4.

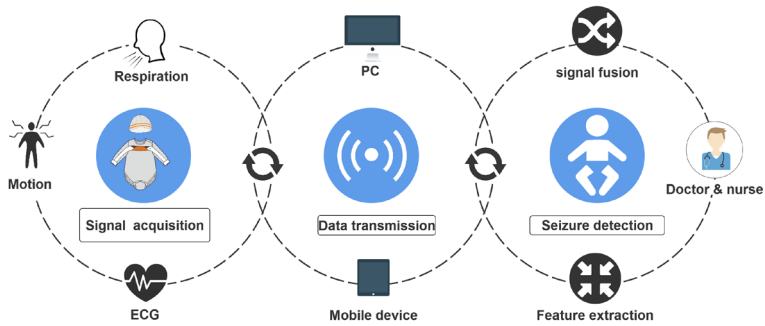


Fig. 3-4. System architecture

In Section 3.2, we introduce the design of the multi-modal wearable sensor system, including system architecture design, hardware design, smart vest design and software design. The system design realizes the function of signal acquisition and data transmission. In Section 3.3, we verify the signals collected by the system. Finally, the clinical data collection of neonatal seizures and the multimodal signal fusion method for detecting seizures are introduced in section 3.4.

3.2 System Design of Multi-Sensor Platform

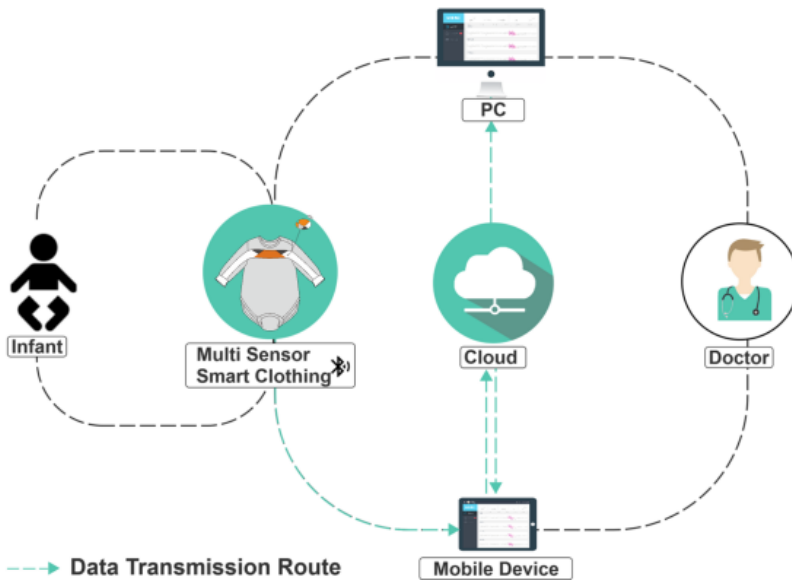


Fig. 3-5. System architecture

The proposed solution is described in Figure 3-5. In the proposed system architecture, a smart vest is introduced with flexible-material based sensors to acquire ECG, motion and respiration signals for signal acquisition. Choice of flexible materials for sensors and cloth for the vest together with the structure of the smart vest have been taken into consideration to achieve high signal quality and a better user experience for newborns. The data generated by the hardware system in the smart vest are transmitted to the local terminal for real-time monitoring with application and uploaded to the cloud platform simultaneously by local terminals. Another control terminal connected with the cloud platform will help doctors to analyze neonatal health status.

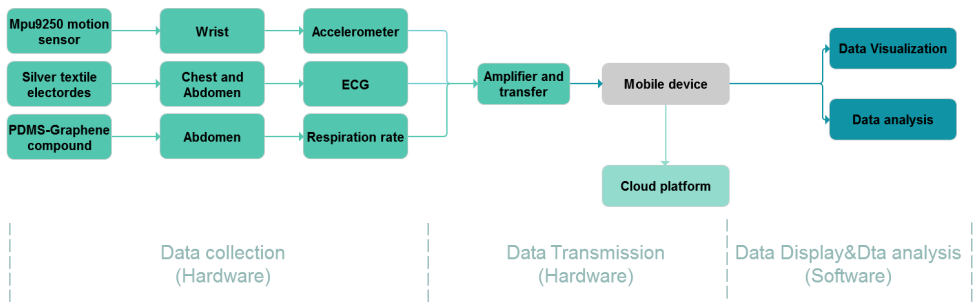


Fig. 3-6. Block diagram of the wireless neonatal monitoring system.

Figure 3-6 shows how the system framework is designed, which was divided into three parts: data collection, data transmission, data display and analysis.

In the data collection section, we designed a smart baby suit embedded with motion sensors, flexible textile electrodes, PDMS-Graphene (PDMS-G) compound and conductive wires to provide a comfortable clinical monitoring environment for infants. The microcontroller system collects the sampling signal of multiple chips, and uses the low-pass filter drop sampling process to transmit the data through the Bluetooth module in the form of packets. The ECG acquisition front end, controller, Bluetooth transmission module, and battery will all be embedded in an external plush toy. Too many components placed on the baby's body affect the baby's movements and reduce the baby's comfort, so we only embedded the inertial measurement unit (IMU), PDMS-G compound and flexible electrodes into the baby suit, while other components were connected by an external connector.

Motion signals, breathing signals, and ECG signals were transmitted via Bluetooth module to software, and the data were visualized on a computer or mobile device. At the same time, the software achieved the operation of the convulsive detection algorithm. When a seizure

was determined, the system automatically alerted. All data were automatically stored on the terminal. The method of neonatal seizure detection based on multi-signal fusion is described in detail in Section 3.4

3.2.1. Hardware Design

Figure 3-7 shows the technical framework of the hardware, including data acquisition, data processing and transmission. The signal acquisition consists of an ECG signal acquisition module, a motion signal acquisition module and a respiration signal acquisition module. The signal processing and transmission module was mainly composed of the ECG front end (ADS1292), the MSP430 microcontroller and the CC2564 Bluetooth and power supply module.

The system works as follows:

- (1) The data was carried out by each signal acquisition modules, including motion sensors, respiratory sensors and ECG sensors.
- (2) Microcontroller MSP430 communicates with each signal acquisition module through the Serial Peripheral Interface (SPI) bus and collects data.
- (3) Low pass filter was used to sample down.
- (4) The collected data will be sent to the computer via Bluetooth module.

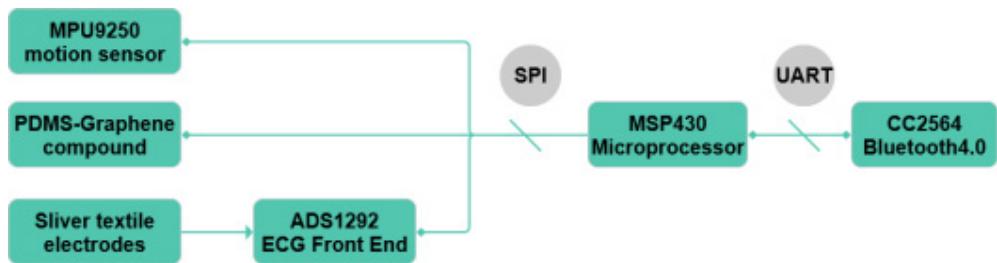


Fig. 3-7. Hardware architecture

a. Data acquisition module

The signal acquisition module consists of a respiration sensor, ECG electrodes and motion sensor, which was used to collect the physiological and motion signals of infants. To accommodate high-quality signals with a comfortable monitoring environment, we have designed PDMS-G compound sensors for capturing respiration

signals, textile electrodes for collecting ECG signals, and small motion sensors for collecting motion signals.

Respiration sensor

There exist a variety of methods to detect respiration, mainly covering Acoustic Based Methods, Airflow Based Methods, Chest and Abdominal Movement Detection, Transcutaneous CO₂ Monitoring, Electrocardiogram (ECG) Derived Respiration Rate and so on [170]. Among them, mercury strain gauges or impedance methods can be deployed to measure chest and abdominal wall movements [171]. Respiration inductance plethysmography is a non-invasive technique that measures respiration rate through two bands, a thoracic strap placed around the thoracic cage and an abdominal belt placed on the abdomen at the level of the umbilicus. Both are made of an extensible/deformable conductive material, an extremely fine wire or thin foil able to maintain its conductivity during the stretching process. The principle of the strain gauge sensor roots in the direct proportion of the resistance and area of the conductor in respiration [172]. In this work, we developed an advanced PDMS-Graphene compound material-based sensor and embed the new sensor into clothing to detect newborns' respiration signals.

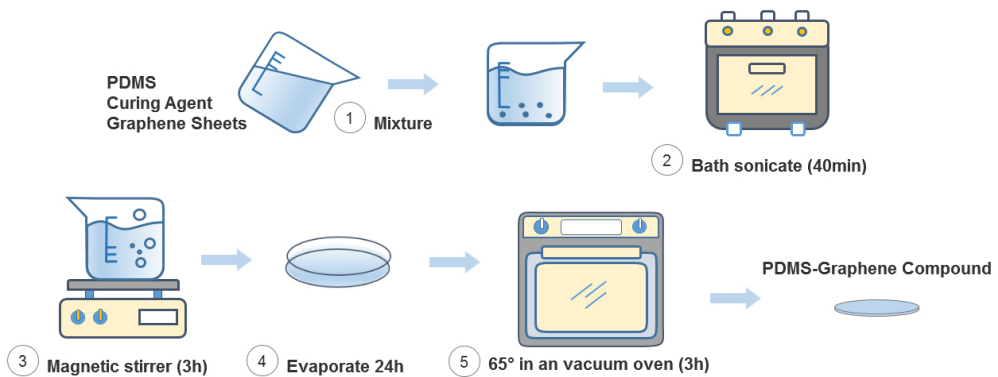


Fig.3-8. Schematic illustrations of fabrication procedures based on solution mixing-casting molding method for PDMS-graphene compound

We manufacture PDMS-G compound to monitor respiratory signals unobtrusively. The steps of the fabrication procedures are presented schematically in Figure3-8. PDMS, Graphene sheets and xylene are the main raw materials of the PDMS-Graphene compound. 8 g PDMS prepolymer, 0.8 g curing agent, 1.2 g graphene sheets are added

into a beaker with 60 mL Xylene. Then the mixture is bath sonicated for 40 minutes and then stirred for another 3 hours to extensively disperse the graphene sheets. After that, we poured the mixture into a glass plate to evaporate the xylene under ambient conditions. In the end, it was cured at 65 °C in an oven for 3 hours to obtain the final product.

Figure 3-9 shows the tensile state and the original state of the new tensile sensor (PDMS-G compound) respectively and demonstrates the feasibility of changing the conductivity of the sensor with the use of the new tool. To better get access to the changes of the abdomen during newborns' respiration, the sensor is designed to be put on the elastic band on the abdomen. Therefore, the length of the elastic band changes with the chest in the process of newborns' respiration, which helps to extract respiration signals through these changes.



Fig. 3-9. Resistance change while PDMS-Graphene compound is stretching. The original state of material (right); The stretched state of material (left).

The respiratory signal acquisition was connected to the analog-to-digital converter (ADC) of the single chip computer by the PDMS-G compound through the voltage dividing circuit. As shown in Figure 3-10, one side of the signal acquisition module was connected to the voltage source VCC while the other side is connected to the 12-bit AD converter on the signal processing module, and the offset resistance R0 was grounded. The change of breath over time was obtained by using the analog-to-digital conversion unit of the single chip computer.

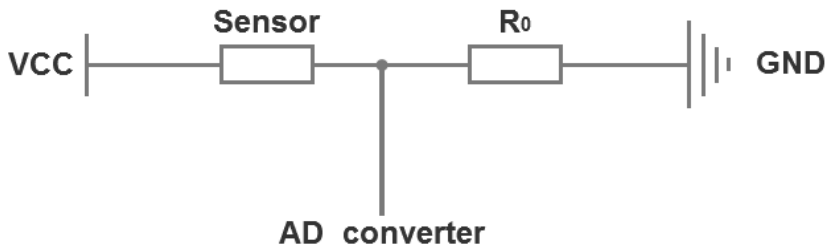


Fig. 3-10. Circuit diagram for respiratory signal acquisition.

ECG sensor

Conductive E-textile material is chosen to obtain ECG signal based on the above mentioned requirements [173]. After several iterations, comparing the properties of different materials, we used a conductive material to make the electrodes. The model of textile electrodes is from Berlin RS of Shieldex Company named as textile-based electrodes. They are flexible, non-irritating, lightweight (0.055 kg/m^2), thin (0.11 mm), low resistance ($< 0.5 \text{ ohms/sq}$) and convenient to be integrated into the side of the clothing. The textile electrode is designed to be disposable, because it will be affected by stains and sweats after use. We put forward a new flexible electrode structure in the proposed system. To ensure the stability of the electrode connection, the connection structure of the flexible electrode is proposed so that the electrode can be replaced, as shown in Figure. 3-b.

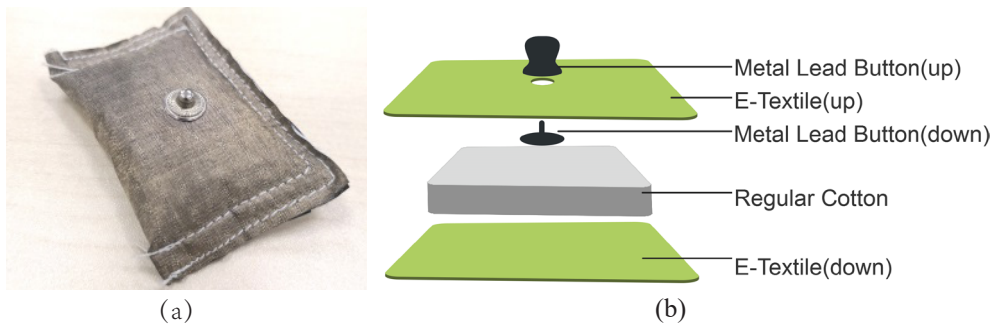


Fig. 3-11. (a) Textile electrode prototype; (b) Construction of textile electrodes

The electrode consists of three parts, a metal lead button, E-textile, and Regular Cotton. E-textile is connected to the metal lead button. Regular Cotton is sandwiched between the E-textile (up) and the E-textile (down), the periphery of E-textiles up and down is stitched by sewing. Motion artifact is one major

challenge that textile electrodes face. The proposed sandwich little cushion style of design improves the contact during a relative movement between the skin and the electrode perpendicular to the skin, which helps to improve the signal quality during motion.

The textile electrode was connected to the ADS1292 module by wire. ADS1292 was adopted as a low-power, 2-channel, 24-bit analog front-end, for ECG measurement. It has the characteristics of low noise, high precision, high resolution, high common mode rejection ratio and high transmission rate. With its high integration and excellent performance, ADS1292 can realize the establishment of a scalable medical instrument system on the premise of greatly reducing size, power consumption and overall cost. It is suitable for the application of this chip in wearable equipment. The chip uses the serial peripheral interface (SPI) protocol to communicate with the microprocessor.

When the register reads the data, the first communication number, CS, was set to 0, and the data input two bytes, with the first representing the first address of the register read and the second representing the number of registers to be read n minus one, followed by the output n byte corresponding to the corresponding number of register-stores stored data. When the register writes the data, the first communication number was set to 0, and the data was entered two bytes, with the first representing the first address of the register written and the second representing the number of registers to be written to the data n minus one, followed by the input n byte corresponding to the corresponding number of registers that will be written data.

Motion sensors

Recently, inertial sensors has been widely used in ambulatory motion analysis [174]. To obtain accurate motion measurements, IMUs, integrating the accelerometers, gyroscopes, and magnetometers are often used.

In the second chapter, we searched for studies related to wearable motion monitoring in newborns in recent years. From the search, it can be found that 20 of the 30 articles used acceleration sensors. With the development of technology, inertial sensors (IMU, accelerometer, magnetic inertia) have become the research hotspot in the field of motion sensing. Due to its low cost, portable size and high performance, more and more researchers believe these sensors are a good choice for infant motion monitoring.

Therefore, the inertial sensor (IMU) MPU9250 is used in this project. It is a nine-axis motion tracking device developed by InvenSense, which combines three-axis acceleration, three-axis gyroscope and 3-axis magnetometer, compatible with SPI

and I2C transmission protocols, and is capable of simultaneously outputting all nine-axis data.

In order to make the sensor smaller and lighter, we integrate MPU9250 into a PCB with a diameter of 0.8cm, and connect it with a signal processing module through SPI. The motion sensor we designed is shown in figure 3-12, which is only 0.9g.



Fig. 3-12. Motion sensor

The motion signals are transferred to MCU via SPI using Flexible Printed Circuit (FPC) cables. Data is stored in byte format and address is also stored in byte format. The highest bit is 1 for reading while the highest bit is 0 for writing.

b. Data processing module

The system uses MSP430F5529 as the control chip. Compared with other microcontrollers, the series of micro-controllers are very suitable for the processing of ECG signals with the advantages of ultra-low power consumption and rich on-chip peripherals. In the MSP430 series of chips, the MSP430F5529 not only meets functional requirements, but also has the advantages of low overall power consumption and cost.

(1) Microprocessor workflow

The workflow of MSP430F5529 is shown in Figure 3-13. The peripheral and SPI configurations are initially initialized, then the configuration sensor is read through the registers and the four flag bits in the diagram are initialized, and the filter is preprocessed for the data to turn on the global interrupt when it is ready. After processing, if the direct memory access (DMA) transmission flag bit DMA-Done is 1, the data bus is connected directly to the Bluetooth side by DMA to send the data.

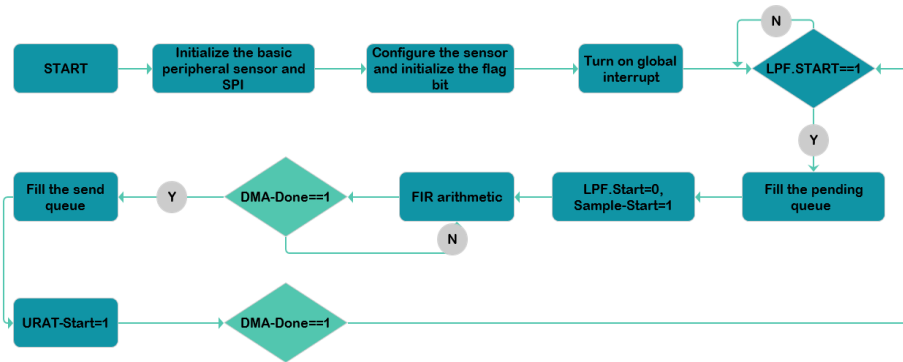


Fig .3-13. Main program

(2) Program architecture

The program is composed of the main program occupying the kernel and two hardware interrupt service programs to realize the scheduling of multiple tasks such as timing sampling, timing sending, data sampling filtering, etc. As shown in Figure 3-14, through four global flags, the system works in a limited finite state machine (FSM) and can start by itself when the hardware works normally. Under this framework, the tasks of sampling, filtering and sending are executed separately. Each task does not affect each other, which ensures the real-time performance of the system, enhances the readability of the program, and improves the efficiency of modification and transplantation.

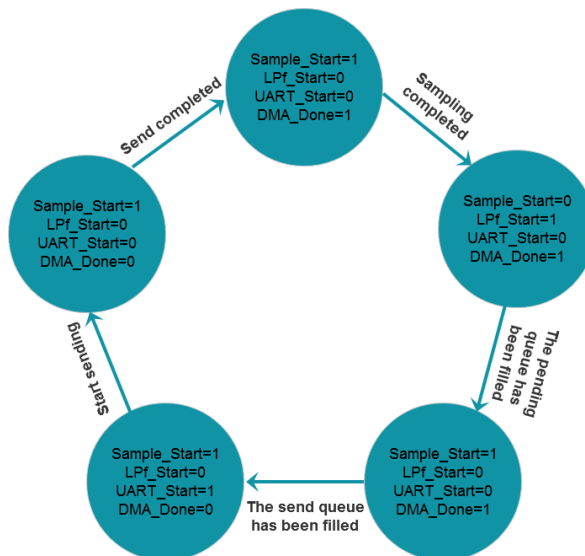


Fig. 3-14. The diagram of system state transition

c. Signal transmission module

(1) Bluetooth module (CC2564)

CC2564 Bluetooth module was used as a wireless transmission module. The CC2564 Bluetooth module is a dual-mode Bluetooth chip, supporting Bluetooth 3.0 and Bluetooth 4.0 transmission. In addition, the CC2564 has good equipment compatibility and is easy to connect with computers, mobile phones, tablets and other devices. The serial port of the Bluetooth module was connected to the serial port of the MSP430F5529.

(2) Data transmission process

All the signal acquisition modules were controlled and managed by the MCU (MSP430, Texas Instruments) at the sample rate of 500Hz. In order to achieve 500Hz sampling, the 'timer interrupt' was called every 2 microseconds to acquire the signals through SPI sequentially. The 'timed interrupt' is a task executed at a fixed interval to process the data. A finite impulse response (FIR) filter was used to control the bandwidth of the data transmission. The optimized signals were sent to the universal asynchronous receiver/transmitter (UART) ports of the wireless transmission module (CC2564, Texas Instruments) through direct memory access (DMA) of MSP430. The block diagram of the system is shown in Figure 3-15. Also, a timestamp was added to the data package every 1 second to synchronize the time interval with the machine in the hospital. The processing procedures were controlled by a restricted finite state machine (FSM).

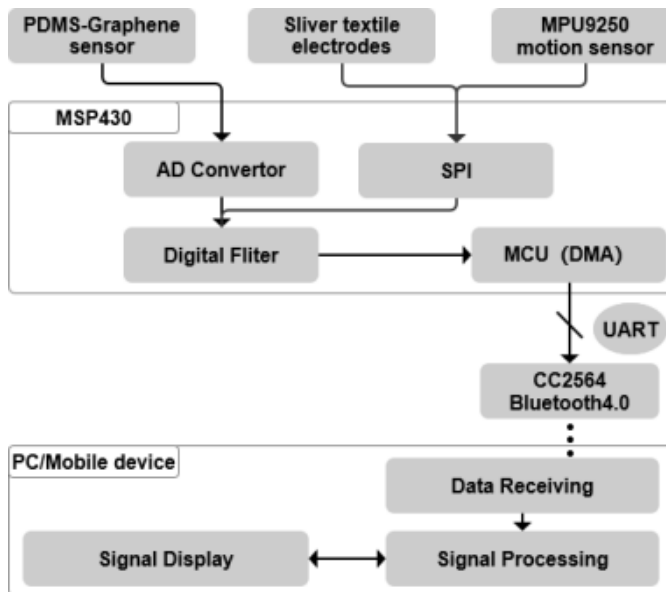


Fig. 3-15. The block diagram of MSP.

(3) Design of data transmission protocol

The data package format is shown in Table 3-5. One data package in the system is 24 bytes. The Frame Header field specifies the beginning of a package and contains 2 bytes. Moreover, the Length field shows the length of one package. The Check field is the odd-even check result for the data in one package. In this project, HEAD_H=0x88, HEAD_L=0x71, LENGTH=22, and the CHECK is odd even CHECK, with the value of the first 21 bits of exclusive OR (xor). The format of the Data field is shown in Table 3-6. ACCEL0_X, ACCEL0_Y and ACCEL0_Z stand for the tri-axis acceleration of the left wrist acquired by the IMU. ACCEL1_X, ACCEL1_Y and ACCEL1_Z stand for the tri-axis acceleration of the right wrist. ECG is the 24-bit digital signal gathered from ADS1292. RESP is the respiration signal gathered from the novel stretching sensor.

Table3-5 Data package format

Frame Header		Length	Data(17 bytes)				Check
Head_H	Head_L	Length	Data0	Data1	...	Data16	CHECK

Table 3-6 data field format

Data byte	0-1	2-3	4-5	6-7	8-9	10-11	12-13	14-16
Data	ACCEL0_X	ACCEL0_Y	ACCEL0_Z	RES_P	ACCEL1_X	ACCEL1_Y	ACCEL1_Z	ECG

3.2.2 Smart vest Design

In the iterative design process of clothing, we mainly focused on the comfort of clothing, signal stability, and operation convenience. Nurses, clinicians, and costume designers participated in the discussion and evaluation during the design process. Figure 3-16 shows the final version of the prototype of the smart garment.

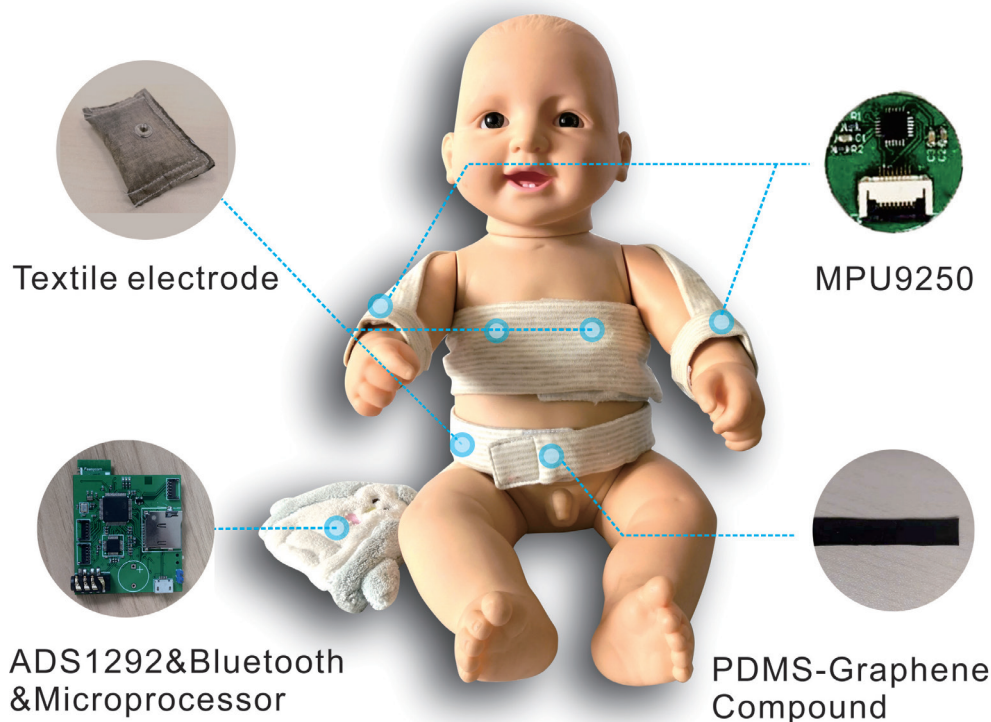


Fig. 3-16. Prototype of the smart vest

According to previous research experience [37], we choose knitted cotton fabrics to ensure comfort. The choice of knitting structure is critical because it is usually more ductile, flexible and breathable than others. In addition, proper elasticity is also very important for sensor immobilization, especially for ECG electrodes. Elastic fabrics can increase the stability of contact between skin and electrodes, which is an important condition for ECG signal detection. The whole structure of smart clothing adopts an open front-end design, in order to expose more skin in the process of continuous monitoring and reduce the impact of clothing on newborns. The bandage design with a magic sticker can make clinical nurses more convenient to operate, which is conducive to the fixing of sensors. In order to ensure comfort for newborns, we only integrate sensors into clothing to reduce the interference of components on newborns. The garment side is connected with a doll for placing the signal processing module, signal transmission module and battery.

The position of electrodes will affect the quality of ECG signals, so several studies have focused on the placement of electrodes on the body to determine the optimal location for ECG signal detection. Cho and Lee studied the signal quality of electrodes placed at 56

locations on an adult and found the best location was near the chest line, which was the smallest dynamic area of the human trunk [175]. Lanjun Yin et al. tested four different electrode positions on adults to verify the optimal electrode position [176]. ECG data were collected and analyzed by Vernier LabQuest device. The best clear signal was obtained by using chest and right waist positions, as shown in Figure 3-17. Later, Lanjun Yin et al. held a test on an infant. The results showed the infant's body was so small and compacted that the three electrodes could cover a large area. So as long as they were located on the trunk and had good contact with skin, there was no significant difference in ECG signals reflected by different electrodes. In this project, the electrodes were placed on the left and right sides of the chest of the newborn, and the reference electrodes were placed on the abdomen, fixed by simple banding. By adjusting the magic tape, it can be suitable for newborns of more sizes. The experimental results show that this method can obtain high quality ECG signals. A detailed description of the experiment is given in Section 3.2

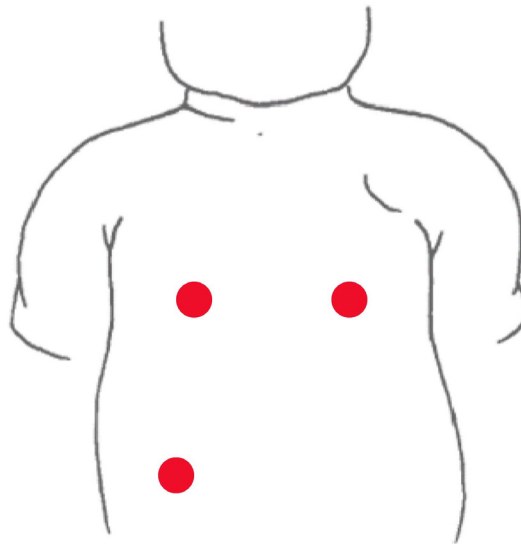


Fig. 3-17. The best placement of electrodes for ECG signal obtained.

The position of the motion sensor is also critical. In Chapter 2, we summarized the placement of motion sensors on newborns in recent studies. Most studies on infant movements have chosen to place sensors on the wrist or ankle. The results are not only related to the purpose of the study, but also because newborns tend to exercise more at the wrists and ankles than other areas, making it easier to obtain useful information. In

addition, in the clinical characteristics of neonatal convulsive attacks, four types of neonatal convulsive seizures may involve abnormal hand movements, such as cycling, boxing, jerking et.al. Therefore, in this project, we attach motion sensors to the newborn's wrists in the form of straps to obtain motion signals from hands.

Unlike adults, newborns mainly depend on abdominal breathing, so we place the respiration sensor sits on their abdomen. The newborns' breathing is reflected by detecting changes in the abdomen. The breathing sensor is placed on the inside of the abdominal strap and can be adjusted by magic paste.

3.2.3 Software Design

In software design, we need to meet three basic requirements of signal visualization, data storage, and seizure alert reminders. The neonatal activity scope is restricted, while the range of doctor/nurse activity is unlimited. Therefore, mobile devices were adopted and placed in the range of neonatal activity. The data of the smart vest was received by mobile software to ensure its integrity and sustainability. Mobile software transfers data to the cloud and stores it while receiving data. Mobile devices and PC (personal computers) can read real-time data from the cloud server for viewing.

Mobile software was designed based on an android development environment. Software programming adopts the method of modularization, with the main function modules like wireless data transceiver module, signal data acquisition module, historical data module and seizure alarm module all edited into independent functions, and called by the main program. The framework of the software system is shown in Figure 3-5. The function of the software system is divided into four modules, including user list, signal display, seizure alarm and history record, as shown in Figure 3-18.

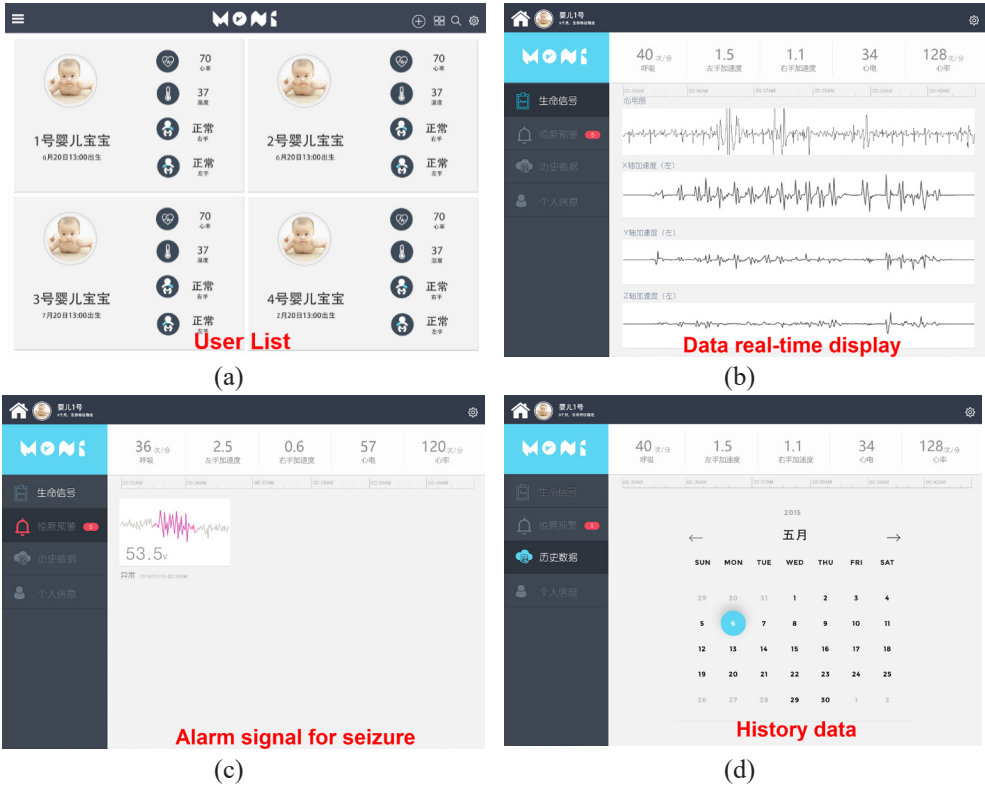


Fig. 3-18. Four modules of software, (a) User list, (b) Data real-time display, (c) Alarm signal for seizure, (d) History data.

User list

The purpose of the user list was to facilitate the monitoring of different neonates by nurses/doctors. When nurses/doctors need to monitor a new neonate, they can add users in the user list module, ensuring that each infant has independent data storage space. When a new user ID is added, basic information of the user can be recorded, including the head picture, name, date of birth, weight and hospital code which is usually set according to different hospital standards.

For the data storage of new users, the ‘Leancloud’ cloud server is selected as the technical support. User information can be stored in the form of a table, as shown in Figure 3-19. Each record corresponds to a user’s information.

objectId	name	birthday	day	ACL	createdAt	img	yu
Sacce939f9f545463f0875d0	baby5		10	{**:{read":true,"wri	2018-04-11 00:41:35	http://1c-jmH06yK.cn-n1.l.	3
Sac9d3a0f9f545420c22949ac	yan hua		15	{**:{read":true,"wri	2018-04-08 17:13:30	http://1c-jmH06yK.cn-n1.l.	3
Sac9d100f9f545420c22947b2	chen chen		5	{**:{read":true,"wri	2018-04-08 17:12:48	http://1c-jmH06yK.cn-n1.l.	3
Sac9dce9f9f54541c80af0109	baby2		30	{**:{read":true,"wri	2018-04-08 17:12:09	http://1c-jmH06yK.cn-n1.l.	3
Sac9dce9f9f54541c80af0109	baby1		4	{**:{read":true,"wri	2018-04-08 17:11:21	http://1c-jmH06yK.cn-n1.l.	3
S0d0b724b123db3f6b0dc795	机器人1号		21	{**:{write":true,"r	2017-03-21 13:16:20	http://ac-jmH06yK.cloudnn.	3
S0a2ba60128fe10065a4454	李村		23	{**:{write":true,"r	2017-02-14 16:06:03	http://ac-jmH06yK.cloudnn.	3
S0a2ba205c4970005644f4ec	承德		14	{**:{write":true,"r	2017-02-14 16:04:56	http://ac-jmH06yK.cloudnn.	3
S0a2b9f4128fe1006cf07ef5	吴云		14	{**:{write":true,"r	2017-02-14 16:04:04	http://ac-jmH06yK.cloudnn.	3
S0a2b9852f301e0009084483	宏宇		14	{**:{write":true,"r	2017-02-14 16:02:13	http://ac-jmH06yK.cloudnn.	3
S032f8f3578c350059e07a3a	龙宝	2016-11-15	21	{**:{write":true,"r	2016-11-21 21:38:59	http://ac-jmH06yK.cloudnn.	3
S038759061f46006cdc4e0	八宝	2016-11-25	24	{**:{write":true,"r	2016-11-26 01:32:00	http://ac-jmH06yK.cloudnn.	3
S02da6c667f35006334a1a	余旭	2016-11-09	4	{**:{write":true,"r	2016-11-17 20:47:32	http://ac-jmH06yK.cloudnn.	3
S02af2c7da3f600063cfa20	宝宝1号	2016-6-11	20	{**:{write":true,"r	2016-11-15 19:34:31	http://ac-jmH06yK.cloudnn.	3

Fig. 3-19. The form of user information in the ‘Leancloud’

Signal display

The Android terminal connects the hardware sensor device via Bluetooth and receives the raw data from the hardware device. The raw data is stored in a global data source for use by the waveform graph control. The waveform controls “Canvas” and “Paint” extract the corresponding ECG, respiration and movement data in real time and display on the interface. The HR, RR and motion characteristic values extracted by the algorithm are also displayed in the interface. Figure 3-18-b shows an overview of the elements in the signal display interface. The core code of the control is as follows:

```
// If the data in the set
if(data.size()>1){
    if(FearActivity.reset){
        data.clear();
        return;
    }
    for (int i = 1; i < data.size(); i++) { // Remove the data in turn for drawing
        canvas.drawLine(xPoint+(i-1)*xScale,(float)( yPoint-(data.get(i-1))*yScale-2*yScale),
xPoint+i*xScale, (float)(yPoint-data.get(i)*yScale-2*yScale), paint);
        if (data. get(i-1)>2||data. get(i-1)<-2){
            canvas.drawLine(xPoint+(i-1)*xScale,yPoint,xPoint+(i-1)*xScale,yPoint-
4*yScale,paint1);
        }
    }
    if (i==599)
        break;
    if (i>=20&i<data. size()) {
        double resultL = 0;
```

```

double resultR = 0;
for (int j = 0; j < 20; j++) {
    resultL = resultL + FearActivity.data3.get(i-j)*FearActivity.data3.get(i-j)+FearActivity.
data4.get(i-j)*FearActivity.data4.get(i-j)+FearActivity.data5.get(i-j)*FearActivity.data5.get(i-j);
    resultR = resultR + FearActivity.data6.get(i-j)*FearActivity.data6.get(i-j)+FearActivity.
data7.get(i-j)*FearActivity.data7.get(i-j)+FearActivity.data8.get(i-j)*FearActivity.data8.get(i-j);
}
resultL = resultL/20;
resultR = resultR/20;
if (resultL> HomeBaseActivity.yuzhi || resultR>HomeBaseActivity.yuzhi){
    canvas.drawRect(xPoint+(i-20)*xScale,0,xPoint+i*xScale,yPoint,paint1);
}
}
}
}

```

Seizure alarm

The seizure alarm module was embedded in the software. The related algorithms will be introduced in detail in chapter 3.4. The storage of seizure data depends on the cloud service “leancloud”. The software will trigger an automatic storage function to store the current data in the “Leancloud” service cloud when a seizure is detected. Each record stores the user information and the time of the seizure. Meanwhile, the software can give visual and auditory alarm feedback.

objectId	STRING	pointerBaby	POINTER	month	NUMBER	day	NUMBER	hour	NUMBER	minute	NUMBER	createdAt	DATE
59da052d954040067ea3ba4		5832f8f3578c350059e07a3a		10		8		19		0		2017-10-08	18:59:57
59da031167f350003ab05a41		5832f8f3578c350059e07a3a		10		8		18		51		2017-10-08	18:50:57
59da064e954040067e09f7d		5832f8f3578c350059e07a3a		10		8		15		40		2017-10-08	15:39:58
59da0c455756f714641d499cc		5832f8f3578c350059e07a3a		10		8		15		6		2017-10-08	15:05:57
59da0c4d167f350003aee79c2		5832f8f3578c350059e07a3a		10		8		14		51		2017-10-08	14:50:57
59da0ca5967f3500042fca2e0		5832f8f3578c350059e07a3a		10		8		14		49		2017-10-08	14:48:57
59da0ca001069e0040b416da		5832f8f3578c350059e07a3a		10		8		14		47		2017-10-08	14:47:28
59da0ca95578c35000c080ea		5832f8f3578c350059e07a3a		10		8		14		46		2017-10-08	14:45:57
59da0c96917d0090063ef02aa		5832f8f3578c350059e07a3a		10		8		14		45		2017-10-08	14:44:57
59be07d8120fe158341da942		58a2ba285c497d005644f4ec		9		17		22		34		2017-09-17	22:34:00
59be079c8d6d810055a30b08		58a2ba285c497d005644f4ec		9		17		22		33		2017-09-17	22:33:00

Fig. 3-20. The form of seizure alarm event in the ‘Leancloud’

Historical data

The historical data module provides a way for doctors to view historical data and diagnose. After receiving the data, the mobile terminal transmits them to “leancloud” through the wireless network. The data interacted between the mobile terminal and the cloud server is

abstracted into [AVOobjects]. After each instance of AVObject is saved to the ‘leancloud’ cloud, the cloud will give the instance a globally unique ID. At the same time, the cloud will automatically add two attributes to the instance: ‘createdat’ and ‘updatedat’, which respectively represent the creation time and the last update time of the instance. For the data on ‘leancloud’, the main operations are data storage and data retrieval.

The operation of save data is as follows:

```
// Build the object
AVObject todo = new AVObject("Todo");
// Assign a value to the property
todo.put("title", "name");
todo.put("priority", 2);
// Save the object to the cloud
todo.saveInBackground().subscribe(new Observer<AVObject>() {
    public void onSubscribe(Disposable disposable) {}
    public void onNext(AVObject todo) {
        // After successful saving, other logic is executed
        System.out.println("Save successfully. objectId: " + todo.getObjectId());
    }
    public void onError(Throwable throwable) {
        // Exception handling
    }
    public void onComplete() {} });
```

The operation of data acquisition is as follows:

```
AVQuery<AVObject> query = new AVQuery<>("Todo");
queryInBackground("582570f38ac247004f39c24b").subscribe(new Observer<AVObject>() {
    public void onSubscribe(Disposable disposable) {}
    public void onNext(AVObject todo) {
        // todo is an instance with objectId 582570f38ac247004f39c24b
        String title = todo.getString("title");
        int priority = todo.getInt("priority");

        // Get built-in properties
```

```
String objectId = todo.getObjectId();
Date updatedAt = todo.getUpdatedAt();
Date createdAt = todo.getCreatedAt();
}
public void onError(Throwable throwable) {}
public void onComplete() {});
```

3.3 Signal Verification of Multi-Sensor Platform

3.3.1 System Signal Verification Framework

A systematic verification method was proposed for wearable hardware systems with new materials involved. Figure 3-21 shows the framework of evaluation to verify the feasibility of the system by evaluating three kinds of acquisition methods respectively. The targets and methods are designed to objectively verify signal quality from a fundamental aspect to an actual use scenario. For the ECG signal acquired by textile electrodes, we first evaluate the electrical properties of designed electrodes by investigating the skin-to-electrode impedance to promise the signal quality at the very beginning. Then some statistical indexes are chosen to assess the signal quality in a standard equipment environment. After the evaluation process of the textile electrodes designed, they are applied to the new hardware system while ECG signals are collected accordingly. Three classical ECG signal quality assessment methods are applied to evaluate ECG signal acquired by the proposed system and finally we compare the ECG waveform with the clinical gold standard. Similarly, for the novel stretching sensor based on the PDMS-G compound, a feasibility experiment is designed at first. After that, the sensor is embedded in the system for comparison with clinical equipment. Moreover, since we use a commercial chip for the motion signal acquisition, the sensor verification method is omitted at this stage and we just compare the signal acquired by the system with the commercial Shimmer device.

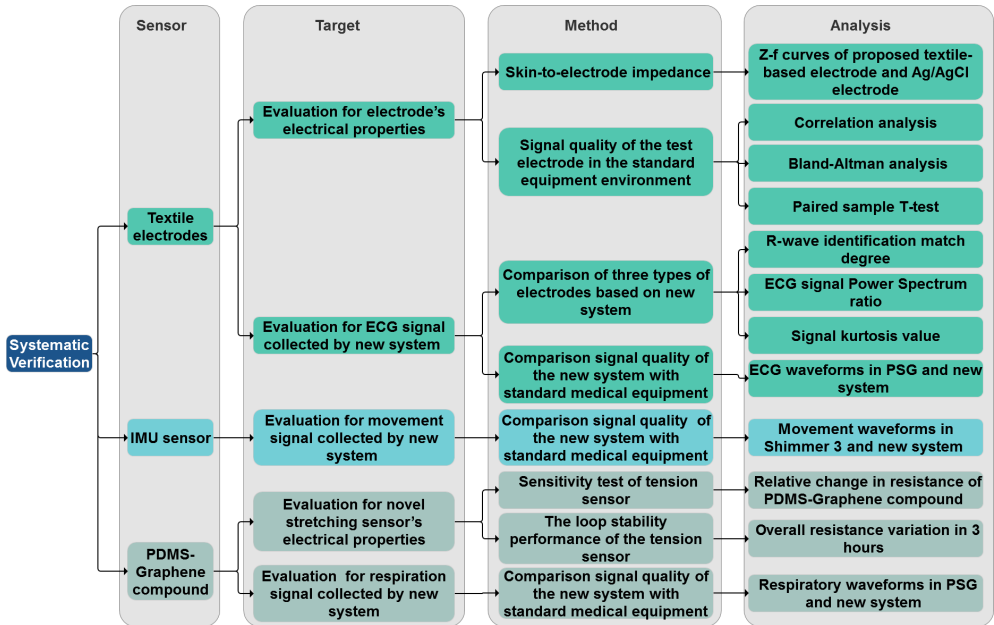


Fig. 3-21. Framework for the evaluation

3.3.2 ECG Signal Verification

3.3.2.1 Flexible Textile Properties

1) Method

To assess the electrode properties, we set up two experiments. One is to test the skin-to-electrode impedance, and the other is about the signal quality of the test electrode in the standard equipment environment.

(a) Skin-to-electrode impedance

The impedance introduced by the skin-to-electrode interface of standard Ag/AgCl electrode and textile electrode is measured on a person's forearm by an electrochemical workstation (ZAHNER - Zennium).

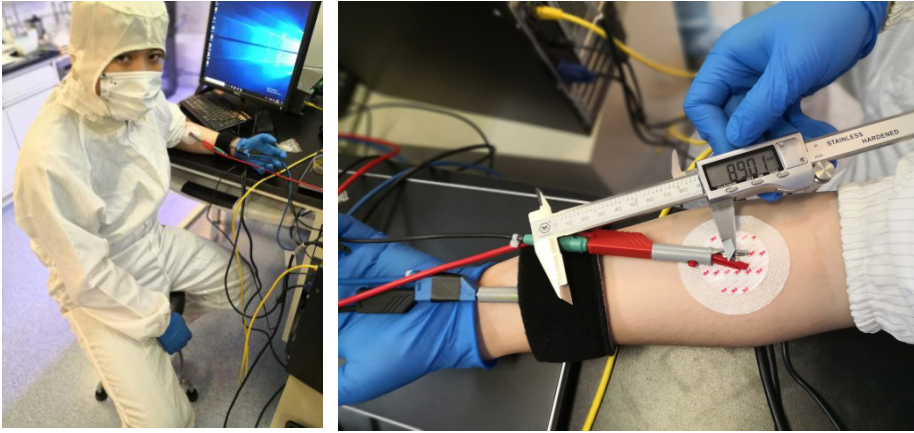


Fig. 3-22. Experimental settings for evaluation of electrodes

The two-electrode system is used as depicted in Figure 3-22. Ag/AgCl electrode is deployed as a reference electrode. The work electrodes are chosen from the textile electrode and Ag/AgCl electrode (Covidien, H124SG). The distance between the working electrode and the reference electrode is approximately 9 cm. We fixed the textile electrode with a strap. The frequency of the input signal sweeps from 0.1 Hz to 100 kHz. An impedance-frequency curve is drawn for each kind of electrode.

(b)Textile electrodes signal quality assessment

We compared the ECG signals acquired by the proposed electrodes and Ag/AgCl electrode (Covidien H135SG) using a standard acquisition system.

We collected data from the textile electrode and Ag/AgCl electrode simultaneously in a static state by shimmer 3 [177]. The study involved a 24-year-old male volunteer. Different electrodes were attached to the adjacent positions on the left and right sides of the subject's chest. We used shimmer-3 as a standard acquisition device. The acquisition time for data was one and a half hours.

The following three statistical analysis methods were conducted to evaluate the signal quality acquired by the novel electrode. Heart rate per minute is extracted by the R wave detection algorithm implemented on MATLAB R2018a based on the classic QRS detection algorithm proposed by Willis. et al [178]. A bandpass filter with a passband of 5-15Hz is used to preprocess the data and the hamming window is applied for the function “fir1” in MATLAB. Then a dynamic threshold is determined every five seconds with 2500 values gathered from the system for the “findpeaks” function with the ‘MinPeakDistance’ index of 150 points which is 0.3 seconds in the time domain.

Correlation analysis

We extracted the average heart rate value per minute and compared the heart rate signals from two different electrodes in each group. Correlation analysis is calculated between heart rate information in each group.

Bland-Altman analysis

Similarly, a „Bland-Altman analysis“ was performed on the average heart rate.

The standard Ag/AgCl electrode is used as the comparison detection system M1, and the textile electrode is the system M2 to be evaluated. The Bland-Altman analysis was performed to show the difference between heart rates detected by the two systems.

Paired sample T-test

Table 3-7. Selected time domain and frequency domain measures of HRV

Variable	Units	Description
Analysis of short-term recordings (5 min)		
SDNN	ms	Standard deviation of all NN intervals
RMSSD	ms	The square root of the mean of the sum of the squares of differences between adjacent NN intervals
SDSD	ms	The standard deviation of differences between adjacent NN intervals
NN50		Number of pairs of adjacent NN intervals differing by more than 50 ms in the entire recording. Three variants are possible counting all such NN intervals pairs or only pairs in which the first or the second interval is longer.
PNN50	%	NN50 count divided by the total number of all NN intervals.
5 min total power	ms ²	The variance of normal-to-normal (NN) intervals over the temporal segment.
VLF	ms ²	Power in very low-frequency range
LF	ms ²	Power in the low-frequency range
LF norm	ms ²	LF power in normalized units $LF / (Total\ Power - VLF) \times 100$
HF	ms ²	Power in the high-frequency range
HF norm	nu	HF power in the normalized unit $HF / (Total\ Power - VLF) \times 100$

In order to compare the differences between the signals acquired by textile electrodes and standard electrodes, we compared a list of physiologically sound parameters (Table 3-7). These parameters are widely used to characterize the heart rate variability which reflects more fine-grained information about the dynamics of heart activity [179]. Five minutes of continuous ECG are taken as a segment of data, and the data collected for each type of electrode can be divided into 18 segments. Paired T-test is adopted to support our claim that no differences in substance exist between those parameters retrieved from signals acquired by these three kinds of electrodes.

2) Results

(a) Skin-to-electrode impedance

Figure 3-23 shows the Z-f curves. Those curves respectively characterize the skin-to-electrode interface of the proposed textile-based electrode and Ag/AgCl electrode (Covidien, H124SG). The frequency ranges from 0.1 Hz to 100 kHz. Test results suggest a decrease in the impedance introduced by the skin-to-electrode interface as the frequency of stimulus signal increases. Within the frequency range of most bio-potential signals, the smallest impedance (~ 500 Ohm in near dc range) is relevant to textile C-based electrodes. However, a slightly larger impedance also appears in correspondence to Ag/AgCl electrode, compared with that of textile C-based electrode about 575 k Ohm in near dc range. The differences of those outcomes are statistically significant with all data points larger than 0.95.

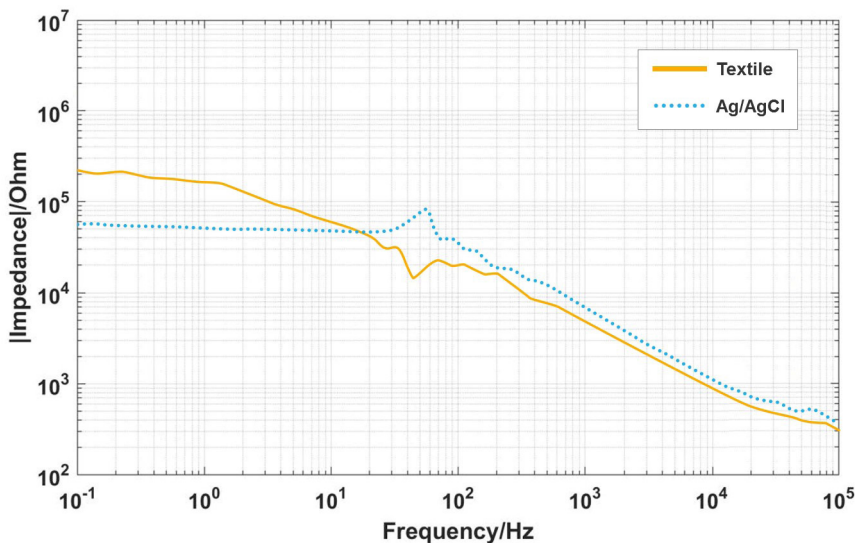


Fig. 3-23. Skin-electrode impedance of different electrodes

(b) Textile electrodes signal quality assessment

Correlation analysis results

We extracted heart rates and did a correlation analysis and Bland-Altman analysis. Figure 3-24 shows the results of the correlation analysis of the data from the utilized 90 epochs for Ag/Cl electrode versus textile-based electrode. The Pearson Correlation (r) of 0.92 demonstrates a strong relationship between textile-based electrodes and Ag/Cl electrode in monitoring HR.

Bland-Altman analysis results

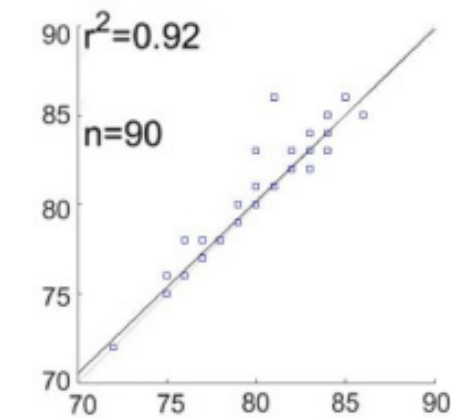


Fig. 3-24. Results of Correlation analysis

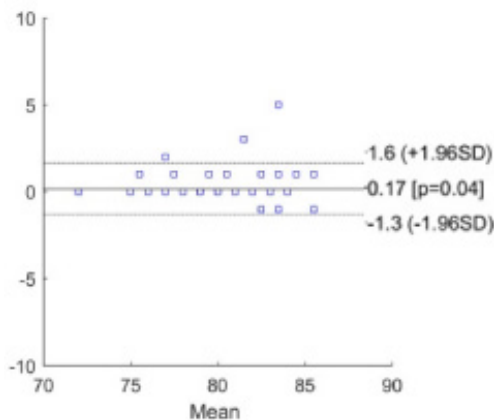


Fig.3-25. Results of Bland-Altman analysis

Figure 3-25 shows the results of the Bland-Altman analysis. It can be seen in Figure 3-25

that the 95% consistency limit is (1.6, -1.3); the 2% point is 95% beyond the consensus limit; the mean difference for average HR between M1 and M2 is less than 1 bpm, mean = -0.17. The results show that the textile electrodes have a good agreement with the standard Ag/AgCl electrodes, and the average value of the results is closest to zero.

Paired sample T-test results

The results are shown in Table 3-8 present that the significance values of each indicator of textile electrodes are all greater than 0.05.

Therefore, there are no differences between the indicators of the ECG signals collected by the textile electrodes and the standard electrodes.

Table 3-8. T-test results

Variable	Statistical significance
NN50(M1)- NN50(M2)	0.072
PNN50(M1)- PNN50(M2)	0.071
SDNN	0.460
RMSDD	0.306
SDSD	0.311
5 min total power	0.700
VLF(M1)- VLF(M2)	0.922
LF(M1)- LF(M2)	0.990
LF norm(M1)- LF norm(M2)	0.015
HF(M1)- HF(M2)	0.484
HF norm(M1)- HF norm(M2)	0.072

3.3.2.2. ECG Signal Collected by MSP

1) Method

(a) Comparison method of textile electrodes and AgCl electrodes based on MSP

After the experiment of electrode's electrical properties, the electrodes are evaluated to acquire ECG signals. An evaluation was operated on the performance of textile electrodes by the proposed system. The evaluation was a test on a 24-year-old male volunteer and a measurement of the ECG signals in different human body motion states. During the experiment, two electrodes were separately fixed on both sides of the ribcage of each test subject. These electrodes were placed in the same position in each measurement to ensure similar test conditions for later comparisons. After the preparation, we firstly measured

ECG signals in a state of sitting. Then the motion artifacts that result from walking and upper body turning of the subject's arms were investigated. The test time of each group is 2 minutes.

We use the three following indicators as the evaluation of signal quality factors which are the critical facts in further research. These indicators are shown below:

R-wave identification match degree

The R-wave belongs to the maximum point in the ECG, and the main characteristic of the QRS complex is the higher amplitude and scope value. In this paper, the R wave detection algorithm is implemented on MATLAB R2018a (MathWorks, U.S.A.) based on the classic QRS detection algorithm proposed by WJ Tompkins et al [180], [181]. A bandpass filter with a passband of 5-15Hz is used to preprocess the data and hamming window is applied for the function "fir1" in MATLAB. Then a dynamic threshold is determined every 5 seconds with 2500 values gathered from the system for the "findpeaks" function with the 'MinPeakDistance' index of 150 points which is 0.3 seconds in the time domain. After finding the peaks of a set of data, we define the R-wave matching degree $M(\omega)$ as

$$M(\omega) = \frac{N(\omega)}{N_A(\omega)} \quad (1)$$

whereby $N(\omega)$ is the number of R waves matched by the algorithm, and $N_A(\omega)$ is the number of R waves manually counted by experts.

We chose this specific preprocessing and R wave detection method to minimize the effect of the algorithm thus verifying the amplitude of ECG signals acquired by different types of electrodes under the same movement.

ECG signal power spectrum ratio

According to Donald et al. and others [30, 31], the QRS complex mainly concentrates in the 2~20Hz, with powerline in 50 or 60Hz and the baseline drift in 0.15~0.3Hz [184]. The main energy of the QRS wave concentrates at 12Hz [185], and the ECG signal is subject to motion artifacts and EMG interference between 3~30Hz [27]. So in this paper, the ratio of ECG signal power density between 5~15Hz and 3~30Hz is calculated to estimate the state of motion ECG signal quality.

$$S(\omega) = \frac{\int_5^{15} P(f)df}{\int_3^{30} P(f)df} \quad (2)$$

$P(f)$ denotes the power spectrum of ECG signal.

Signal kurtosis value

ECG signals are collected as discrete signals. According to the central limit theorem, the kurtosis of the discrete signal reflects the Gaussian of the signal.

$$K = \frac{1}{M} \sum_{i=1}^M \left[\frac{x_i - \mu_x}{\sigma} \right]^4 \quad (3)$$

μ_x denotes the mean of the signal x_i , σ denotes the standard deviation of the signal, and M is the number of sampling points of the measured data segment. The corresponding level of the ECG signal quality evaluation is presented in table3-9.

Table 3-9. Signal quality factors

Signal quality factors	Good	Normal	Bad
R-wave matching degree (M)	$M \geq 0.8$	$0.8M \geq 0.6$	$0.6 > M$
Power Spectrum ratio (S)	$S \geq 0.5$	$0.5 > S \geq 0.4$	$0.4 > S$
Signal Kurtosis (K)	$K > 5$	$5 > K \geq 4.3$	$4.3 > K$

(b) Comparison method of the MSP with standard medical equipment

After obtaining experiment results about the textile electrodes proposed, we used PSG (Polysomnography) as the gold standard to compare the waveform in this experiment. We compared the ECG signals acquired by MSP with textile electrodes and PSG with AgCl electrodes. Altogether six electrodes were fixed on the volunteer simultaneously with an experiment time of five minutes.

(2)Results

(a) Comparison result of three types of electrodes based on proposed system

To analyze the electrode performance under motion artifacts, the measurements were performed in sitting state, upper body turning state and walking state.

Sitting state results

QRS wave group and T wave can be detected obviously under sitting state. The results of R-waves detection results are shown as Figure 3-26 and Table 3-10. The R-wave recognition rate is generally high, with a small difference between textile electrode and Ag/Cl electrodes. Power spectrum ratio and signal kurtosis values of 1000 points selected during the test time of two minutes are listed in Table 3-11 and 3-12. The S and K values of the textile-based electrodes and the Ag/AgCl electrodes were all in good level, but the S and K values of the former one were better than those of the latter.

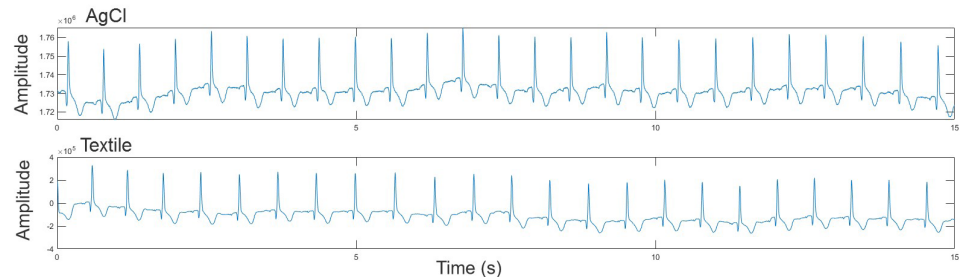


Fig. 3-26. ECG waveform under sitting state

Table 3-10. R-wave Recognition under sitting state

Type of electrode	AgCl	Textile
Missed	0	0
N (ω) Identified by algorithm	161	171
NA (ω)Detected by experts	161	171
R-wave matching degree (M)	1	1

Table 3-11. Power spectrum of ECG under walking state

Type of electrode	AgCl	Textile
Power Spectrum ratio (S)	0.7407	0.7709

Table 3-12. Signal quality under walking state

Type of electrode	AgCl	Textile
Signal Kurtosis(K)	10.3668	11.2188

Upper body turning state results

Detection data of QRS wave and T wave is displayed in Table 3-13 and Figure 3-27. Power spectrum ratio and signal kurtosis values during the sitting state are listed in Table 3-14 and 3-15.

Compared with sitting state, ECG signal is more prone to drift in upper body turning state. According to the signal quality factors in Table 3-9, the results showed that the values of K, S and M of the AgCl electrode and the textile-based electrode were all at a good level.

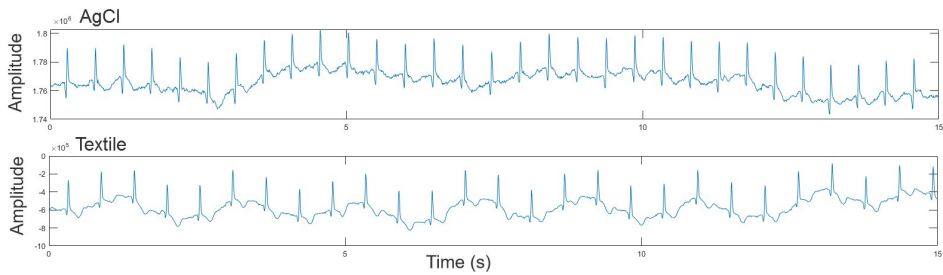


Fig. 3-27. ECG waveform under turning state

Table 3-13. R-wave Recognition under turning state

Type of electrode	AgCl	Textile
Missed	0	0
N (ω) Identified by algorithm	0	0
NA (ω)Detected by experts	201	181
Detected	201	181
R-wave matching degree (M)	1	1

Table 3-14. Power spectrum of ECG under turning state

Type of electrode	AgCl	Textile
Power Spectrum ratio (S)	0.8481	0.7039

Table 3-15. Signal quality under turning state

Type of electrode	AgCl	Textile
Signal Kurtosis (K)	8.2667	7.4293

Walking state results

Table 3-16 and Figure 3-28 show the ECG waveforms collected from different electrodes under the walking state. Power spectrum ratio and signal kurtosis values are listed in Table 3-17 and 3-18. Like the upper body turning state, the ECG signal is prone to drift in the walking state. In the state of walking, the M value of textile-based electrode is the largest. The K and S values of the textile-based electrodes were not as good as those of the AgCl electrodes. However, the K and M value of textile-based electrode reached a good level.

Three indexes of R-wave recognition, power spectrum ratio, and signal kurtosis value are used to make a comprehensive evaluation of electrodes under each state. According to these indexes, the performance of textile-based electrodes is similar to that of the AgCl electrode.

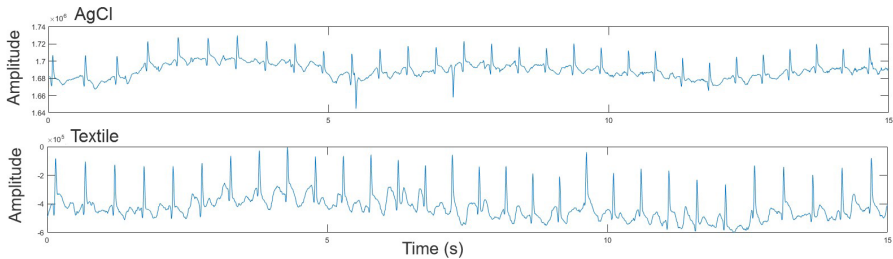


Fig. 3-28. ECG waveform under walking state

Table 3-16. R-wave Recognition under walking state

Type of electrode	AgCl	Textile
Missed	3	1
False alarm	0	0
N (ω) Identified by algorithm	205	202
NA (ω)Detected by experts	208	203
R-wave matching degree (M)	0.986	0.995

Table 3-17. Power spectrum of ECG under walking state

Type of electrode	AgCl	Textile
Power Spectrum ratio (S)	0.6386	0.4119

Table 3-18. Signal quality under walking state

Type of electrode	AgCl	Textile
Signal Kurtosis (K)	9.1456	7.1517

(b)Comparison results of the MSP with standard medical equipment

ECG waveforms acquired by the MSP and PSG under static state are given in Figure 3-29. We can see that the smart vest can acquire ECG signals of comparable signal quality with respect to PSG.

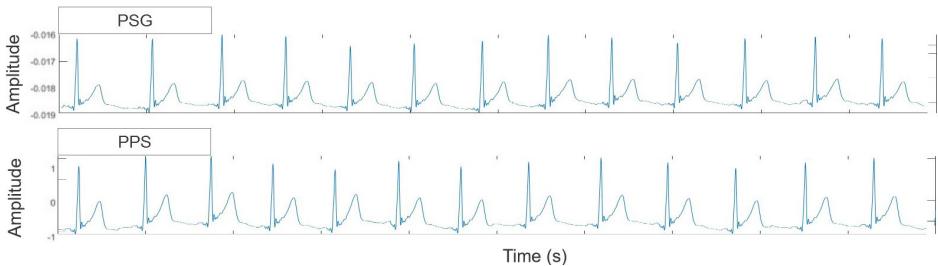


Fig. 3-29. ECG signal collected by proposed system and PSG

3.3.3. Movement Signal Verification

1) Method for motion signal collected by proposed system

Experiments on adults were carried out to validate the motion analysis part of our system. The prototype and Shimmer 3 were attached to the left wrist as is shown in Figure 3-30 a. A standard protocol was followed, where different types of movements, including boxing, arm swing, arm tremble etc.

2) Results

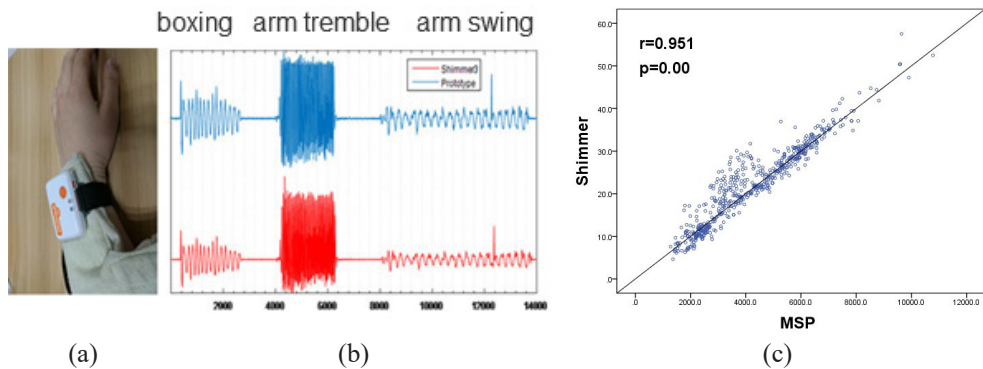


Fig.3-30. (a) Motion signal experimental setup; (b) Motion signal waveforms; (c) Results of Correlation analysis

Figure 3-30 b shows the comparison of the mean square values of 3-axis accelerations, demonstrating that the IMU data measured by the prototype has the comparable data quality of the commercial shimmer device. Figure 3-30 c shows the correlation analysis for the readings obtained from the MSP. The vertical axis represents the reference reading given by Shimmer 3, and the horizontal axis represents the values provided by the MSP for the corresponding time segments. The MSP was found to have a pearson correlation(r) of 0.951 with the reference values.

3.3.4. Respiration Signal Verification

3.3.4.1. PDMS-G Compound Properties

The method of obtaining the abdominal respiration signal by stretching the sensor mainly involves resistance change caused by the stretching of this material. Therefore, we tested the sensitivity and cycle stability of PDMS-G compound. The resistance of this sample

sensor at first was approximately 85k Ω with the original length of about 35cm and rose to 320k Ω correspondingly after it was stretched to 42cm length. In order to test the properties of materials, we set up the following two experiments.

(a) Sensitivity test of tension sensor

In this experiment, the Inductance Capacitance Resistance (LCR) meter (E4980AL, Keysight) was used to measure the change of sensor resistance at different lengths accurately. One end of the sensor was fixed and the sensor was stretched to change the length. The lengths of the sensor with its resistance were recorded correspondingly. The deformation range was 0-50% (8cm-12cm) with a step length of 5% (4mm) for each recorded point. The resistance value and the sensitivity of the sensor were studied in this experiment. The sensitivity of the tensile sensor was defined as

$$S = \frac{\delta \left(\frac{R - R_0}{R_0} \right)}{\delta (L - L_0)}$$

where, R was the resistance of the material at the time of strain, R₀ was the initial resistance of the material without strain, L was the length of the material at the time of strain and L₀ was the initial length of the material. The resistance showed the electrical property of the sensor under different lengths and sensitivity was investigated to demonstrate the stretching capability.

Figure 3-31 showed the relative change in resistance for various elongation values. No linear behavior of the sensor was found, but three different areas of the sensitivity were identified. In the first area, the length of the sensor was from 8cm to 10.4cm, as a result, the sensitivity (S) was 4.67cm⁻¹. In the second area, elongation of the sensor was from 10.4cm to 11.6 range, as a result, the S value was 61.15cm⁻¹, and the third area showed a further increase of the S value to 152.68cm⁻¹ when the sensor was fully stretched to 12cm. In the strain range of 30% to 50%, the material has better sensitivity. In fact, this is the strain range when the elastic band is connected to the body.

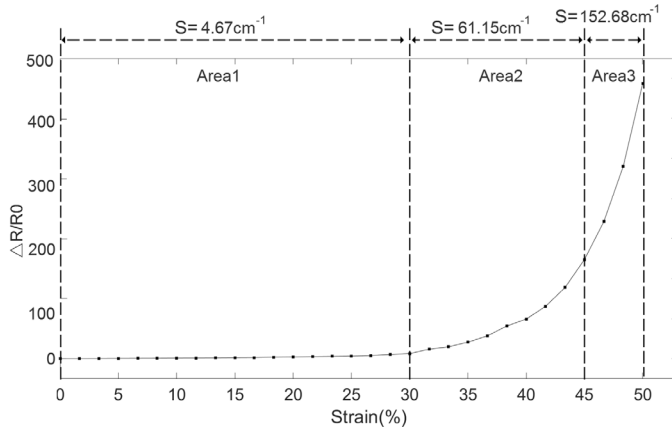


Fig. 3-31. Relative change in resistance of PDMS-G compound tensile sensor versus strain within strain range of 0-50%.

(b) The loop stability performance of the tension sensor

This section demonstrates the process and results to verify the resistance change of the new sensor after repeated stretching. The stepper motor (FLS 40, Chengdu Fuyu Technology Co., Ltd) was used to conduct the cyclic stability experiment. The length of the sensor was set from 10cm to 11.5cm with a frequency of 20 cycles per minute, which was similar to the normal respiratory situation. The duration of the cyclic stability test was 3 hours. The 10-bit ADC on Arduino (Arduino Uno) was used to acquire the resistance change during the 3-hour's experiment at a sampling rate of 100Hz. Since the respiratory rate of the neonate was between 20 and 40 breaths per minute, the 100Hz sampling rate ensured the signal not be distorted.

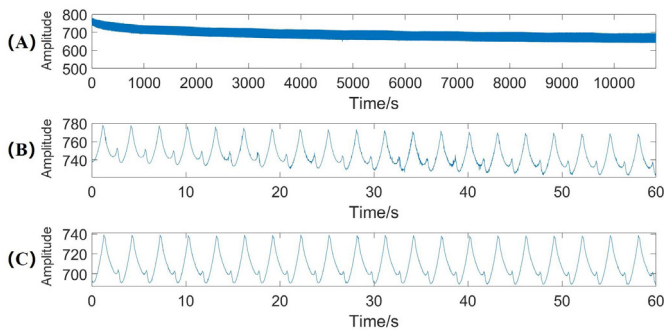


Fig. 3-32. Results of the three hours' stability test (A) overall resistance variation in 3 hours, (B) detailed waveform in the first 1 minute of the whole test, (C) detailed waveform in the last 1 minute of the whole test

Figure 3-32 A showed the 3-hour stability test results. Figure 3-32 B and Figure 3-32 C showed the portions of the results during the first and last 1 minute correspondingly. From these diagrams, the sensor proved to have the advantage of stability. After 3,600 cycles of 3 consecutive hours, the response signal barely changed. At the beginning of the test, the decline of the baseline didn't affect respiration monitoring. According to the experimental results, the sensor based on the PDMS-G compound tensile sensor had a stable signal output under the condition of continuous stretching for three hours.

(c) Response/relaxation time of the sensor

In this experiment, Arduino was also used to test the response/relaxation time of the sensor. The real-time change of the voltage when the resistance of the sensor changes was recorded. The strain range of the sensor was fixed at 0-40%. In the process of strain, the time spent by the voltage jumping from the first stable state to the second stable state was considered to be the response/relaxation time of the sensor.

The result of response time experiment was given in Figure 3-33. The response time of the sensor was 308 ms in tension and 372 ms in relaxation. The above response satisfies the scenario of the respiration rate measurement.

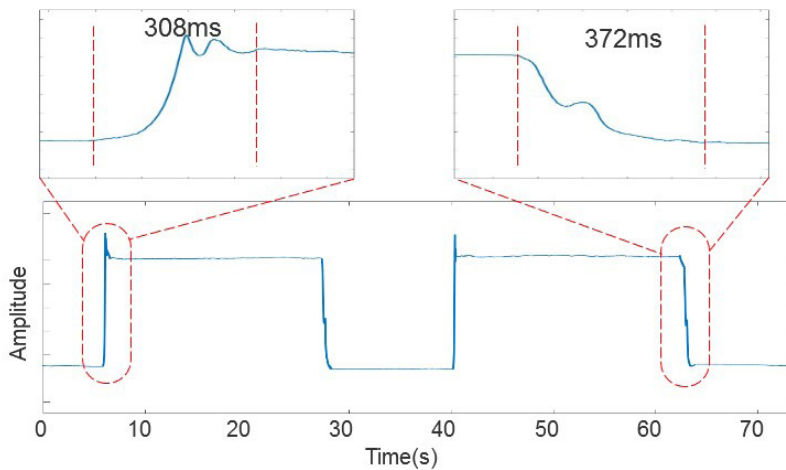


Fig. 3-33. Response/relaxation time test of the sensor

(d) Stress test of the sensor

In order to prevent the excessive pressure of the respiratory bandage on the subject from affecting the respiration, a sensor stress test was conducted. The RIP module in the medical level multi-parameter device-polysomnography (PSG) was compared with the new sensor.

The purpose of the test was to ensure that within the same strain pressure generated by the PDMS-G was less than that generated by the RIP module in PSG. The test used the electronic universal testing machine (RGWT6000, SHENZHEN REGER INSTRUMENT). The stress curves of new sensor and RIP module in PSG were compared, as shown in Figure 3-34. The stress of PDMS-G was much smaller than that of the RIP module in PSG at the same tensile ratio. Therefore, PDMS-G in MSP for respiration monitoring was more comfortable than RIP module in PSG, especially for neonates.

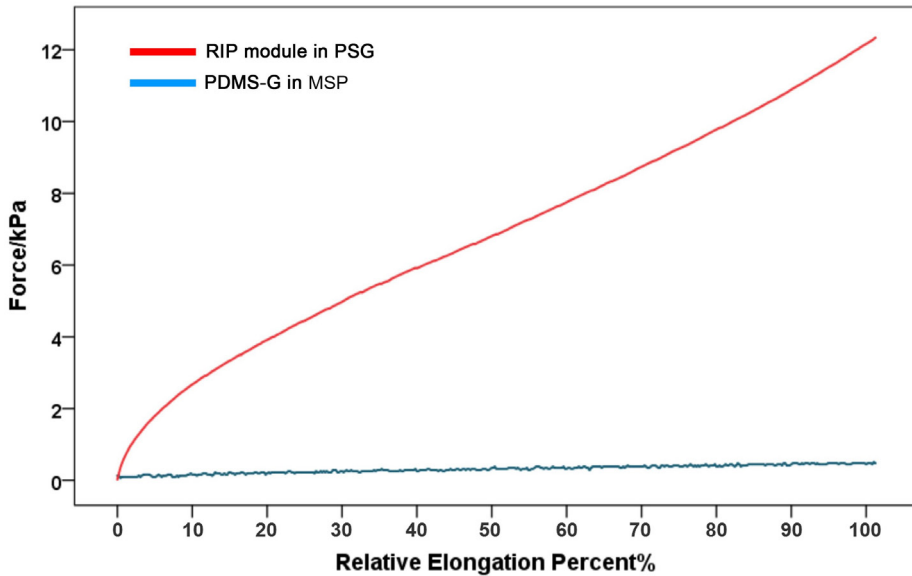


Fig. 3-34. Stress curves of RIP module in PSG and PDMS-G in MSP

3.3.4.2. Respiration Signal Collected by MSP

1) Method

Firstly, to assess the basic monitoring performance of MSP, the system performance of respiration monitoring function under different frequencies was verified. we compared our system with the RIP module as part of the PSG apparatus. Unlike the proposed MSP, the respiratory band used in PSG was based on inductance change formed by the coil inside the band. The data from PSG were gathered through the PSG software (Greal-PAG Oline 3). The stepper monitor used in this test was the same as the cyclic stability performance experiment. The frequency range was set from 60 cycles per minute to 20 cycles per minute, which covered the range of neonatal respiratory rate [15], [16]. There were 21 groups in this

frequency range. In each group, the waveform of the proposed sensor with the RIP module in PSG was compared. A digital bandpass filter with a passband of 0.01Hz to 5Hz was implemented for the sensor data on MATLAB 2018b (MathWorks).

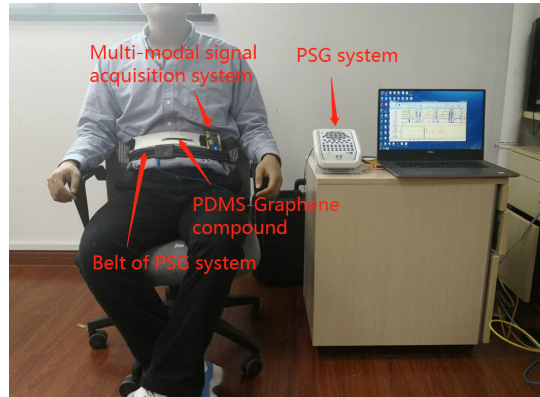


Fig. 3-35. Respiratory signal experimental setup;

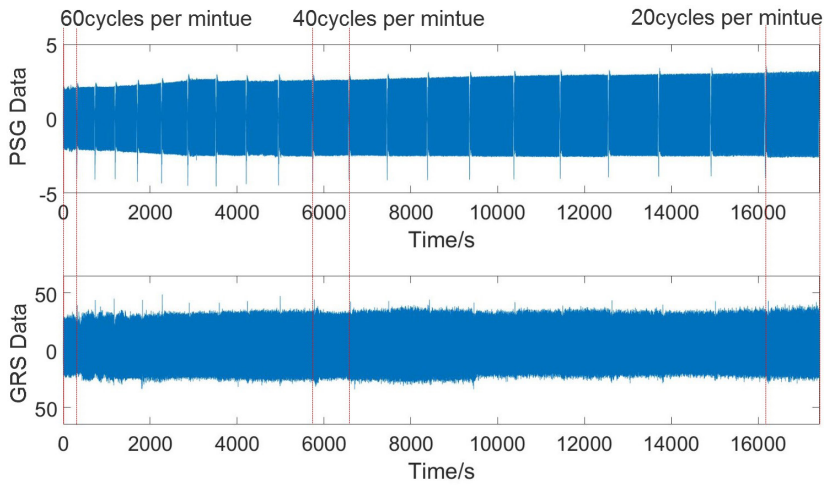
Secondly, we collected adult respiratory signals based on MSP and PSG for comparison. Both systems were installed on the subject for simultaneous recording of respiration. As shown in Figure 3-35, PSG respiratory detection band is attached to the abdomen, and PDMS-G tensile sensor is attached lower than PSG band. PSG has a respiration sampling frequency of 32Hz. The following three aspects are used for analysis and comparison.

1. We compare the respiration signals of adult acquired by the MSP and PSG to perform a visual comparison. We compare the similarity of the original waveform output of the MSP and the PSG.
2. Mean difference in average RR between propose system and PSG was studied in the second outcome measure. Each RR point was output for a 30 second interval. The correlation analysis between the respiratory rates measured for MSP and PSG was also conducted. Values from mean, standard deviation, median and range helped us generalize the differences in average RR between monitoring techniques over the 30 second interval. The 95 % confidence intervals enabled us to determine the effectiveness of the MSP monitor versus PSG-derived RR for the mean difference in average RR between techniques. The difference of three breaths per minute (bpm) denotes the minimum clinical relevance chosen from the early warning system (EWS). The system identifies meaningful 3 bmp in score difference through a definition where the respiration scores in steps are no greater than 3 bpm.

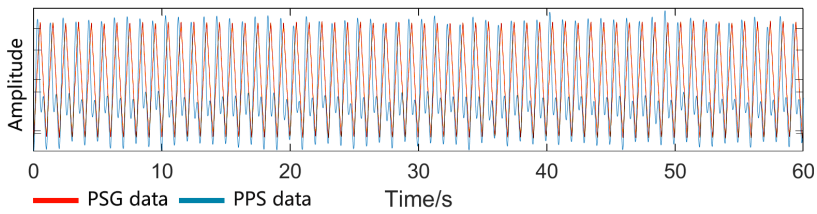
3. We performed an individual's Bland-Altman analysis in the third analysis to assess the direct relationship or correlation between the respiratory rates measured by the MSP device and each measuring technique involved. Given a correlation coefficient (r) up to greater than 0.8, we could view MSP as effectiveness in detecting changes in RR comparable to PSG. Moreover, as a higher correlation is possible to present due to the continuous nature of both MSP and PSG-derived monitoring, we set the expected correlation with PSG-derived RR of 0.8. Bland-Altman analysis was used to present the results graphically.

2) Results

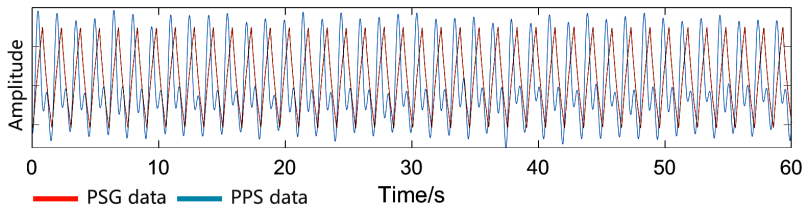
Firstly, Figure 3-36-A showed the overall waveform. Figure 3-36-B, Figure 3-36-C and Figure 3-36-D showed the portions of the results with 60, 40 and 20 cycles per minute correspondingly. From this experiment, the proposed system had a stable performance under different frequencies.



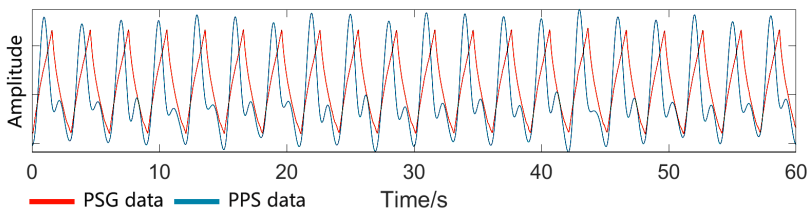
(A) Overall



(B)60cycles per minute



(C)40cycles per minute



(D)20cycles per minute

Fig. 3-36. Performance of the proposed system under different frequency compared with PSG (A) overall waveform, (B) detailed waveform with 60 cycles per minute, (C) detailed waveform with 40 cycles per minute, (D) detailed waveform with 20 cycles per minute

4. Secondly, the respiration signal of adult was carried out on a 30-year-old male volunteer for 4 hours. The subjects sat in a chair without strenuous exercise, during the trial. Firstly, we compare the signal quality in time domain, as show in Figure 3-37. From Figure 3-37, we see that the signals obtained using the MSP show the similar beat structure of the same frequency with those of the PSG. Though the attaching positions of the MSP and the PSG are a little different from each other in the abdomen region, the overall similarity of the data obtained during the inspiratory intervals can be noted implying the accuracy of the MSP in measuring the breathing rate.

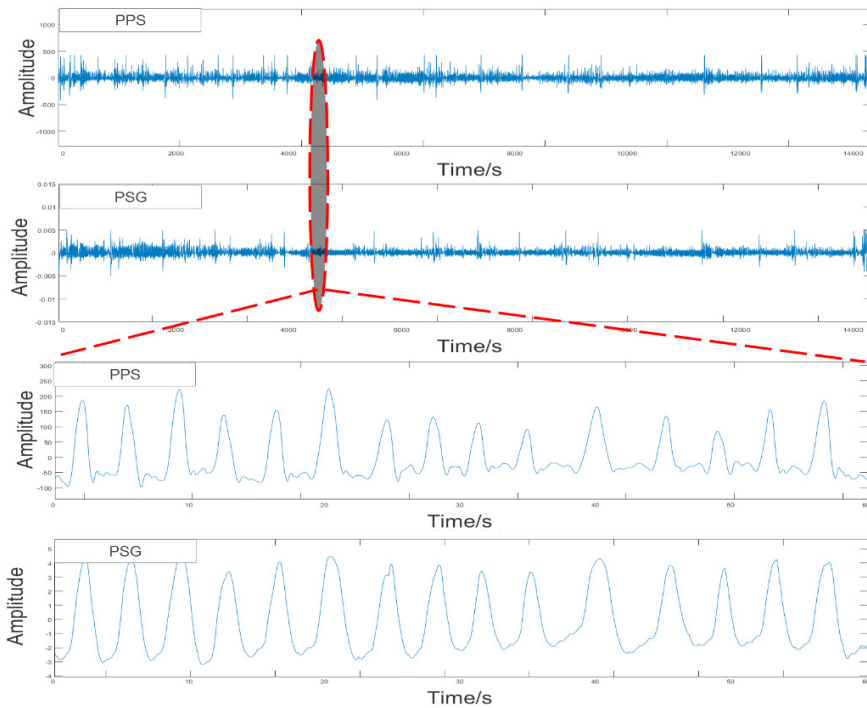


Fig. 3-37. Respiration signals measured by MSP and PSG.

5. From the total 160 records, an interval of one minute was adopted between RR points to ensure the independence of variables in Bland–Altman analysis. Of them, 154 time points were available engaged in the analysis. The PSG wire fell off when the subject left the chair to rest. Six time points were thus lost. Table 3-19 presents comparisons between the MSP and PSG-derived RR. Figure 3-38-a summarizes the data from the utilized 154 epochs for PSG versus MSP in the form of a Bland–Altman plot. The direction of difference is: (MSP–PSG). The red dashed line is a marker indicating the bias of the differences. The solid lines represent the 95% confidence limits for the differences. The

average RR between MSP and PSG is showed with a mean difference less than one bpm, where the mean (SD) = -0.15 (0.86). The 95 % confidence interval (CI) for the difference in average RR is calculated to be [-1.84, 1.55], which does not exclude the clinically relevant difference of 3 bpm. However, there was an exception. When only two intervals (1.3% of intervals) were presented, the difference was greater than three bpm. Figure 3-38-b reports the results of correlation analysis on the data harvested from the 154 epochs used for PSG versus MSP. The Pearson Correlation (r) of 0.977 demonstrates a very strong relationship between MSP and PSG in monitoring RR.

Table 3-19. Comparison of average respiratory rate in breaths per minute between MSP and PSG

MSP-PSG	
Number of data points	154
Mean	-0.15
Standard deviation	0.86
Minimum–maximum	-4.26,3.10
95 % confidence interval	-1.84,1.55

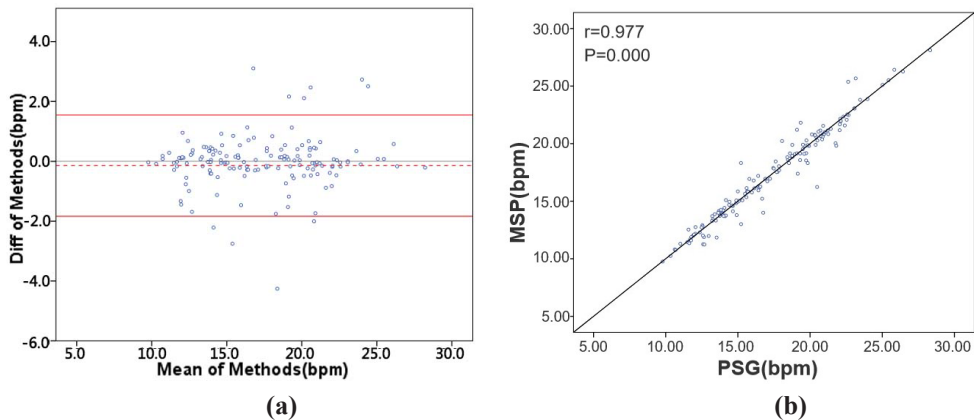


Fig. 3-38. (a) Bland-Altman plot showing MSP versus PSG. Direction of difference is (MSP-PSG); (b)Results of Correlation analysis

3.3.5. Clinical Test in Neonates

1) Method

After the performance tests on adults, permission was obtained from the Children's Hospital affiliated to Fudan University Research Ethics Committee (approval No. (2017) 89) to recruit infant patients for multi signal monitoring. Inclusion criteria were as follows: (1) age

under 60 days;(2) in stable health conditions;(3) about to discharge from neonatal intensive care unit (NICU). Exclusion criteria were as follows: (1) with diagnosed respiratory disorders history;(2) allergy to medical grade skin adhesive or latex.

15 patients, seven males and eight females, who did not violate our exclusion criteria were enrolled in the experiments. The mean age of the subjects was 36 days (median 33, standard deviation 12.5, range 18-59). The average data collection time per subject was 10 min. No adverse respiratory events and skin allergy occurred during the test. The subjects lie in an incubator, keeping awake during the trial.

We compared our system with the PSG, when both systems were attached on the subject for simultaneous recording of ECG and respiration, as show in Figure 3-39. Data analysis methods including visual comparison, and accuracy analysis.



Fig.3-39. Clinical experimental setup

2) Result

First, we compared the ECG and respiration signal quality in time domain. ECG waveforms acquired by PSG and MSP were given in Figure 3-40. The figure shows that the proposed electrode can acquire ECG signals of comparable signal quality and amplitude (thus, also average power) with respect to PSG. The respiration signal quality in time domain was compared also, as shown in Figure 3-41. As shown in Figure 3-41, the signal with the same beat frequency structure can be obtained by using MSP and PSG. Although MSP and PSG have slightly different attachment locations in the abdominal region, the overall similarity of the data obtained during the inspiratory interval can be noted.

The second outcome measurement for the study was correlation in average heart rate (HR)

and average respiratory rate (RR) between the proposed system and PSG. A total of 150 HR data point and 150 RR data point, Each HR and RR point was output for a 60 second interval. Figure 3-42-a shows the correlation analysis for the HR obtained from the clinical study. Vertical axis represents the reference reading given by the PSG and the horizontal axis represents the results given by the MSP for the corresponding time segments. The value of Pearson correlation(r) between PSG and PPG in HR monitoring was 0.967. Figure 3-42-b shows the correlation analysis for the RR obtained from the clinical study. Vertical axis represents the reference reading given by the PSG and the horizontal axis represents the results given by the MSP for the corresponding time segments. The value of Pearson correlation(r) between PSG and PPG in RR monitoring was 0.969. The r value of HR and RR demonstrate a very strong relationship between MSP and PSG in monitoring HR and RR.

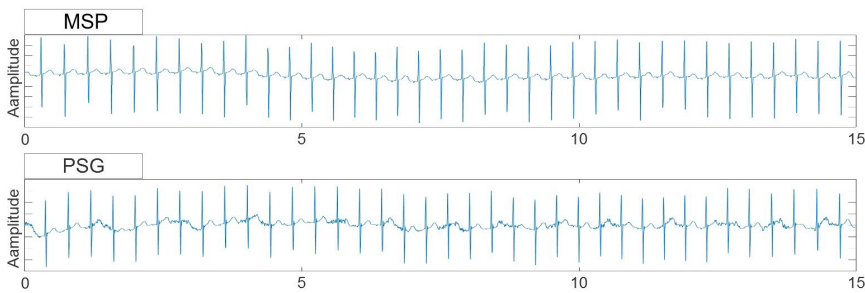


Fig. 3-40. Clinical ECG data measured by MSP and PSG

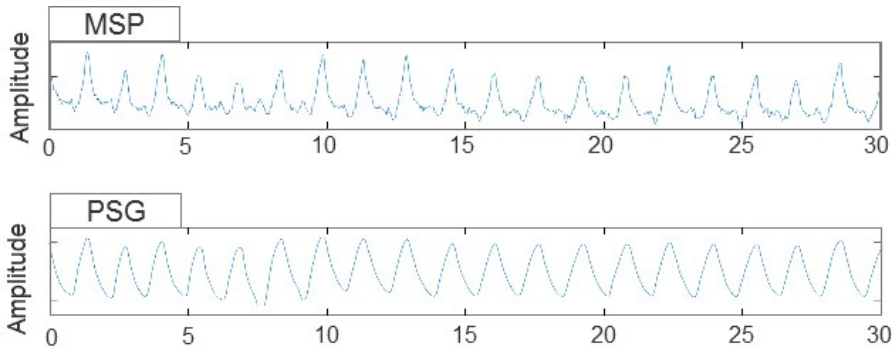


Fig. 3-41. Clinical respiration data measured by MSP and PSG

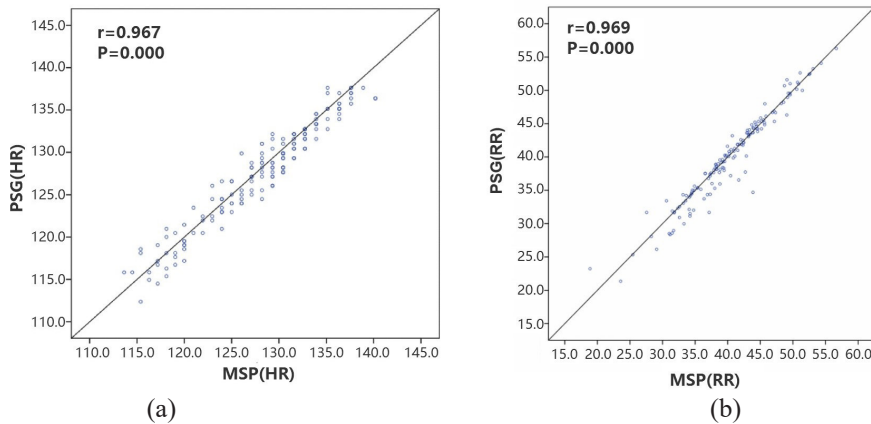


Fig. 3-42. (a) Correlation regression analysis for the results obtained from the heart rate clinical data collection exercise; (b) Correlation regression analysis for the results obtained from the respiration rate clinical data collection exercise

3.4. Neonatal Seizure Detection

In order to verify the clinical feasibility of multi-sensor platform for neonatal seizure detection, permission was obtained from the Research Ethics Committee of Children's Hospital of Fudan University (approval No. (2017) 89) to recruit infant patients for neonatal seizure detection. The whole research of neonatal seizure detection includes three parts, namely data collection, data analysis strategy, data analysis results.

3.4.1. Clinical Data Collection

The VEEG acquisition system (niocolet) in the hospital and the multi-sensor platform (MSP) were used for data acquisition at the same time. EEG signal and video information of neonate were collected by the VEEG acquisition system, while ECG signal, respiration signal, and motion signal were collected by the proposed multi-modal wearable sensor system (MSP). The EEG signal and video were used as the gold standard of neonatal seizure detection.

The recruitment criteria for patients covering inclusion criteria, exclusion criteria and stop criteria and details are as follows.

Inclusion criteria include: (1) Age less than 60 days; (2) Patients who have had a seizure in the clinic; (3) No anticonvulsant treatment before admission;

Exclusion criteria include: (1) Patients with diagnosed respiratory disorder history; (2) A history allergy to medical-grade skin adhesive or latex. (3) Patients with life-threatening diseases such as shock, cerebral infarction, and severe congenital malformations.

Stop criteria include: (1) The subjects' continuous worsen condition and even dangerous events during the study; (2) The subjects' some inappropriate changes in comorbidities, complications or special psychology; (3) Subjects with adverse events.



Fig. 3-43. The environment of neonatal seizure data collection

Neonatal seizures appear suddenly, thus requiring long-term monitoring. Wearing the EEG cap of the EEG collection system for long-term monitoring will damage the neonatal skin, so the time of collecting data is only about 4 hours one time. A 24-hour interval was required between the first and the second acquisition experiment of the same subject. The experimental setup for data acquisition is shown in Figure 3-43. The EEG cap is worn on the neonatal head to collect EEG signals. The camera is placed on the top of the incubator to collect the video information. The smart vest is worn on the neonate, with the flexible electrode placed on the chest to collect ECG signals, the IMU at the wrist to collect body motion signals, and the respiration sensor on the abdomen to collect respiration signals. The sampling rate of EEG acquisition system is 500 Hz, and that of multi-sensor platform is 250 Hz. During the experiment, the data received by the multi-sensor platform are stored in the laptop and processed on the desktop with MATLAB R2019a (MathWorks Inc., Natick, MA,

USA). EEG signals and video information are sent to the data storage center of the hospital and analyzed by medical experts to judge the neonatal seizure occurrence. During each trial, the following measurements were obtained by the principal investigator:

1. Subject age, gender.
2. The start time and end time of the neonatal seizure. The timing of the seizures was determined by hospital experts through video and EEG analysis.
- 3 Attending NICU nurse rating of ease of device use, using 11point VRS (0 = least difficulty imaginable to use, 10 = most difficulty imaginable to use)

The following measurements were recorded electronically:

- ECG signal, respiration signal, motion signal, collected by the MSP prototype, recorded on Dell Laptop.
- EEG signal, collected by EEG acquisition system, record on local data platform of the hospital.

38 patients, 23 male and 15 females, who had already experienced seizure at the hospital and who did not violate exclusion criteria were enrolled in the trial. The average age of subjects was 36.8 days (median 37, standard deviation 8.3, range 20–57). Since the interval between multiple records of a subject was more than 24 hours, the mean age of subjects was calculated based on the time of each record. The mean time spent by the subjects for one experiment was 228.8 min (median 240, standard deviation 36.8, range 78–292). No patients suffered an adverse respiratory event or skin irritation during the trial. In terms of comfort, 12 nursing staff (100 %) rated the multi-sensor platform as 10 on a VRS for the ease of use (application of device only).

During the test, seizures were finally detected on four patients, with 30 seizures occurring in total. Most of the patients did not detect seizure for several reasons. For example, the early diagnosis is wrong, and the patient does not have the problem of brain nerve damage, so the EEG detected is normal. It may also be because the detection time is limited, within 4 hours did not appear seizure symptoms. Seizures were labeled by an experienced neurologist reviewing video-EEG recordings and annotating the onset and offset of the manifestation of the seizures. Table 3-20 gives a broad overview of the patients with seizures.

Table 3-20. Overview of the patients with seizures

No.	Sex	Average age	Records	Record duration per time	Seizures
1	male	36	1	236min	1
2	male	41	1	132 min	1
3	female	30	6	249 min, 230 min , 232 min , 78 min , 191 min , 244min	24
4	male	34	2	98 min ,231 min	4

3.4.2. Data Processing

These data from Table 3-20 were used to develop the classification algorithms. Full recordings were included in the analysis regardless of the record length, record quality and the child's awake or asleep state. A non-overlapping sliding window of 5-minute length was applied to ECG, acceleration and respiratory recordings to divide the data into epochs. The data were then preprocessed to remove the artifacts and reduce the data for further processing.

For ECG recordings, ECG is processed for R wave detection and HRV spectrum analyses. Many interfering signals can affect the ECG signal, such as the 50 Hz power line interference, the interferences from EMG signals, and the baseline wandering. Therefore, in the preprocessing stage, these interfering noises are eliminated first by means of a 5–15 Hz band pass filter. Next, in order to detect R waves of the ECG, the Hamilton and Tompkins algorithm (Pan and Tompkins 1985, Hamilton and Tompkins 1986) is employed [180], [181] The RR-interval signal is then constructed by measuring the time intervals between the successive R peaks. A heart rate variability spectrum is calculated with a serial FFT (Fast Fourier Transform) using a Hanning window.

For respiratory recordings, acceleration data is processed for extracting breathing rate. First, to remove noise and signal drift, the signal from y axis of the segment is left-right padded and mean-smoothed by a 25-ms window. Global linear drift is removed by subtracting the slope of the linear regression model of the data. Local signal drifts are corrected to continuous, minute-long sliding mean baseline windows, and padding is removed. Next, in order to extract breathing rate, we estimated the onset of inhales and exhales by performing zero-crossing point detection algorithm. According to respiratory flow, the upward and

downward zero-cross points are recognized as the onset of inhales and exhales, respectively. For movement recordings, acceleration data from each axis were low-pass filtered with 47 Hz as cutoff frequency in order to remove the powerline and high-frequency interference. After down sampling acceleration signals by a factor 2, a high-pass filter of 0.2-Hz cutoff frequency was applied to remove the baseline drifts [188].

Seizures typically last for 1-2 minutes whereas the patients were monitored continuously throughout their stay (days) in the hospital. As such, there is a vast amount of non-seizure data (forming the majority class), which causes the data set to be highly imbalanced. To decrease the computational workload as well as reduce the degree of data imbalance during supervised learning, we labeled the 5-minute signal after the onset of seizure as a seizure epoch, which contains seizure activity. The 25-minute signal before the onset of seizure and the 20-minute signal after the offset of seizure were labeled as non-seizure epochs. In cases where more than one seizure close to each other in 5 minutes, these seizures are regarded as one seizure to evaluate. Thus, we trim our dataset to balance the number of seizure and non-seizure epochs, where the ratio of seizure and non-seizure epochs for each patient is around 1:9.

3.4.3. Feature Extraction

A range of parameters have been used for neonatal seizure classification, describing ECG, respiration and movement modalities. Features extracted from ECG signals were found in the literature [189]–[191]. Features used in acceleration-based seizure detection [58] and respiration activity recognition [192] were also added to the list.

ECG feature:

10 features were computed to characterize each epoch, describing time and frequency characteristics of the ECG signals. There are mean RR, SDNN, SDSD, PNN50, SD1, SD2, CCM (Complex Correlation Measure), LF power, HF power and range of RR-interval signal.

Respiratory feature:

Breathing rate is calculated as the reciprocal of average time between inhale onsets.

Movement feature:

The major energy band for daily activities falls between 0.3 and 3.5 Hz whereas during seizures the power is typically concentrated at frequencies above 2 Hz [58], [193]. To capture the spectral information of the net acceleration, we computed the power spectral density with Welch's method. The integrated power within the spectral band of 0-2 Hz and

2-5 Hz are included as features. The total power within each epoch also was computed as a feature. Moreover, zero-crossing rate of the net acceleration was included for classification. To summarize, a total of 15 features were computed from each epoch constituting feature vectors, including 10 ECG features, 4 acceleration features and 1 respiratory feature. Each feature vector will be assigned to a seizure or non-seizure class by using a Support Vector Machine (SVM).

3.4.4. Classifier

Support Vector Machines (SVMs) are state-of-the-art binary classification methods that usually exhibit good resistance to overfitting and have shown excellent performance in complicated pattern recognition problems [194]–[196]. An SVM can learn a decision boundary in the form of a hyperplane that separates two classes. This hyperplane is selected such that the classification margin, which is the geometric distance between the hyperplane and the boundary cases of each class (i.e. the support vectors), is maximized [197], [198]. Moreover, SVMs can map the original finite dimensional feature space into a much higher dimensional space through the use of a kernel function to improve the separability of the data. We chose the Gaussian Radial Basis kernel function (RBF) as it provides non-linear mapping of the original feature vectors into a higher dimensional space. An SVM is a good choice for the task of seizure detection because its unique learning mechanism allows it to perform well with moderately imbalanced data without any modifications [199]. Since an SVM only takes into account those instances that are close to the boundary for building its model, it is unaffected by negative instances far away from the boundary even if they are large in number, which is important given that the number of non-seizure instances far outnumber the seizure instances.

3.4.5. Performance Evaluation

We implemented a patient-independent seizure detection algorithm that excluded all data from a test patient in the training phase (leave-one-patient-out cross-validation). To allow the SVM to learn from previous examples of seizures from the test patient if that patient had more than a single seizure recording available, we also implemented double leave-one-seizure-out cross-validation.

The performances of the developed seizure detectors were characterized in terms of sensitivity, specificity, accuracy, false alarm rate per hour, F-measure and AUC (Area Under

Curve). Sensitivity and specificity show the percentage of test seizures and test non-seizures respectively identified by the algorithm. Accuracy gives the overall classification accuracy. False alarm rate refers to the number of times, over the course of one hour, that the system declared the onset of seizure activity in the absence of an actual seizure. However, in learning imbalanced data, the overall classification accuracy is not an appropriate measure of performance since a trivial classifier that predicts every instance as the majority class (non-seizure) would achieve very high accuracy but be of little use. As such, we used the F-measure to evaluate the performance of the SVM.

To evaluate the utility of combining ECG, respiration and movement, we compared the performance of three seizure detectors. The first detector included features from both the ECG, respiration and acceleration recordings, the second incorporated respiratory-motion based features from respiration and acceleration recordings, and the third used ECG-based features from the ECG recordings solely.

3.4.6. Result

We respectively reported the evaluation results of neonatal seizure detection algorithm in the ECG based mode, respiratory based mode, and aggregated (full) mode (Table 3-21). Assessment indicators include sensitivity, specificity, accuracy, false alarm rate per hour, F-measure and AUC.

To visualize the performance of three neonatal seizure detection modes tested on data from the four patients with seizures, we performed receiver operating characteristic (ROC) curve analysis (Figure 3-44). The ROC curves depict the trade-off between sensitivity (percentage of recorded seizures that were identified by the detector) and false alarm rate as the decision threshold is varied.

The results show that the false alarm rate of the algorithm in the ECG based mode, is higher than that in respiratory based and multi-modal based modes, reaching 1.29 times/hour while its accuracy, specificity and AUC value are lower than those under respiratory based and aggregated (full) mode, 85.16%, 90% and 0.69 respectively. On the other hand, the specificity, accuracy and F-measure value of seizure detection algorithm are higher than those of aggregated (full) based and also aggregated (full) based modes, reaching 96.43%, 90.97% and 0.461. And the false alarm rate of the algorithm under this mode is the lowest, only 0.46 times per hour. Overall, the seizure detection algorithm based on aggregated (full) mode improved the performance.

Table 3-21. Results of neonatal seizure detection algorithm in the ECG based mode, respiratory based mode, and aggregated (full) mode

Detector based on	Sensitivity	Specificity	Accuracy	False alarm rate	F-measure	AUC
ECG+ acceleration +Respiration	40%	96.43%	90.97%	0.46 per hour	0.461538	0.77
ECG	40%	90%	85.16%	1.29 per hour	0.342857	0.69
acceleration +Respiration	30%	92.86%	86.77%	0.92per hour	0.305085	0.77

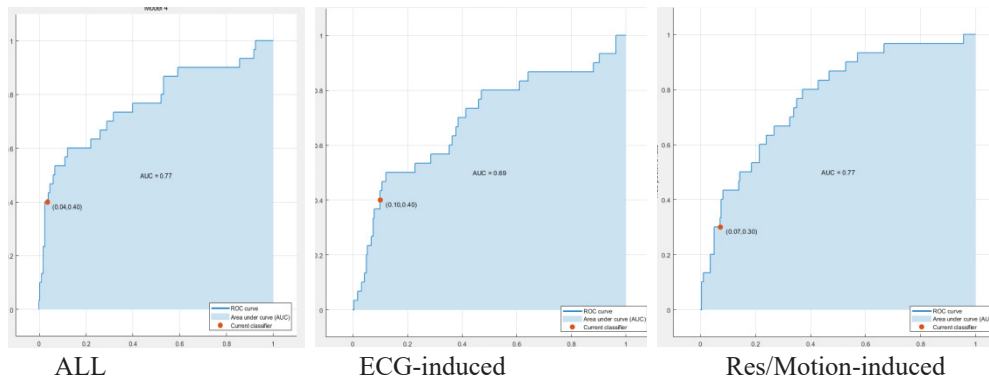


Fig. 3-44. Receiver operating characteristic (ROC) curve analysis from three seizure detectors.

3.5. Discussion

We propose a smart vest as a multi-sensing platform embedded with flexible material based non-invasive sensors for neonatal seizure monitoring. We carried out systematic verification about the platform which includes electrical properties of the new sensing materials, signal quality evaluation and comparison with gold standard to verify the feasibility of the system. Verification experiments prove that quality ECG signals can be obtained through the proposed flexible electrode materials with comparable performance to the commercial AgCl adhesive electrodes, accurate respiration data can be obtained through a new PDMS-Graphene compound based stretching sensor and movement signal of wrist can be obtained based on IMU sensor.

In addition, we developed an algorithm for automatic detection of neonatal seizures based on ECG, respiration and acceleration. The algorithmic evaluation of the records of 4 patients with seizures were performed. To evaluate the utility of combining ECG, respiration and movement, we compared the performance of three seizure detectors. The first detector included features from both the ECG, respiration and acceleration recordings, the second incorporated respiratory-motion based features from respiration and acceleration recordings, and the third used ECG-based features from only the ECG recordings.

Our study illustrates the overall performance was better when multi-modal features were included, reducing false alarm rate and achieving higher F-measure compared to the detector utilizing individual modal features. However, the results show that the sensitivity of non-EEG based method is low. The reason for low sensitivity may be small sample size under representation. In addition, poor data quality, unknown seizure types (some are asymptomatic without abnormalities in respiration, electrocardiography, motor activity, etc.), and rebalancing approaches may result in deviation in results and limitation in interpretation.

For future work, we will further improve the structure and electronic properties of the innovative materials to enhance the stability of the measured signal, especially during motion. Furthermore, we will conduct more clinical trials to verify the performance of the wearable platform for neonatal seizure detection. Data fusion techniques and optimization algorithms will be explored with the help of clinical data.

4

Exploration of New sensors for Physiological Parameter Measurement

This chapter is based on:

1 **Chen H**, Zhao Y, Mei Z, et al. Characterization of a novel carbonized foam electrode for wearable bio-potential recording[C]//2018 IEEE 15th International Conference on Wearable and Implantable Body Sensor Networks (BSN). IEEE, 2018: 173-176.

2 **Hongyu Chen**, Shenjie Bao, Jianhua Ma, et al. A Wearable Daily Respiration Monitoring System Using PDMS-graphene Compound Tensile Sensor for Adult” 2019IEEE 41th International Conference on Engineering in Medicine and Biology(EMBC)

3. Ma, J., Wang, P., **Chen, H.**, Bao, S., Chen, W., & Lu, H. (2019). Highly sensitive and large-range strain sensor with a self-compensated two-order structure for human motion detection. ACS applied materials & interfaces, 11(8), 8527-8536.

4. Chen C, Wang Z, Li W, et al. Novel flexible material-based unobtrusive and wearable body sensor networks for vital sign monitoring[J]. IEEE Sensors Journal, 2018, 19(19): 8502-8513.

In chapter 3, we propose a smart vest as a multi-sensing platform and developed an algorithm for automatic detection of neonatal seizures based on ECG, respiration and accelerometry. In addition, the study illustrates how a seizure detector that combines information from both ECG, respiration and accelerometry recordings can perform better than a detector that relies on one signal. In order to improve the comfort of the system and the stability of the signal, we further study the sensors with different signals. Firstly, we compare the influence of electrodes made of different intelligent textile on the quality of ECG signal. Secondly, a novel dry disposable electrode made of carbonized foam was presented. We tested the electrical properties and feasibility as an electrocardiogram electrode. Finally, we explored the mesh graphene-based sensor for respiration monitoring. The basic properties of mesh PDMS-G (M-PDMS-G) and PDMS-G were compared. In addition, we used the RIP band based on polysomnography (PSG) device as the gold standard to carry out a systematic validation experiment compared with mesh PDMS-G sensor based on MSP.

4.1. Smart Textile Electrodes for ECG Monitoring

4.1.1. Introduction

The miniaturization of electronic devices made it possible to produce wearable electronic devices. More and more research has integrated electronics reliably directly into clothing, such as into a shirt. Traditionally, clothing was used to cover and protect the body from injury or for aesthetic purposes. If intelligence can be part of everyday clothing, then the people can monitor his/her own physiology during exercise. Smart textile technology provides higher value opportunities for clothing design to protect, monitor and determine physical condition to avoid potential dangerous. In the future, smart clothing can become part of daily clothing, enabling the monitoring of physiological and movement signals of the wearer during daily activities. In medical applications, clothing can be used as a measurement platform, and textile electrodes can be used for bio-signal measurement. ECG data collection is widely used in infant health examination [200]. Experienced clinicians can diagnose various heart conditions by visual analysis of abnormal ECG patterns [201]. ECG consists of three parts: QRS complex, P wave and T wave. These signals are produced in different parts of the heart, and their shape and duration depend on many different factors, such as the pressure of the heart during measurement. The amplitude of the wave depends

on the location of the measurement and the distance between the electrodes. The role of the electrode is to convert the ionic flow into electric current. Electrodes are very sensitive to interference. The interference sources in ECG measurement include patients, electrodes, environment and instruments. The biggest interference is caused by contact between the skin and the electrodes [202]. Nowadays, Ag/AgCl electrode is commonly used for ECG measurement.

One of the weaknesses of these electrodes is their short lifespan, which can only be used for a few days and cannot be reused [65], [203]. In addition, due to the fragile infants' skin, it is easy to damage the skin if such electrodes are used for a long time.

However, the appearance of smart textile electrode makes it possible for long-term smart wearable ECG monitoring. The term "Smart Textiles" refers to a broad field of studies and products that extend the functionality and usefulness of common fabrics. Smart Textiles are defined as textile products such as fibers and filaments, yarns together with woven, knitted or non-woven structures, which can interact with the environment/user. The convergence of textiles and electronics (e-textiles) can be relevant to the development of smart materials that are capable of accomplishing a wide spectrum of functions, found in rigid and non-flexible electronic products nowadays. Conductive textile, a kind of smart textile, can be used to collect ECG signals. Smart textile electrode is a typical flexible ECG electrode, combining the traditional textile materials with conductive material, which meets the requirement of comfort and long-time measurement to a certain extent. In recent years, the common textile ECG electrode materials are polypyrrole-cotton fabric electrode [167], [204], silver-plated electrode, etc. However, different materials and structures will affect the quality of ECG signal. In this chapter, we compare the influence of electrodes made of different intelligent textile on the quality of ECG signal.

4.1.2. Material Selected and Electrode Design

In this study, the raw materials used in electrode production were smart fabrics made by Shieldex. Shieldex produces different types of intelligent fabrics, including Woven Fabrics, Non-Woven Fabrics, Medical Fabrics, Technical Fabrics, RTF Fabrics, Mesh Fabrics and Wearable Fabrics.

In the chapter 3, we use the electrode based on the RTF (Ready to Fabricate) Fabrics (*Berlin RS*). In order to compare the influence of different materials on the signal acquisition, we choose another two Fabrics for comparison. The basic information of the three materials is

as follows:

Medical Fabrics (Balingen)

Medical fabrics are offered in various weights and textures including both knits, and elastic knits with single (SD) or double direction (DS) stretch as well as some woven forms. These fabrics are usually silver plated only, with 99% silver (Ag). Medical fabrics are available with an anti-tarnish coating (+B). Silver is a natural antimicrobial treatment that limits the infections from bacteria.

We use a medical fabric of the type "Balingen". The specific parameters are as follows:

- Description: Silver (Ag) plated Nylon fabric
- Plating: 99% pure silver
- Surface Resistivity: $< 0.6 \text{ Ohmm}$
- Radio Frequency (RF) RF Shielding Effectiveness: Average $> 55 \text{ dB}$ from 30Mhz to 10Ghz
- Temperature Range: -40°C to 100°C / -40°F to 212°F
- Total Thickness: $0.010'' (0.260\text{mm}) \pm 10\%$
- Abrasion Resistance: 10,000 cycles
- Weight: $62 \text{ g/m}^2 \pm 10\%$

Technical Fabrics (Techniktex P130+B)

Technical fabrics are conductive silver knitted fabrics with elastic that come in a single direction (SD) or double direction (DS) stretch. While these fabrics can be used in the same applications as medical fabrics, technical fabrics are generally used for applications that require a higher conductivity like smart wear. Applications include; sensors (vital signs, stimulation of nerves and muscles, etc.), EMI shielding, and reflection to name a few. We use a technical fabric of the type "Techniktex P130+B". The specific parameters are as follows:

- Description: Silver (Ag) plated knitted fabric
- Raw Material: 78% Nylon + 22% Elastomer
- Plating: 99% pure silver
- Coating: Polyurethane as additional protective coating
- Stretch: DS (double stretch direction –warp—weft)
- Surface Resistivity: $< 2 \text{ Ohmm}$ (front / visible side)
- Temperature Range: -30°C to 90°C / -22°F to 194°F
- Total Thickness: $0.021'' (0.55\text{mm}) \pm 10\%$
- Abrasion Resistance: 10,000 cycles

- Weight: $141 \text{ g/m}^2 \pm 10\%$

RTF Fabrics (Berlin RS)

RTF Fabrics include some of woven or non-woven metalized fabrics containing additional coatings including; carbon (C2), hot melt adhesives (HMA), pressure sensitive adhesives (PSA) or low-density thermoplastics (LDPE). These fabrics are typically used in similar applications such as woven fabrics, as well as wallpaper, tapes, medical electrodes and fingertips for touch screen gloves.

We use an RTF Fabric of the type “Berlin RS”. The specific parameters are as follows:

- Description: Conductive PUR-coated silver-plated fabric RS
- Raw material: parachute silk (polyamide 6.6 rip stop fabric)
- Plating: 99% pure silver
- Coating: one sided conductive PUR-coating(functional)
- Surface Resistivity: Average 0.3 Ohmm (max< 0.5 Ohmm)
- Shielding Effectiveness: Average > 60 db from 300Mhz to 5Ghz
- Abrasion Resistance: 200,000 Cycles
- Temperature Range: -30°C to 90°C / -40°F to 212°F
- Weight: $55\text{g/m}^2 \pm 10\%$
- Total Thickness: $0.110\text{mm} \pm 10\%$
- Number of Splices: 1/200 Lm nominal

The above three materials we selected are named as textile A (Medical Fabrics), textile B (Technical Fabrics) and textile C (RTF Fabrics) respectively. Based on these three materials, three types of textile electrodes were developed. Figure 4-1 shows the Ag/Cl electrode and three textile electrodes based on different materials.

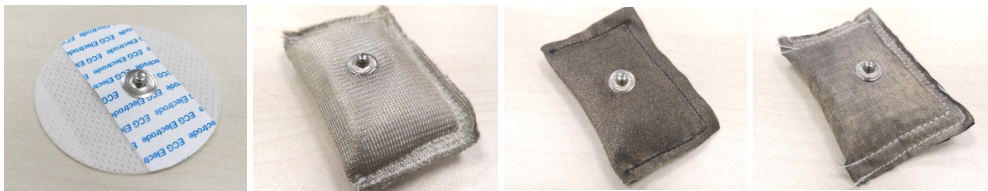


Fig. 4-1. AgCl-adhesive ECG electrode (left 1), Textile A (left 2), Textile B (right 2), Textile C (right 1).

4.1.3. Textile Electrodes Properties

1) Method

To assess the electrode properties, we set up two experiments. One is to test the skin-to-electrode impedance. The other is the signal quality of the test electrode in the standard equipment environment.

(a) Skin-to-electrode impedance

The impedance introduced by the skin-to-electrode interface of standard Ag/AgCl electrode and textile electrode are measured on a person's forearm by an electrochemical workstation (ZAHNER - Zennium).

The two-electrode system is used. Ag/AgCl electrode is deployed as a reference electrode. The work electrodes are chosen from each textile electrode and Ag/AgCl electrode (Covidien, H124SG). The distance between the working electrode and the reference electrode is approximately 9 cm. We fixed the textile electrode with a strap. The frequency of input signal sweeps from 0.1 Hz to 100 kHz. An impedance-frequency curve is drawn for each kind of electrode.

(b) Textile electrodes signal quality assessment

We compared the ECG signals acquired by the proposed electrodes and Ag/AgCl electrode using standard acquisition system.

We collected three sets of data. Each set of data was collected from two different kinds of electrode simultaneously in a static state by shimmer 3 [27], respectively. The study involved a 24-year-old male volunteer. Different electrodes were attached to the adjacent positions on the left and right sides of the subject's chest. The combination of different electrodes was group 1: textile A electrode and Ag/AgCl electrode; group 2: textile B electrode and Ag/AgCl electrode; group 3: textile C electrode and Ag/AgCl electrode. We used shimmer-3 as a standard acquisition device. The acquisition time for each set of data was one and a half hours.

Three statistical analysis methods were conducted to evaluate the signal quality acquired by the novel electrode. Heart rate per minute is extracted by R wave detection algorithm implemented on MATLAB R2018a based on classic QRS detection algorithm proposed by Willis. et al [28]. A bandpass filter with passband of 5-15Hz is used to preprocess the data and the hamming window is applied for the function "fir1" in MATLAB. Then a dynamic threshold is determined every five seconds with 2500 values gathered from the system for the "findpeaks" function with the 'MinPeakDistance' index of 150 points which is 0.3

second in the time domain.

Correlation analysis

We extracted the average heart rate value per minute and compared the heart rate signals from two different electrodes in each group. Correlation analysis is calculated between heart rate information in each group.

Bland-Altman analysis

A "Bland-Altman analysis" was performed on the average heart rate of each group. The standard Ag/AgCl electrode is used as the comparison detection system M1, and the textile electrode is the system M2 to be evaluated. The Bland-Altman analysis was performed to show the difference between heart rate detected by the two systems.

Paired sample T-test

In order to compare the differences between the signals acquired by textile electrode and standard electrode, we compared a list of physiologically sound parameters (Table 3-5). Five minutes of continuous ECG are taken as a segment of data, and the data collected for each type of electrode can be divided into 18 segments. Paired T-test is adopted to support our claim that no differences in substance exist between those parameters retrieved from signals acquired by these three kinds of electrode.

2) Results

(a) Skin-to-electrode impedance

Figure 4-2 gives the Z-f curves which characterize the skin-to-electrode interface of the proposed textile-based electrode and Ag/AgCl electrode (Covidien, H124SG) respectively. The frequency ranges from 0.1 Hz to 100 kHz. Test results demonstrate that the impedance introduced by skin-to-electrode interface also decreases as the frequency of stimulus signal increases. In the frequency range of most bio-potential signals, the impedance corresponding to textile C-based electrode is the smallest (~500 kOhm in near dc range) while the impedance corresponding to textile A-based is the largest (~725 kOhm in near dc range). The impedance corresponding to Ag/AgCl electrode is slightly larger than that of textile C-based electrode, about 575 kOhm in near dc range. The significances of all data points are all larger than 0.95.

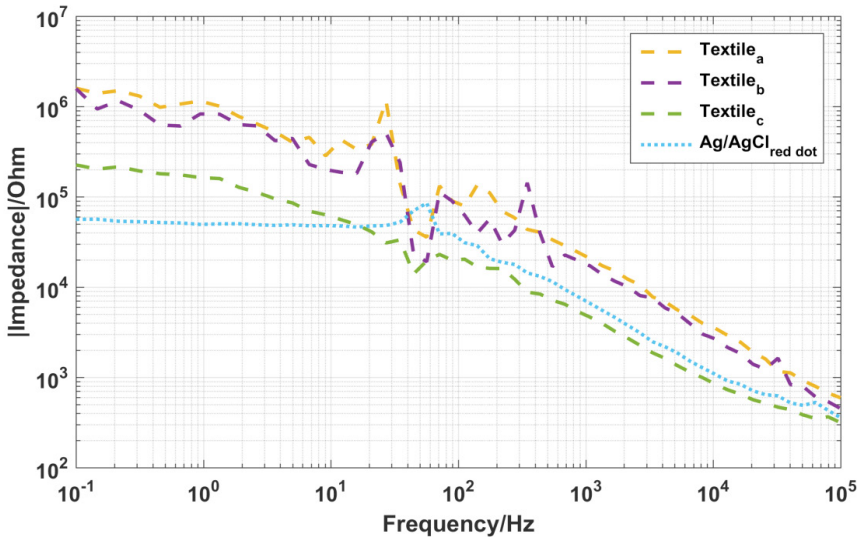


Fig. 4-2. Skin-electrode impedance of different electrodes.

(b) Textile electrodes signal quality assessment

① Correlation analysis results

We extracted heart rates and conducted a correlation analysis and Bland-Altman analysis. Figure 4-3 shows the analysis results of the three sets of data. Correlation analysis results showed that the R^2 values of the three A, B, C groups were all within the range of 0-1, and the R -value of the C electrode was the largest, 0.92. Therefore, the signals collected by the three textile electrodes were positively correlated with the signals acquired by the standard electrodes.

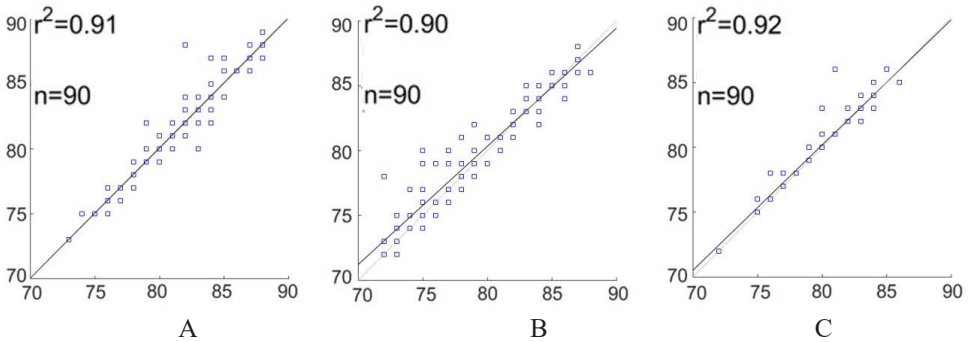


Fig. 4-3. Results of Correlation analysis.

② Bland-Altman analysis results

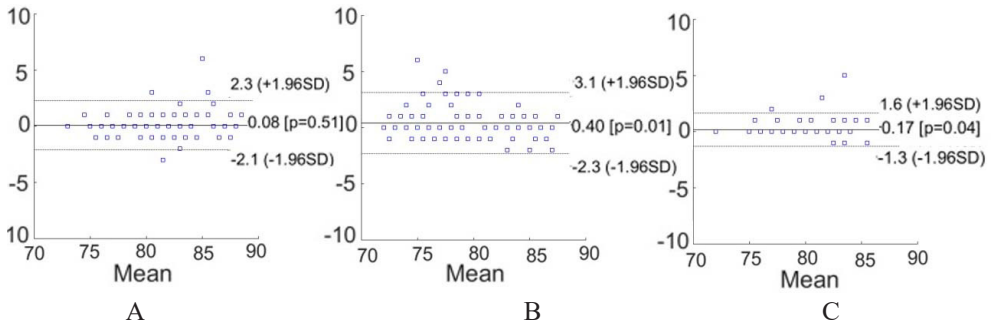


Fig. 4-4. Results of Bland-Altman analysis.

Figure 4-4 shows the results of Bland-Altman analysis. It can be seen in Figure 4-4- A that the 95% consistency limit is (2.3, -2.1); the 3% point is beyond the 95% consensus limit; The mean difference for average RR between M1 and M2 is less than 1 bpm, mean (SD) = 0.08 (1.13). As can be seen in Figure 4-4-B, the 95% consistency limit is (3.1, -2.3); the 2% point is 95% beyond the consensus limit; The mean difference for average RR between M1 and M2 is less than 1 bpm, mean (SD) = 0.40 (1.38).. It can be seen in Figure 4-4-C that the 95% consistency limit is (1.6, -1.3); the 2% point is 95% beyond the consensus limit; The mean difference for average RR between M1 and M2 is less than 1 bpm, mean (SD) = 0.17 (0.73). The results also show that the three groups of textile electrodes have a good agreement with the standard Ag/AgCl electrodes.

③ Paired sample T-test results

Table 4-1. T-test results of Group A, B, C

Variable	Statistical significance (Group A)	Statistical significance (Group B)	Statistical significance (Group C)
NN50 (M1) - NN50 (M2)	0.660	0.106	0.072
PNN50 (M1) - PNN50 (M2)	0.598	0.105	0.071
SDNN	0.529	0.501	0.460
RMSDD	0.596	0.370	0.306
SDSD	0.606	0.349	0.311
5 min total power	0.525	0.500	0.700
VLF (M1) - VLF (M2)	0.782	0.185	0.922

LF(M1)- LF(M2)	0.606	0.186	0.990
LF norm (M1)- LF norm (M2)	0.510	0.852	0.015
HF (M1)- HF (M2)	0.938	0.396	0.484
HF norm (M1)- HF norm (M2)	0.067	0.577	0.072
VLF (M1) - VLF (M2)	0.782	0.185	0.922
LF (M1)- LF (M2)	0.606	0.186	0.990
LF norm (M1)- LF norm (M2)	0.510	0.852	0.015
HF (M1)- HF(M2)	0.938	0.396	0.484
HF norm(M1)- HF norm(M2)	0.067	0.577	0.072

The results are shown in the Table 4-1. The results show that the significance values of each indicator of three kinds of electrodes are all greater than 0.05.

Therefore, there are no differences between the indicators of the ECG signals collected by the three textile electrodes and the standard electrodes.

4.1.4. ECG signal Collected by Proposed System

1) Method

In order to compare the performance of different electrodes under the MSP, the MSP was used for data acquisition and the ECG signal quality collected by different electrodes was compared. ECG signals were measured in different human body motion states in a 24-year-old male volunteer. Two electrodes were fixed on the left and right sides of the ribcage of each test subject. To ensure similar test conditions for comparison, these electrodes were positioned in the same locations for every measurement. The sitting-state ECG signals were measured first, and then the motion artifacts that resulting from walking and upper body turning of the subject's arms were investigated Test time of each group was 2 minutes.

We use following three indicators as the evaluation of signal quality factors which are the critical facts in the further research. These indicators are shown below:

R-wave identification match degree

Using the same heart rate detection method aforementioned, we define the R-wave matching

degree $M(\omega)$ as

$$M(\omega) = \frac{N(\omega)}{N_A(\omega)} \quad (1)$$

whereby $N(\omega)$ is the number of R waves matched by the algorithm, and $N_A(\omega)$ is the number of R waves manually counted by experts.

ECG signal power spectrum ratio

In this section, the ratio of ECG signal power density between 5~15Hz and 3~30Hz is calculated to estimate the state of motion ECG signal quality.

$$S(\omega) = \frac{\int_5^{15} P(\omega) d\omega}{\int_3^{30} P(\omega) d\omega} \quad (2)$$

$P(f)$ denotes the power spectrum of ECG signal.

Signal kurtosis value

ECG signals are collected as discrete signals. According to the central limit theorem, the kurtosis of the discrete signal reflects the Gaussian of the signal.

$$K = \frac{1}{M} \sum_{i=1}^M \left[\frac{x_i - \mu_x}{\sigma} \right]^4 \quad (3)$$

μ_x denotes the mean of the signal x_i , σ denotes the standard deviation of the signal, and M is the number of sampling points of the measured data segment.

2) Results

To analyze the electrode performance under motion artifacts, the measurements were performed in sitting state, upper body turning state and walking state.

Sitting state results

Firstly, ECG signals were measured in sitting state. The subjects put their hands on both sides and sat in a chair. The electrodes were attached to the left and right sides of the chest. Each electrode was tested for 2 minutes.

Figure 4-5 shows the waveform of ECG signals collected by three textile electrodes and Ag/Cl electrode through the MSP in 15 seconds. As can be seen in the figure, QRS complex and T wave can be detected obviously in sitting state.

The results of R-waves detection by computer and expert are presented in Table 4-2. R-wave recognition rate was generally high, reaching 100%. There was a small difference among three kinds of textile electrodes. Power spectrum ratio and signal kurtosis values of 1000 points selected during the test time of two minutes were listed in Table 4-3 and 4-4.

The S and K values of the three textile electrodes and the Ag/AgCl electrodes were all at a good level. The S and K values of textile C electrode were better than those of Ag/AgCl electrode.

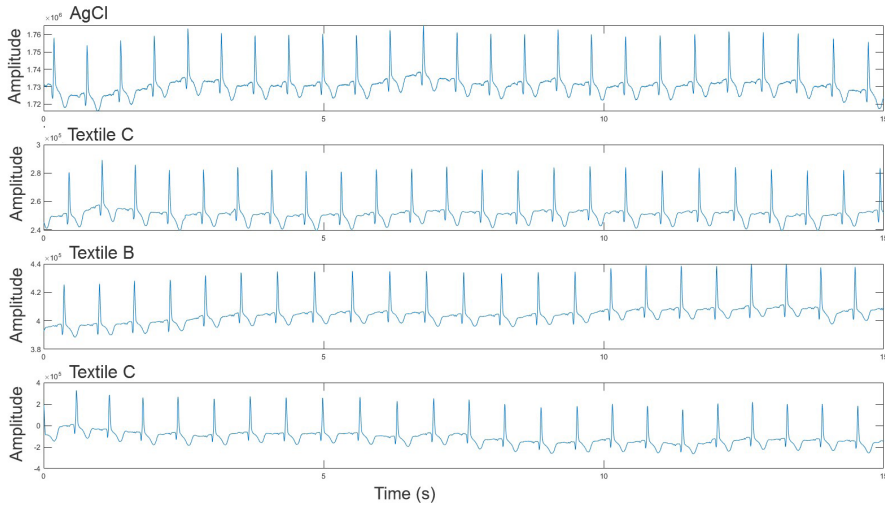


Fig. 4-5. R-wave Recognition under sitting state.

Table 4-2. R-wave Recognition under sitting state

Type of electrode	AgCl	Textile A	Textile B	Textile C
Missed	0	0	0	0
N (ω) Identified by algorithm	161	167	173	171
NA (ω) Detected by experts	161	167	173	171
R-wave matching degree (M)	1	1	1	1

Table 4-3. Power spectrum of ECG under sitting state

Type of electrode	AgCl	Textile A	Textile B	Textile C
Power Spectrum ratio (S)	0.7407	0.7291	0.7283	0.7709

Table 4-4. Signal quality under sitting state

Type of electrode	AgCl	Textile A	Textile B	Textile C
Signal Kurtosis(K)	10.3668	9.8756	7.4843	11.2188

Upper body turning state results

In this part, the ECG signal with the upper body turning was measured. The subject sat on the chair with their hands raised flat and rotated their upper body left and right. The

electrodes were attached to the left and right sides of the chest. The test time of each electrode was 2 minutes.

Figure 4-6 shows the ECG waveforms of three kinds of textile electrodes and Ag / CL electrodes in 15 seconds under the Upper body turning state. QRS wave group and T wave also can be detected obviously under the upper body turning state. Compared with the sitting state, the ECG signal was more prone to drift in the upper body turning state. Textile electrode A was the most stable among the three kind of textile electrodes.

Table 4-5 shows the R-wave recognition rates of the three textile electrodes and Ag/CL electrodes under the upper body turning state. The R-wave recognition rate of textile electrode A and textile electrode B decreased to 0.994 and 0.97 respectively. Power spectrum ratio and signal kurtosis values during the upper body turning state were listed in Table 4-6 and 4-7. The results showed that the values of K, S and M of the AgCl electrode and the textile electrode C were all at a good level. The K values of the textile electrodes A and B are at the normal level.

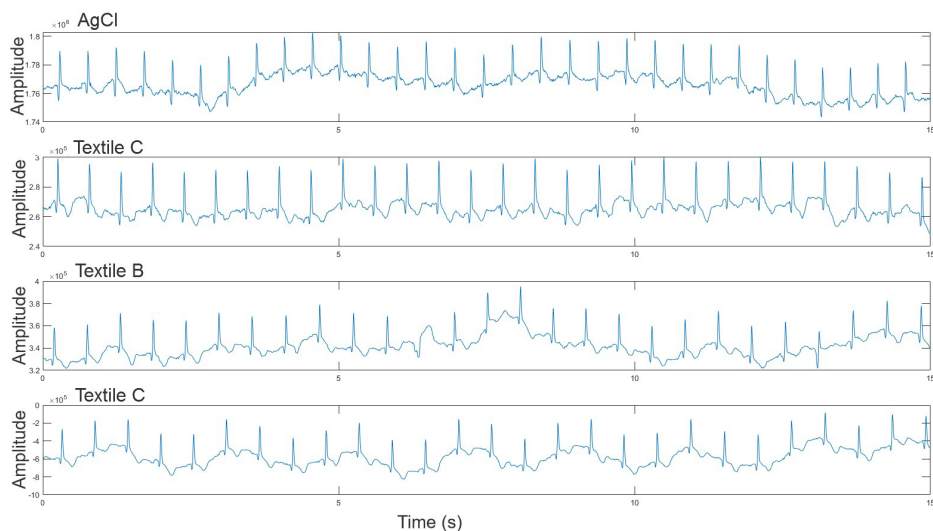


Fig. 4-6. R-wave Recognition under turning state.

Table 4-5. R-wave Recognition under turning state

Type of electrode	AgCl	Textile A	Textile B	Textile C
Missed	0	1	6	0
False alarm	0	0	0	0
N (ω) Identified by algorithm	201	186	191	181

NA (ω)Detected by experts	201	187	197	181
R-wave matching degree (M)	1	0.994	0.97	1

Table 4-6. Power spectrum of ECG under turning state

Type of electrode	AgCl	Textile A	Textile B	Textile C
Power Spectrum ratio (S)	0.8481	0.7051	0.6477	0.7039

Table4-7. Signal quality under turning state

Type of electrode	AgCl	Textile A	Textile B	Textile C
Signal Kurtosis (K)	8.2667	4.7987	4.9923	7.4293

Walking state results

Finally, ECG waveforms acquired by the MSP and PSG under walking state were compared. The subject put his hands on both sides and raised his left and right legs alternately and keep his original position. The electrodes were attached to the left and right sides of the chest. The test time of each electrode was 2 minutes.

Figure 4-7 shows the ECG waveforms of three kinds of textile electrodes and Ag / CL electrodes in 15 seconds under walking state. Like the upper body turning state, the ECG signal was prone to drift in the walking state. As can be seen in the figure, compared with the upper body turning state, the ECG signal is more vulnerable to be affected in the walking state.

Table 4-8 shows the R-wave recognition rates of the three electrodes and Ag / CL electrodes in the walking state. The R-wave recognition rate of four electrodes in the walking state is lower than that in other states. The R wave recognition rate of textile electrode A was only 90.1%, while that of textile electrode C was 99.5%. The power spectrum ratio and signal kurtosis values are listed in tables 4-9 and 4-10. The results show that the K and S values of the three textile electrodes were not as good as those of the AgCl electrodes. However, the K and M values of textile electrodes B and C reached a good level.

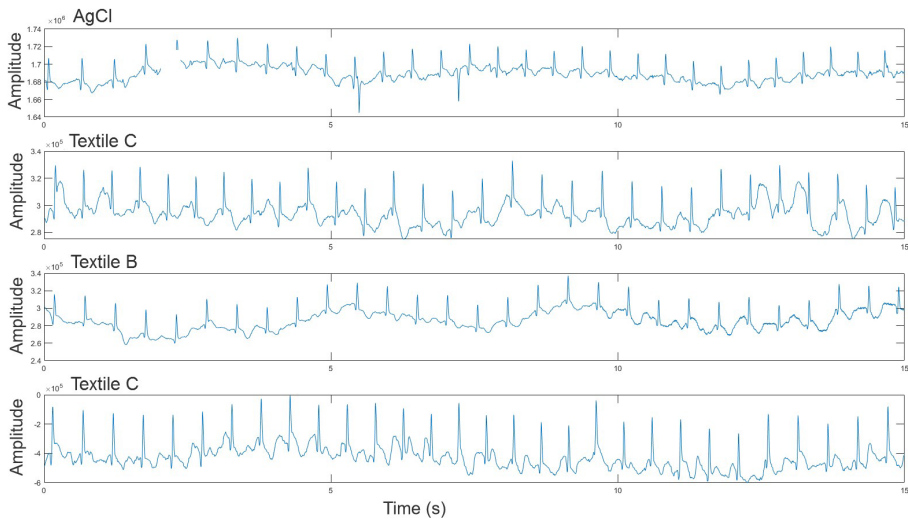


Fig. 4-7. R-wave Recognition under walking state.

Table 4-8. R-wave Recognition under walking state

Type of electrode	AgCl	Textile A	Textile B	Textile C
Missed	3	21	7	1
False alarm	0	0	2	0
N (ω) Identified by algorithm	205	193	204	202
NA (ω)Detected by experts	208	214	209	203
R-wave matching degree (M)	0.986	0.901	0.976	0.995
N (ω) Identified by algorithm	205	193	204	202
NA (ω)Detected by experts	208	214	209	203
R-wave matching degree (M)	0.986	0.901	0.976	0.995

Table 4-9. Power spectrum of ECG under walking state

Type of electrode	AgCl	Textile A	Textile B	Textile C
Power Spectrum ratio (S)	0.6386	0.3603	0.4223	0.4119

Table 4-10. Signal quality under walking state

Type of electrode	AgCl	Textile A	Textile B	Textile C
Signal Kurtosis (K)	9.1456	6.7123	5.0471	7.1517

Three indexes of R-wave recognition, power spectrum ratio, and signal kurtosis value are

used to make a comprehensive evaluation of electrodes under each state. According to these indexes, the performance of AgCl-adhesive is the best, and textile electrode C is better than A and B.

4.1.5. Conclusion

In this experiment, we mainly compared the material properties of the four electrodes and the quality of the signals collected by the MSP with the four electrodes in different states. The results show that the textile electrode has great potential in ECG signal acquisition. The signals collected by the three kinds of textile electrodes and Ag/Cl electrodes under sitting states showed good quality. However, Ag/Cl electrodes and textile electrodes based on RTF textile materials showed advantages under the upper body turning state and walking state. Due to the effects of motion and the material, the quality of the signals collected by the electrodes based on Medical Fabrics and Technical Fabrics will obviously decrease under the motion state. The textile electrode made of RTF textile material has more advantages than that made of the other two kinds of textiles. During the motion state, the signal obtained by the electrode based on the RTF material is more stable and not easily affected by the movement. The R-wave recognition rate of electrodes based on RTF material in walking state is higher than that of Ag/CL electrode. However, the power spectrum ratio value and signal kurtosis (K) value of electrodes based on RTF materials are lower than those of Ag/Cl electrodes under motion state, which means that the electrode based on RTF materials is easily affected by the external environment.

So far, Ag/Cl electrodes are still widely used. With the innovation and development of smart fabrics, textile electrodes have gradually demonstrated its advantages. It is also expected to be a substitute for traditional electrodes in the future.

4.2. Carbonized Foam Electrode for ECG Monitoring

4.2.1. Introduction

The development of wearable sensor systems and body sensor network (BSN) enables healthcare providers to narrow the gap between the existing medical infrastructures and the growing need for mobile healthcare.

An exclusive advantage of a wearable sensor systems over traditional monitors is the

possibility of continuously and unobtrusively monitoring the user's long-term physiological and behavioral signals in parallel by embedding multiple sensors in the system [205]. For acquiring the electrophysiological signals like ECG, EEG and EMG, it is necessary to record the surface bio-potentials by electrodes.

The term 'electrode' originated from Faraday's research about electricity and electrochemistry [206]. In 1903, Einthoven used a string galvanometer and cumbersome electrodes to obtain the first ECG and opened up clinical electrocardiography [207]. Nowadays, the most commonly used electrode in clinical practice is Ag/AgCl electrode with electrographic gel, which provides good conductivity and small and stable offset potential, guaranteeing the very finite distortion on signals introduced by the electrode's deviation from the ideal condition. However, this kind of electrode may lead to skin irritations and even tears.

For wearable sensor systems, the wet electrodes are dissatisfactory because the use of conductive gel is, to some extent contradicted with portability and long-term unobtrusive monitoring. Various electrodes based on polymer materials and e-textiles without the needs for conductive gel are developed as alternatives for the electrode used in wearable sensing platforms [208][209]. Although these electrodes are comfortable with stable signals in the non-moving state, the signal quality is easily affected in the moving state.

In this section, we present a novel dry disposable electrode prototype. The conductive part is made of carbonized foam (CF). A test protocol focusing on characterizing several important electrical properties of the electrode is designed to investigate its performance when it is applied to record the surface potential. Experimental results show that the presented CF electrode is capable of acquiring surface potential like ECG with competitive signal quality. Lower powerline interference is observed from the signal acquired by CF electrodes. The issue about biocompatibility and future work about improving the intension of the material and the durability of the electrode are also discussed.

4.2.2. Material and Manufacturing

1) Production of Material

Figure 4-8 is the outlook of the whole electrode. It is light and manifests good mechanical strength, thus enabling them to be easily integrated in electrodes and e-cloth. In Figure 4-8 (a) and (b), the CF exhibits high flexibility, and can be bent to an arbitrary degree without fracture. Besides, it is also compressible. A 1.0cm thick CF in Figure 4-8 (c) is compressed

to around 0.3 cm under the applied forces in Figure 4-8 (d). When the external forces were released, it returned to the original shape without deformation.

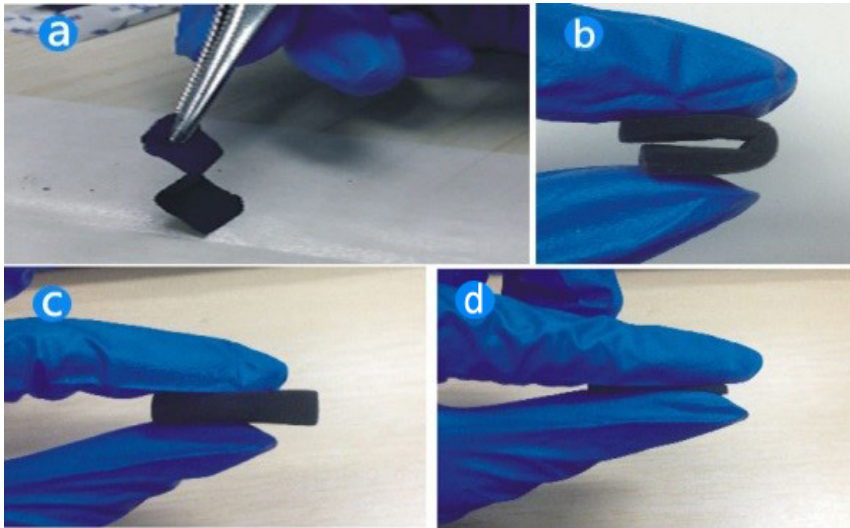


Fig. 4-8. Carbonized foam

2) Production of the Electrode

Figure 4-9-a shows the structure of the novel dry disposable electrode. The electrode consists of four parts, carbonized foam ①, electret gel layer ②, non-woven fabric ③ and metal lead button ④. CF is connected to the metal lead button. The nonwoven fabric is sandwiched between the electret gel layer and the metal lead button as a protective layer. An electret gel layer serves as a paste layer surrounding the carbonized foam. A prototype is given in Figure 4-9-b.

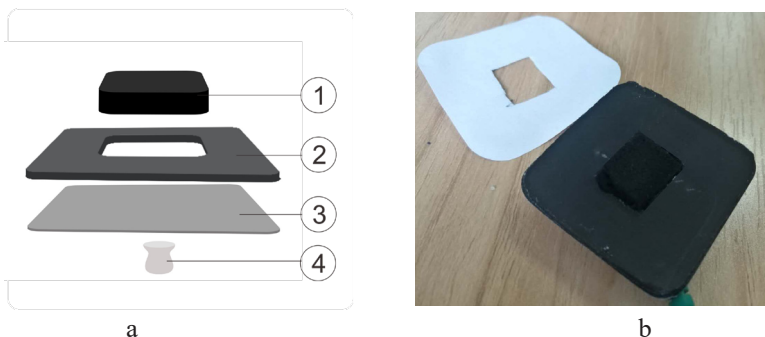


Fig. 4-9. Conceptual structure and prototype of CF electrodes

The thickness of the CF is higher than that of the surrounding electret gel layer. When the electrode is pasted on the skin, the carbonized foam tends to dilate. This characteristic

increases the stability of the contact between the electrode and the skin automatically and thus enhances the quality of the acquired signal during movements.

4.2.3. Method of Evaluation

To characterize the performance and applicability of the proposed carbonized foam electrode, we designed a test protocol to evaluate and compare its electrical properties with that of the state-of-art Ag/AgCl electrode.

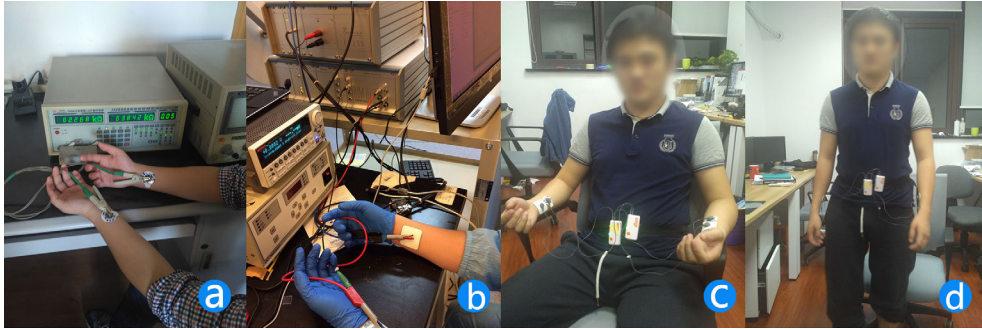


Fig. 4-10. Experimental settings for evaluation of electrodes

First of all, we measured and compared the impedances when the proposed electrodes and Ag/AgCl electrodes (Covidien H135SG) were placed by the convention of Lead-I. The measurement was done by a LCR meter (Tonghui Electronics, TH2816, Figure 4-10-a). The in-vitro impedance is comprised of the impedance of the human body in series, the impedance of the electrodes in series and the impedance introduced by the skin-to-electrode interface [210]. These impedances as a whole serve as equivalent internal signal source resistance of the hypothetical signal source where the bio-potential field of interest is stimulated. Large signal source impedance results in obvious attenuation of the input signal amplitude of the post-stage amplifier. Tolerable in-vitro impedance is necessary for post-stage conditioning. To eliminate the change of conditions of the human body as much as possible, we removed the sweat on the subject's skin before. The subject keeps static during the test. And the whole test (including preparation) about in-vitro impedance was performed within one hour with an assumption that the physiological state of the subject would not shift significantly in such a short period.

Secondly, an electrochemical workstation (ZAHNER - Zennium) was used to measure and compare the impedances introduced by the skin-to-electrode interface of the proposed electrodes and Ag/AgCl electrodes. A two-electrode system was used as depicted in Figure

4-10-b [7]. Ag/AgCl electrodes were deployed as reference electrodes. The work electrodes were chosen from the CF electrode and Ag/AgCl electrode (Covidien, H124SG) as illustrated in Figure 4-11. The working electrode and reference electrode are arranged as Lead-I. The frequency of the input signal swept from 0.1 Hz to 100 kHz. An impedance-frequency curve is got for every work electrode.



Fig. 4-11. Ag/AgCl electrodes

hirdly, we compared the ECG signals acquired by the proposed electrode and Ag/AgCl electrode (Covidien H135SG) to perform a visual comparison. The measurements were performed in static and motion conditions (the subject marches on the spot in with arms swing, Lead-I, Figure 4-10-c, (d)). Signal acquisition was done by a Shimmer-3 unit where an inertial measurement unit (IMU) was integrated so motion data can be provided. ECG signals and 3-axis acceleration data were recorded simultaneously at a sampling rate of 512 Hz. Waveforms, acceleration data and power spectrum densities (PSD) of signals acquired by both electrodes under both situations respectively were compared to investigate the performance comprehensively.

4.2.4. Result

In this section, detailed information about the electrical properties of the presented carbon foam was given. We measured the in-vitro impedance when using proposed CF electrodes and Ag/AgCl electrodes. The skin-to-electrode impedance of CF electrode, textile-based electrode and Ag/AgCl electrode were measured and compared. Furthermore, we evaluated the signal quality of ECG signals acquired by our electrodes and standard electrodes with or without motion.

(a) Impedance in vitro

As mentioned before, we want to estimate the equivalent signal source internal impedances

with respect to the post-stage conditioning circuit when using different kinds of electrodes. A comparable or even smaller quantity is welcomed since a considerable difference in magnitude leads to attenuation.

Figure 4-12 shows that impedance decreases as the frequency of stimulus signal from the LCR meter increase from 50 Hz to 100 kHz. Generally, the in-vitro impedances caused by CF electrodes and Ag/AgCl electrodes do not differ in the order of magnitudes, implying no obvious attenuation on the magnitude of the input signal to a post-stage amplifier will happen when proposed electrodes are applied.

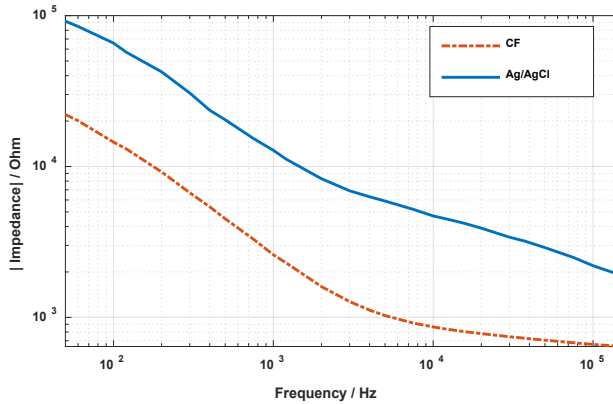


Fig. 4-12. In-vitro impedance test

Furthermore, most of the energy of the ECG signal falls in the frequency range from dc to 100 Hz. For electromyography (EMG), the range is about dc to 500 Hz. In these frequency ranges, the in-vitro impedances when CF electrodes are used are 75% averagely lower than that when Ag/AgCl electrodes (Covidien H135SG) used. Part C will show no obvious difference in the total power of acquired signals observed.

(b) Skin-to-electrode Impedance

When recording bio-potential with electrodes, there is a potential drop between skin and electrode. This potential drop can be equivalent to a circuit consist of resistors and capacitors [212]. Thus the equivalent impedance is frequency dependent.

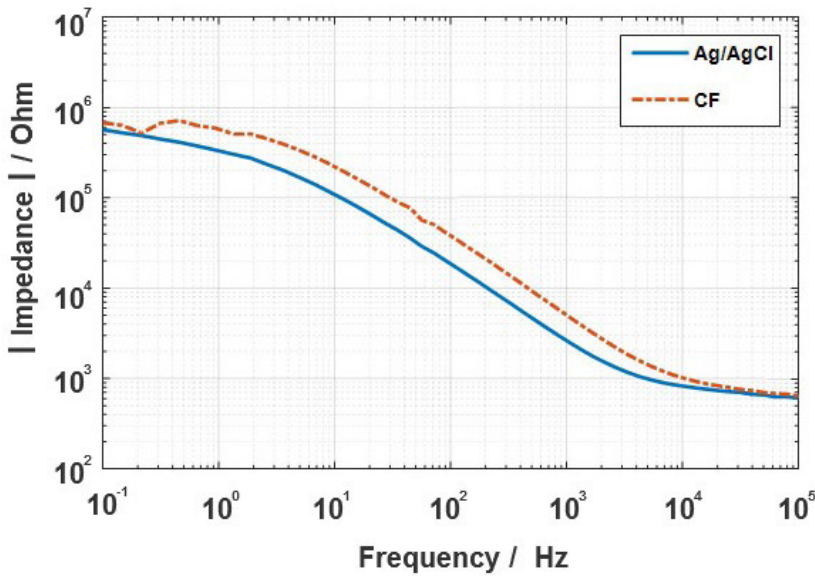


Fig. 4-13. Skin-electrode impedance of different electrodes

Figure 4-13 gives the Z-f curves which characterize the skin-to-electrode interface of CF electrode and Ag/AgCl electrode (Covidien, H124SG) respectively. The frequency ranges from 0.1 Hz to 100 kHz. Test results demonstrate that the impedance introduced by skin-to-electrodes interface also decreases as the frequency of stimulus signal increases.

In the frequency range of most bio-potential signals, the impedance corresponding to Ag/AgCl electrode is the smallest (~566 kOhm in the near dc range). The impedance corresponding to the proposed CF electrode is slightly larger than that of the Ag/AgCl electrode, about 675 kOhm in near dc range. The significances of all data points are larger than 0.95.

(c) Signal Quality

An undistorted signal waveform is the “final purpose” when surface bio-potential is recorded, so we compare the signal quality in the time domain. ECG waveforms (100 points median filtering applied for the convenience of the display) acquired by Ag/AgCl electrodes and CF electrodes and simultaneous accelerations (denoted as Acc, whose value is the modulus of all 3 axis accelerations) are given in Figure 4-14.

During both the static and motion (stepping on the spot) conditions, the proposed electrode can acquire ECG signals of comparable signal quality and amplitude (thus, also average power) with respect to the Ag/AgCl electrode.

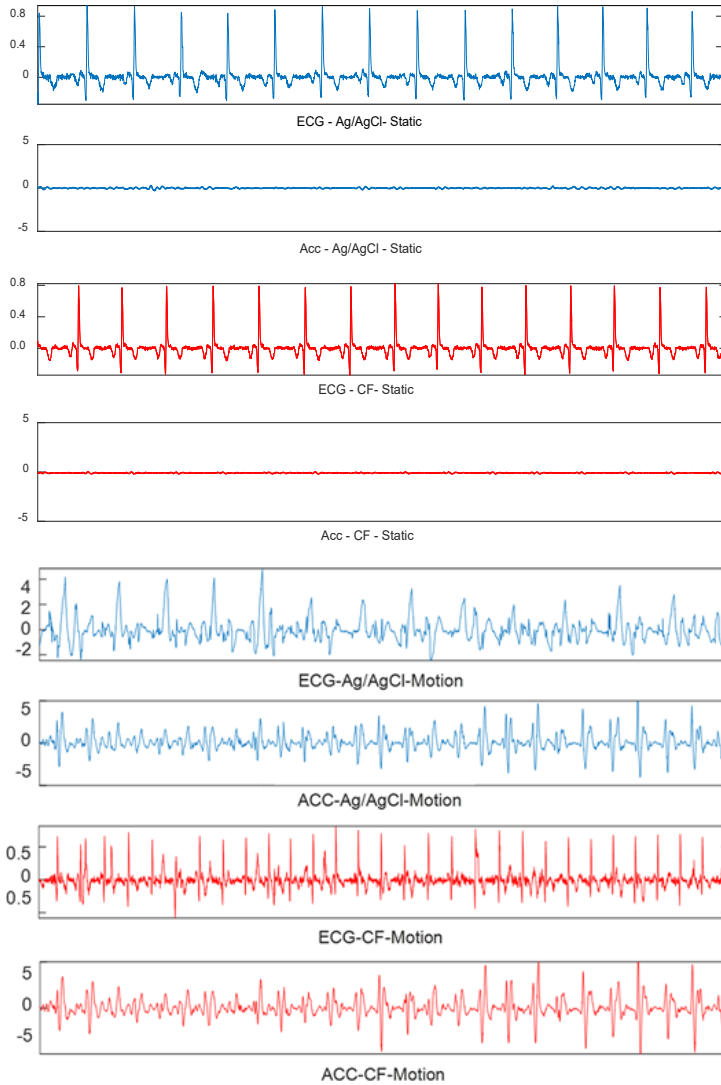


Fig. 4-14. ECG waveforms and accelerations

During the motion condition, the proposed CF electrode represents even better tolerance on motion artefacts, probably due to the mechanical properties of the material and less power line interference.

PSDs estimated by Welch Periodogram (Figure 4-15) reveal that less power line interference is contained in the signal acquired by proposed electrodes. Note that no filtering or driven-

leg circuits or any other noise rejection technique were implemented before the PSD estimation. This difference seems to be caused by the new conductive material itself. And we will identify the true reason in future work.

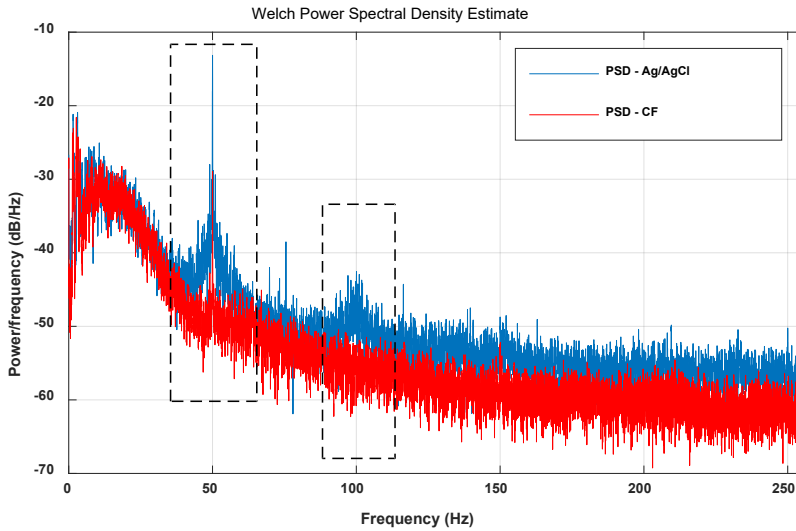


Fig. 4-15. PSD of signals acquired by CF and Ag/AgCl electrode

4.2.5. Discussion and Conclusion

Electrodes that better suit wearable sensor systems and mobile healthcare scenarios can help pave the way for further popularization of wireless and wearable sensing and monitoring devices.

For the reasons mentioned above, we proposed a novel carbonized foam electrode. Test of in-vitro impedance when novel electrode used excludes the worry about attenuations. And the skin-to-electrode impedance introduced by the proposed electrodes is comparable with state-of-art Ag/AgCl electrode. The signal quality acquired by the CF electrode is competitive during static and motion conditions, especially during motion conditions. Furthermore, the proposed CF electrode has no need for conductive gel. The conductive part is flexible which may explain why the CF electrode has a higher tolerance on motion artefacts than Ag/AgCl electrode.

State-of-art textile-based electrode usually has a worse contact with the subject, which degrades the performance under motion condition. So the proposed CF electrode or

other electrodes with similar mechanical properties are potential to be an alternative or complements for improving the performance of wearable bio-potential monitoring systems for daily use.

It should be noticed that the structure of the prototype is designed to justify the usability and performance of CF as the conductive material. To integrate CF into real-world wearable sensor systems, a new structure is needed and the mechanical intensity of CF should be improved, which remains to be our future work with the assessment of material's biocompatibility.

It should also be noted that we use a different subtype of Ag/AgCl electrode when performing the evaluation described in section 4.2.3. The two-electrode system as the experimental setting is different from that used for measurement in [213]. These reasons may account for the different relative relationships between the impedance values corresponding to the CF electrode and Ag/AgCl electrode as depicted in Figure 4-11 and Figure 4-12. And the operating principals of the electrochemical workstation and LCR meter are different in many respects, so the values corresponding to the same frequency should be interpreted respectively. Great care must be taken before any direct contrast. But it's already confirmed that measured values do not differ in the order of magnitudes under the same condition. Together with the comparison of signal waveforms, the usability of the CF electrode can be justified. And we will eliminate the irrelevant variable in further work and improve the data consistency.

We encountered that the CF electrode seems to be able to reduce powerline interference. This characteristic is serendipity given the fact that shielding measure and driven-leg circuits, which can be realized under well-structured environments with powerful but unwieldy medical instruments, are impractical on wearable sensor systems. Less need for high order digital filters circumvents continuous and intensive computation, which helps to maintain low power consumption of the whole system.

This discovery is tested repeatedly and is validated under our experimental settings. The influence of electrode structure, especially the electret gel, has been excluded.

We have made two unverified hypotheses about this characteristic. First, when Cf is used, its polarization could be very low so that the CF electrode may have smaller and more stable offset potentials. The imbalance between input terminals is reduced and the common-mode rejection ratio (CMRR) of the whole front-end circuit is thus improved. Second, the reticular microstructure of CF may serve as a shielding case, which makes the effective contact area between the CF and the skin a region free from direct electrostatic coupling

and magnetic field interference from the environment. So only interference conducted from the uncovered region and interference coupling through other approaches will take effect. We try to identify its root cause and exclude the influence from possible irrelevant variables in our further work.

4.3. Mesh PDMS-G Compound Sensor for Respiration Monitoring

4.3.1. Introduction

Respiratory rate, also called breathing rate, defined as the number of breathing and exhaling movements per unit time, is crucial in neonatal surveillance [24], [214]. In fact, the respiratory rate is ordinarily determined by calculating the number of times the diaphragm expands and contracts per minute. Respiratory problems are the most common causes of admission for newborns, whether in both term infants and premature [215]–[217]. Common respiratory diseases that cause abnormal respiratory rates in newborns include pneumonia, pulmonary hemorrhage and Respiratory Distress Syndrome (RDS). Among them, RDS is very common in premature infants. It can escalate to respiratory failure and cardiopulmonary arrest, if not identified and treated quickly. Therefore, the pediatricians must be able to easily identify the symptoms and signs of respiratory distress, distinguish various causes, and adopt treatment strategies to prevent complications [215].

Current techniques for monitoring respiratory rate include thoracic electrical impedance, respiratory induction plethysmography (RIP), three-dimensional acceleration-derived breathing rate (ADR) and piezoelectric sensor plethysmography, which can record volume changes in the chest and abdomen [218], [219]. Thoracic electrical impedance is the most common method of respiratory monitoring in the clinic. This method adopts adhesive electrodes attached to the skin to obtain signals. However, long-term attachment of these patches to the skin may cause irritation [13]. Researchers studied the feasibility of several sensors for wearable respiratory monitoring systems: piezoelectric sensors or three-dimensional accelerometer signals [75], [76], [220], [221]. However, the breathing signals collected by piezoelectric sensors or three-dimensional acceleration sensors contain a large number of motion artifacts, which affect the accuracy of breathing rate measurement. Therefore, respiratory induction plethysmography (RIP) came into being, proposed by T. Chadha et al. [75]. The RIP method includes an induction band that can be connected to the abdomen or chest. The resistance of the band varies with stretching. Because the chest/

abdomen circumference changes during breathing, RIP-based breathing monitoring is a valid breathing monitoring method. A wearable respiratory monitoring device based on RIP for respiratory biofeedback training was proposed by Zhang et al. [77], [169]. However, the method to manufacture the band of this device is complex and difficult to be embedded in wearable devices.

Hence, there is an unmet demand for a practical, comfortable, affordable and easy-to-use technology to continuously measure the respiratory frequency of newborns in a minimally invasive manner, which can easily be incorporated into the current monitoring program. Such a device could overcome problems resulting in respiratory infection by aiding in early detection and diagnosis.

Nowadays, the research of new materials is an important direction of sensor research and development [222]–[224]. In our previous work, the carbonized foam we proposed can be used as an ECG electrode, which can not only obtain a stable ECG signal, but also reduce the power line interference [225]. The innovation of new materials provides a good opportunity to provide comfortable, economical and practical wearable technology.

In Chapter 3, we proposed the PDMS-G sensor, which has a good performance in obtaining respiratory signals with 0 -100% strain range around. In order to improve the sensor performance, we designed a tensile sensor of graphene composite with mesh structure (M-PDMS-G). A larger strain range and smaller stress can be obtained by using graphene with a mesh structure. Smaller stresses have less effect on neonatal respiration.

In this section, the fabrication process of the M-PDMS-G sensor is introduced. The basic properties, including strain range, stability and sensitivity, between M-PDMS-G and PDMS-G are compared. We used the polysomnography (PSG) device-based respiration belt module as the gold standard to carry out a systematic validation experiment compared with the MSP-based respiration module. Finally, we conducted a clinical test for neonatal respiration detection in Children's Hospital affiliated with Fudan University in Shanghai.

4.3.2. Material and Manufacturing of Mesh PDMS-G Compound

PDMS-graphene ink is the first step to prepare mesh PDMS-G composite, and then a mesh structure is built through the 3D printer. The PDMS-graphene ink was prepared as follows. 1g Graphene sheets were dispersed in 100 mL ethyl acetate; the mixture was ultrasonicated for 2 h, and then 10g PDMS prepolymer was added to the suspension with magnetic stirring for another 2 h. After that, the mixture was transferred onto a heating stage with a

temperature of 80 °C for 6 h to evaporate the ethyl acetate solvent. Finally, 1 g of PDMS curing agent was added into the composite and stirred for 10 min to acquire the PDMS–graphene ink.

The 3D-printing process was performed by a Biological 3D printer (Regenovo 3D Bio-Architect WS); in this experiment, the PDMS–graphene ink was transferred to a 30 mL syringe and the ink was extruded through a 400 μm nozzle to obtain the designed physical structure, as the nozzle's moving speed was 5 mm/s. The as-printed structure was then cured at 80 °C for 3 h to obtain the M-PDMS-G strain sensor. Through 3D printing, we can tune the physical structure and elongation capability of M-PDMS-G composites. Figure 4-16 shows the different structures of printed M-PDMS-G composites.



Fig. 4-16. Different structures of printed M-PDMS-G composites.

Next, for the preparation of the M-PDMS-G sensor, the printed M-PDMS-G composite was treated with oxygen plasma (200 W, 0.2 mbar, 120 s) followed by immersion in PEI solution (3 mg/mL) for 10 min. Then, the composite was washed with deionized (DI) water and gentle blow drying with N₂ air; after that, the composite was immersed in GO suspension (2 mg/mL) for 10 min before washing with DI water and dried with N₂ air again. For the layer-by-layer self-assembly of PEI and GO on the surface of the PDMS–graphene macrostructure, the pH values of both GO and PEI solutions were adjusted to 9.0 by ammonia and hydrochloric acid. Finally, the GO-coated M-PDMS-G composite was reduced through HI acid solution treatment in a sealed container at ambient conditions for 30 min to obtain the M-G-PDMS sensor.

Through 3D printing, we can tune the physical structure and elongation capability of M-PDMS-G composites. In order to choose a structure with better elongation capability, we compared the strain ranges of different structures as shown in Figure 4-17. The mesh of the parallelogram revealing a deformation capability of over 400%. Large elongation is the prerequisite for strain sensors to achieve large workable ranges, like elastic waistband.

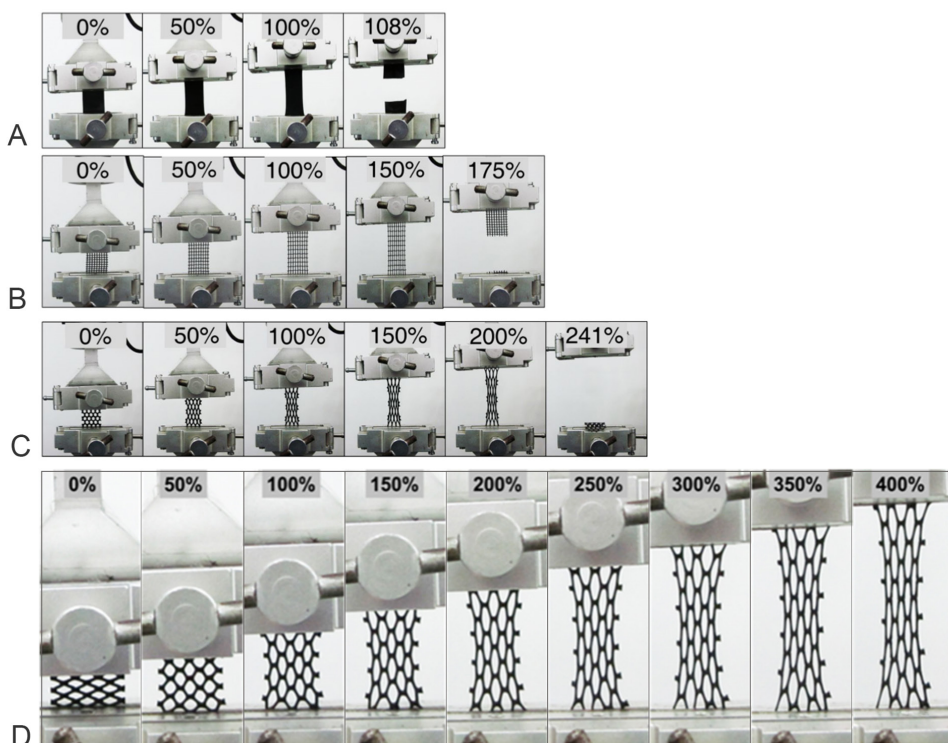


Fig. 4-17. Digital images of PDMS-G composites with different structures, planar(a), square mesh (b), hexagonal mesh (c), parallelogram mesh (d) at different strain states.

Figure 4-18-a and Figure 4-18-b present a structure model and scanning electron microscope (SEM) image of a two-order structural cross section of M-G-PDMS sensor, in which region A represents the inner M-G-PDMS part and B represents the outer reduced graphene oxide (RGO) coating. Figure 4-18-c shows the image of the fracture surface of the sensor, indicating the uniform dispersion state of graphene sheets in the inner M-G-PDMS part. The SEM image of the RGO coating is presented in Figure 4-18-d, and the characteristic wrinkled morphology signifies that RGO sheets were successfully coated onto the M-G-PDMS surface.

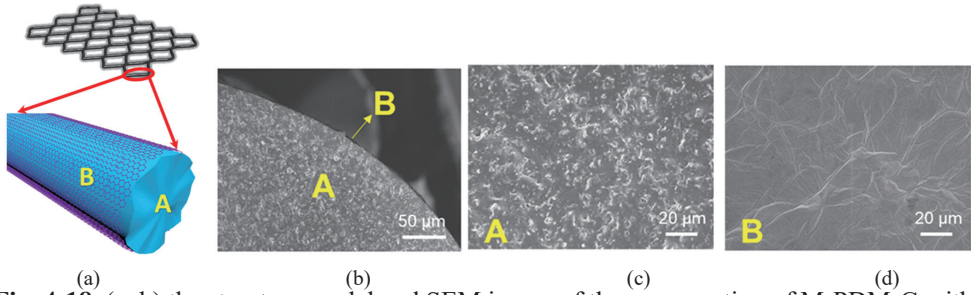


Fig. 4-18. (a, b) the structure model and SEM image of the cross section of M-PDM-G with RGO sensor (top view) (letters A and B represent the inner M-PDM-G part and outer RGO coating, respectively); (c, d) SEM images of the fracture surface of the sensor (c) and RGO coating layer (d), respectively;

Figure 4-19-a shows the version of M-PDMS-G with RGO and without RGO. Due to the presence of RGO coating, M- PDMS-G with RGO reveals significantly improved electrical conductivity, compared with M-PDMS-G without RGO (Figure 4-19-b). The reasons mainly include two aspects. First, the sliding and disconnection of reduced graphene oxide (RGO) sheet coated on the surface (a crack mechanism) of the strain sensor result in high sensitivity at a small strain range. Second, the graphene layer coated on the open mesh provides additional conductive paths that can compensate spontaneously for the conductivity loss of the percolation network at large strains through a combination with the inner network (self-compensation mechanism), so that a large workable strain range can be achieved along with high sensitivities.

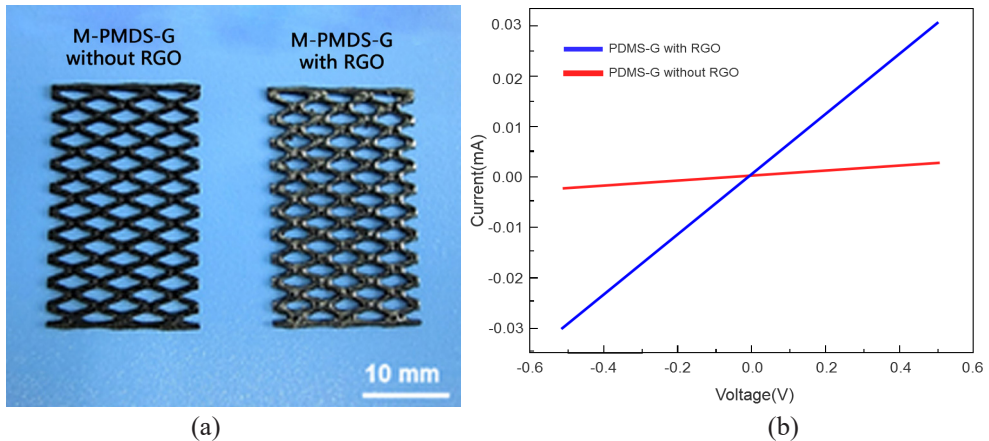


Fig. 4-19. (a) Photograph of M-PDMS-G with RGO and M-PDMS-G without RGO; (b) current-voltage curves of M-PDMS-G with RGO and M-PDMS-G without RGO.

4.3.3. Material Properties

The feasibility of the respiration sensor depends on the basic performance of the material. We compare the sensitivity, stability, stress change curve and response/relaxation time of the M-PDMS-G and PDMS-G materials, but also compare the stress change curve of the two sensors. In the same strain range, the lower the stress, the smaller the effect on respiration, especially for neonates.

1) Stress test of the sensor

Firstly, we compared the mechanical strength of PMDS-G and M-PDMS-G materials. The mechanical properties of the sensors were evaluated by stress-strain curves, as shown in Figure 4-20. Compared with planar structures, the meshed structures reduced the value of stress under the same strain. It can be seen from Figure 4-17-a and 4-17-d that the length of M-PDMS-G at break exceeded 400%, while that of PDMS-G at break was only 108%. Therefore, The M-PDMS-G sensor for respiration monitoring was more comfortable than the PMDS-G sensor, especially for neonates.

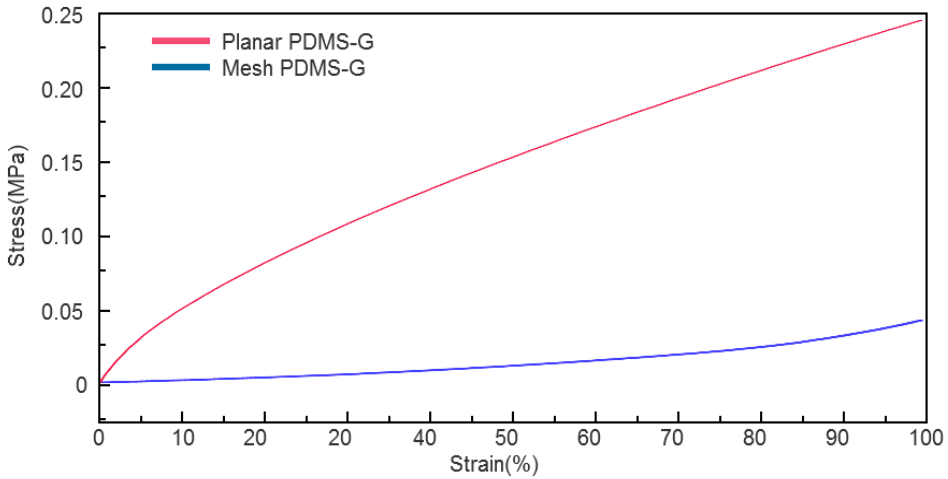


Fig. 4-20. Stress curves of planar PMDS-G and meshed PDMS-G

2) Sensitivity test

Figure 4-21-a shows the curves of relative resistance as a function of strain for G-PDMS and M-PDMS-G in 0-50%. The M-PDMS-G sensor and the PMDS-G sensor have similar sensitivity in the 0-40% strain range. The sensitivity of the M-PDMS-G sensor shows stability in the range of 0-50%, while the sensitivity of the PMDS-G sensor changes significantly from 30%. Figure 4-21-b and 4-21-c show the resistance vs strain of PDMS-G

in 50–100% and resistance vs strain of M-PDMS-G in 50–350%, respectively. The resistance value of the M-PDMS-G sensor has reached the maximum value measured by the test equipment before the break. Here, we set the value of 106 k Ω as the upper limit according to the maximum value of resistance that can be detected by the test equipment. It can be seen from Figure 4-21-b and Figure 4-21-c that the sensitivity of the PMDS-G sensor has changed greatly from 60%, while the sensitivity of the M-PDMS-G sensor changes significantly from 300%.

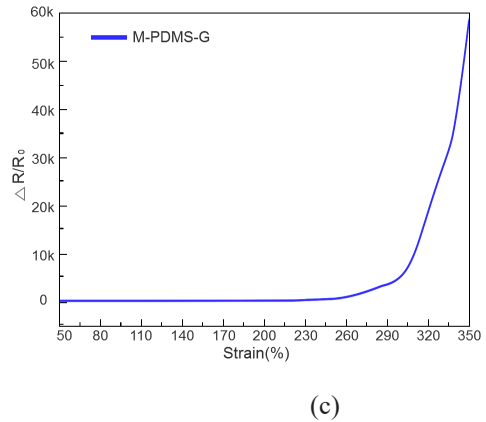
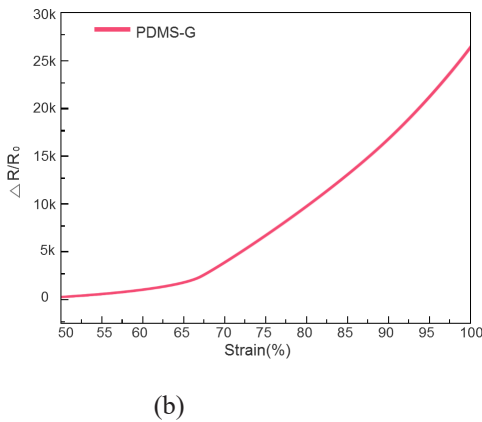
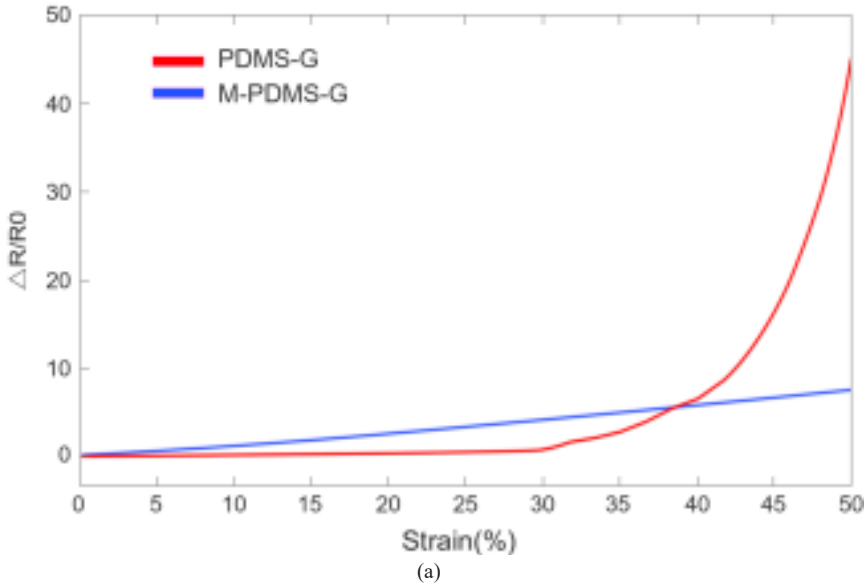


Fig. 4-21. (a) Resistance vs strain of PDMS-G and M-PDMS-G in 0–50%; (b) Resistance vs strain of PDMS-G in 50–100%; (c) Resistance vs strain of M-PDMS-G in 50–350%;

3) Cyclic stability performance

This section was designed to compare the resistance change of the two sensors after repeated stretching. Figure 4-22-a and Figure 4-22-c showed the 3-hour stability test results. Figure 4-22-b and Figure 4-22-d showed the portions of the results of two sensors for 30 seconds separately. From these diagrams, two kinds of sensors proved the advantage of stability. After 3,600 cycles of 3 consecutive hours, the response signal of two sensors barely changed. At the beginning of the test, the baseline of both sensors dropped. However, the baseline of the M-PDMS-G sensor drops more gently than that of the PDMS-G sensor.

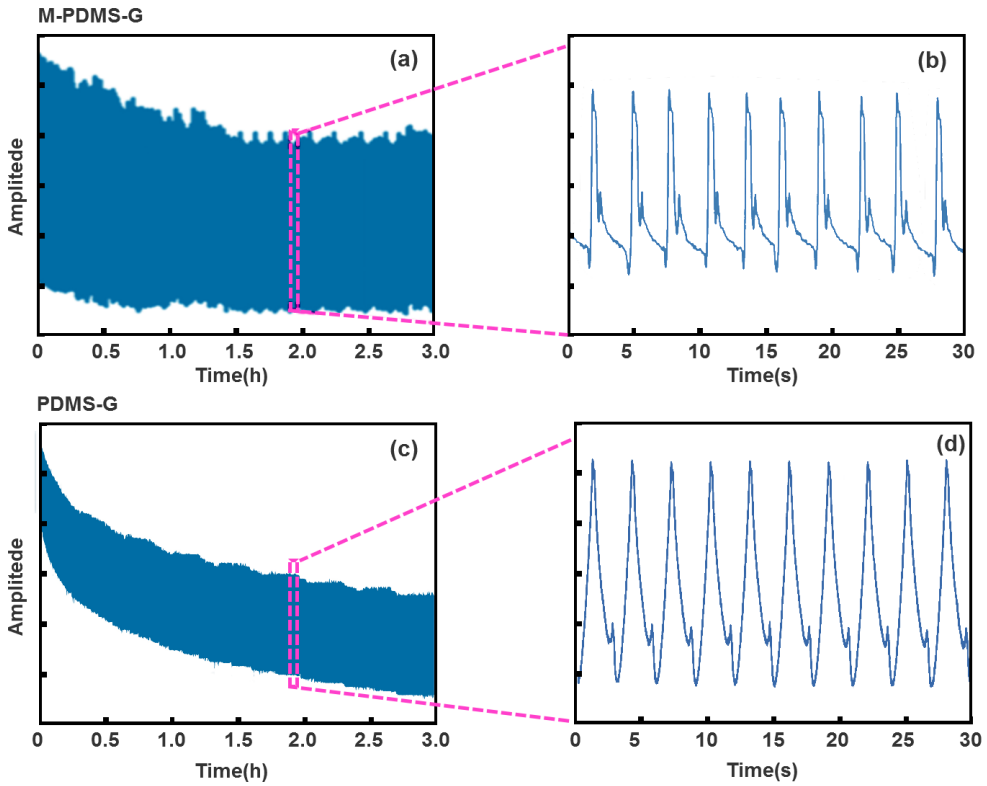


Fig. 4-22. Results of the three hours' stability test (a) overall resistance variation of M-PDMS-G sensor, (b) detailed waveform in 30 seconds of the whole test, (c) overall resistance variation of PDMS-G sensor; and (d) enlarged signals during 2370–2378 cycles.

4) Response/relaxation time of the M-PDMS-G sensor

In this experiment, Arduino was also used to test the response/relaxation time of the sensor. The real-time change of the voltage when the resistance of the sensor changes was recorded. The strain range of the sensor was fixed at 0-40%. In the process of strain, the time spent by the voltage jumping from the first stable state to the second stable state was considered to

be the response/relaxation time of the sensor.

Figure 4-23 shows the comparison of the test results of the M-PDMS-G sensor and PDMS-G sensor. The results show that the response times in tension of M-PDMS-G and PDMS-G at 0% -40% are 145ms and 308ms, and the response times in relaxation are 245ms and 372ms, respectively. The relaxation/tension response time of M-PDMS-G is shorter than that of PDMS-G, which is fast enough for respiration monitoring [226], [227].

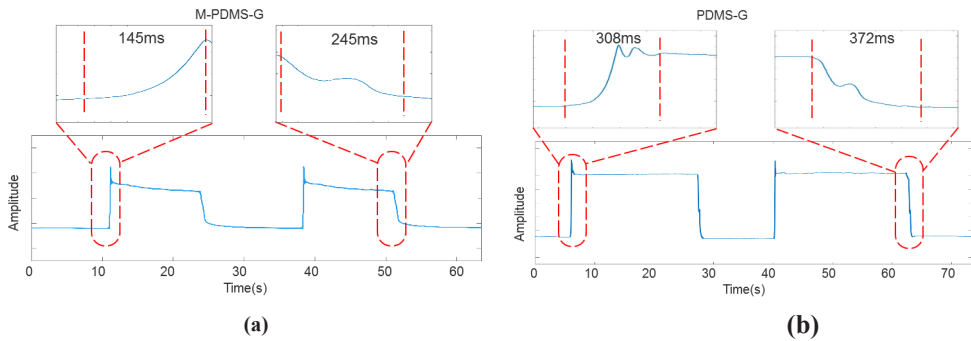


Fig. 4-23. Response/relaxation time test of the M-PDMS-G (a) and PDMS-G (b).

4.3.4. Respiration Signal Evaluation

In order to compare the performance of M-PDMS-G sensors under the multi-sensor platform (MSP), the MSP based on the M-PDMS-G sensor was compared with the respiration band of the PSG.

The experiment on the adult was carried out on a 31-year-old male volunteer for one hour. The PSG respiratory detection band was attached to the abdomen, and the PDMS-G compound tensile sensor was attached slightly lower than the PSG band. The subject sat in a chair without strenuous exercise during the experiment. PSG had a respiration sampling frequency of 32Hz. There were three aspects to be focused on, including visual comparison, mean difference in average RR and correlation between the measured RR for MSP and PSG.

The first aspect was the visual comparison. The respiratory signals acquired by MSP and PSG were compared. The similarity of the original waveform output of MSP and PSG was studied, as shown in Figure 4-24.

From Figure 4-24, the signals obtained using M-PDMS-G showed a similar beat structure of the same frequency with those of the PSG. Though the attaching positions of MSP and

PSG were a little different from each other in the abdomen region, the overall similarity and cycles of the data obtained during the inspiratory intervals were noted implying the accuracy of MSP in measuring respiration rate.

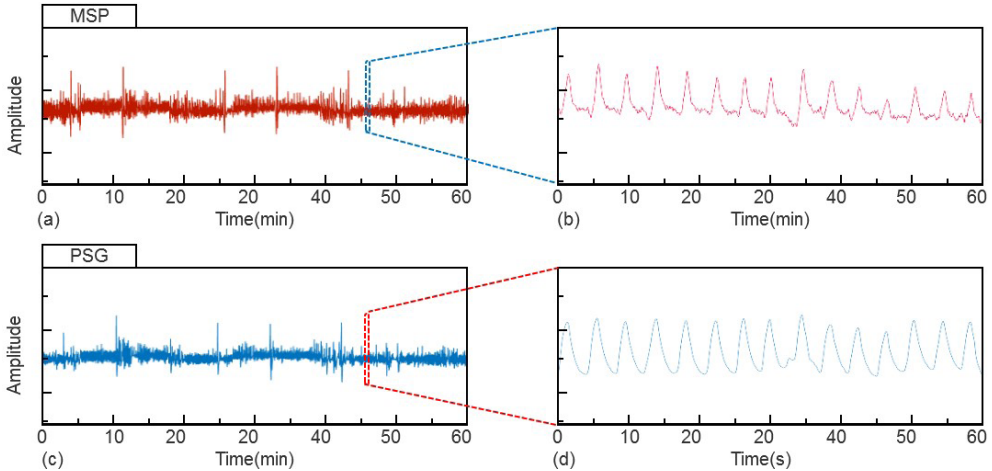


Fig. 4-24. One hour signals measured by MSP (a) and PSG (c). Detailed waveform with one minute for MSP (b) and PSG (d)

The second outcome measurement for the study was to assess the direct relationship between the average measured respiratory rate (RR) for the M-PDMS-G sensor in MSP and respiration band in PSG. Each RR point was output for a 30-second interval. The difference in average RR between monitoring techniques over this 30-second interval was summarized in the aspects of the mean, standard deviation, median and range. The effectiveness of M-PMDS-G-monitored RR versus respiration band-monitored RR was determined by 95% confidence intervals for the mean difference in average RR. A difference of three breaths per minute (bpm) was considered of minimum clinical relevance. This was chosen from the early warning system (EWS) which identifies a score difference of 3 bpm to be meaningful by defining the respiration scores in steps of 3 bpm [228]. The Pearson's Bland-Altman analysis between the RR measured for M-PDMS-G and respiration band was conducted. A total of 60 recorded RR data points were extracted from the experiment. Each RR point was spaced 30 seconds apart to ensure variable independence in Bland-Altman analysis. Comparisons of the RR (column 1) monitored by M-PMDS-G and RR (column 2) monitored by PMDS-G with RR monitored by respiration band are presented in Table 4-11. Figure 4-25-a summarized the data from the utilized 60 epochs for M-PMDS-G versus respiration band in the form of a Bland-Altman plot. The direction of difference was:

(M-PMDS-G- respiration band). The red dashed line represented the bias of the differences. Red solid lines represented the 95 % confidence limits for the differences.

The mean difference for average RR between M-PMDS-G and respiration band was less than 1 bpm, mean (SD) = 0.019 (0.59). The 95% confidence interval (CI) for the difference in average RR was calculated to be [-1.137, 1.176]. 100% of data points were within the clinically accepted error intervals of ± 3 bpm.

Table 4-11. Comparison of Average Respiratory Rate Per Minute between MSP based on M-PDMS-G with and PSG based on RIP bandage

MSP-PSG	
Number of data points	60
Mean	0.019
Standard deviation	0.59
Minimum–maximum	-1.86,1.23
95 % confidence interval	-1.137,1.176

Finally, Figure 4-25-b showed the results of the correlation analysis of the data from the utilized 60 epochs for M-PMDS-G versus respiration band. The correlation coefficient (r) of 0.988 demonstrated a very strong relationship between M-PMDS-G of MSP and the respiration band of PSG in monitoring RR. Similarly, the r of 0.988 demonstrated a strong relationship between PMDS-G and the respiration band in monitoring RR.

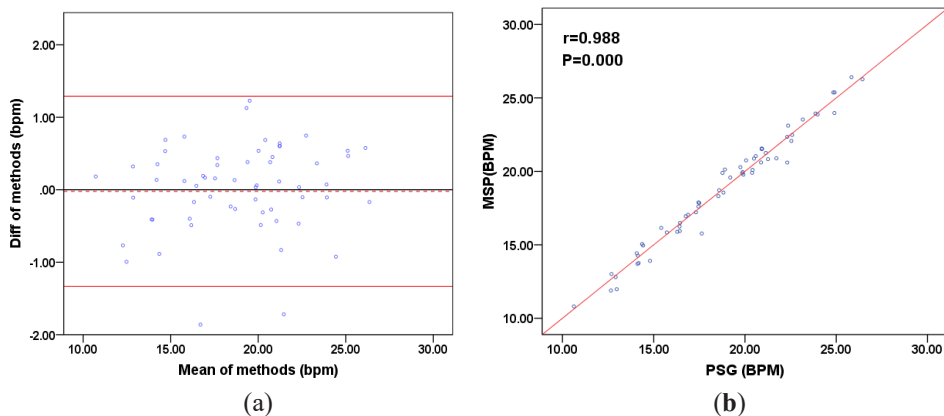


Fig. 4-25. (a) Bland-Altman plot showing MSP versus PSG. Direction of difference is (MSP-PSG); (b)Results of Correlation analysis

4.3.5. Discussion

In this section, we have shown that the M-PMDS-G sensor in MSP can measure RR on adults, with values that showing a clinically relevant agreement with those derived from respiration band in PSG. Compared with the PMDS-G sensor, the M-PMDS-G sensor has a better deformation capability and wider application scenarios.

We chose to compare the M-PMDS-G sensor in MSP to the respiration band in PSG. Although the accuracy of respiratory assessment based on the respiratory band in PSG is not as high as that based on capnography, this method is still used in hospitals.

Respiratory rate measurement derived from capnography is likely the nearest to a gold standard but is currently used only in intubated patients and is thus even more restricted in use. Future analysis of the M-PMDS-G sensor in MSP will compare it to capnography. Neonatal RR based on abdominal changes are different from adults. As a result, it is unclear whether the M-PMDS-G in MSP would detect RR of a neonate as well as respiration band in PSG. Further trials are required to demonstrate the practical aspects of device use in different populations.



Conclusion



5.1. Summary of Thesis

The thesis explored the feasibility of the application of a wearable sensor system in the field of newborn seizure monitoring, and developed a multi-mode wearable system for newborn convulsion monitoring. In addition, we also explored the performance of different ECG electrodes and graphene sensors in the detection of neonatal physiological signals. In chapter 2, we review the research status of neonatal seizure detection from following three aspects: 1. the physiological and pathological basis and present situation of monitoring physiological and behavioral signals and predicting neonatal seizure; 2. research status of wearable sensor systems for infant monitoring; 3. research status of signal processing methods for detection and prediction of neonatal seizure. There are many types of neonatal seizures. The most widely-used method is to divide neonatal seizures into four categories: subtle seizures, clonic seizures, tonic seizures and myoclonic seizures. The existing neonatal seizure detection methods mainly include EEG based detection, ECG based detection, EMG based detection and respiratory signal-based detection. For wearable technology, different wearable sensors have been used to detect different physiological signals and movement signals of neonates. Textile electrodes, various conductive electrodes and conductive ink are used to detect ECG signals. Patch electrode, three-dimensional accelerometer, piezoelectric sensor, electrochemical sensor and infrared sensor are used to detect respiratory signal. A transmission SpO₂ sensor is used to detect the SpO₂ signal. The sensors for neonatal motion detection are mainly divided into 5 types, including IMU, accelerometer, magneto-inertial, pressure sensor and flexible sensor. In addition, some researchers have developed different multi-parameter wearable monitoring systems, such as the smart jacket proposed by Chen et al. to detect ECG signals and the baby swaddle proposed by Baker et al. to detect temperature, humidity, and pulse. In data processing, different methods are utilized to tackle the complexity of physiological signals, mainly for seizure detection. Among them, three subjects as fountainheads, e.g., non-stationary signal processing, nonlinear dynamics and network science, can be roughly identified. We explore these three approaches in this chapter.

In chapter 3, we proposed to solve the problems occurring in neonatal seizure monitoring through a combination of "flexible sensor network" and "multimodal signal fusion technology". We introduced the development process of the system from three aspects: requirement discovery, technical realization and system verification. We summarized the development requirements of a wearable neonatal seizure detection system through

information retrieval, clinical observation and user interview. Based on the development requirements, we developed a wearable multi-sensor system for neonatal seizure detection. The smart vest we proposed is a unified sensing platform embedded with flexible material based non-invasive sensors. We used IMU sensors to collect infants' movement signals. At the same time, we developed flexible textile electrodes and a PDMS-G sensor to collect neonatal ECG and respiratory signals. The overall design focuses on comfort and accuracy. We carried out systematic verification about the platform which includes electrical properties of the new sensing materials, signal quality evaluation and comparison with gold standards to verify the feasibility of the system. Verification experiments proved that quality ECG signals can be obtained through the proposed flexible electrode materials with comparable performance to the commercial AgCl adhesive electrodes and accurate respiration data can be obtained through the new PDMS-Graphene compound based stretching sensor. In order to verify the clinical feasibility of the multi-sensor platform for neonatal seizure detection, permission was obtained from the Research Ethics Committee in Children's Hospital of Fudan University (approval No. (2017) 89) to recruit infant patients for neonatal seizure detection. The whole research of neonatal seizure detection includes three parts, data collection, data analysis strategy, data analysis results. 48 patients who had already experienced a seizure at our hospital and did not violate exclusion criteria were enrolled in the trial. Four patients were finally diagnosed with neonatal seizure during the test.

Based on ECG, respiration and movement signal, we implemented a patient-independent seizure detection algorithm that excluded all data from a test patient in the training phase (double leave-one-patient-out cross-validation). To allow the SVM to learn from previous examples of seizures from the test patient if that patient had more than a single seizure recording available, we also implemented double leave-one-seizure-out cross-validation. Because there exists variability between patients, we also implemented a patient-dependent seizure detection algorithm that used the data from one patient to train and test the SVM classifier.

The results show that the algorithm can automatically detect neonatal seizures. Among the four patients, 2 cases showed high sensitivity, reaching 100%, and the other two cases showed 50% and 25% sensitivity respectively. In addition, we also explored the effect of multi-signal fusion on the detection performance of neonatal seizures. The results show that multi-parameter fusion can improve the performance of neonatal seizure detection, which provides a feasible direction for the follow-up research. We tested the algorithm

through the data from four subjects with neonatal seizures occur. The results show that the algorithm can automatically detect neonatal seizures. The sensitivity of the two subjects was 100% while the sensitivity of the other two subjects was 50% and 25%, respectively. In addition, we also explored the effect of multi-signal fusion on the performance of neonatal seizure detection. The results show that multi-parameter fusion can improve the performance of neonatal seizure detection, which provides a feasible direction for the follow-up research.

In Chapter 4, we explored different new flexible sensors of ECG signal and respiration signal. For ECG monitoring, we compare the influence of electrodes made of different intelligent textiles on the quality of ECG signal, and discussed the structure of the sensor. The results present that the ECG electrodes based on RTF Fabrics show better performance than the ECG electrodes based on Medical Fabrics and Technical Fabrics. However, the performance of AG/cl electrodes is still better than that of textile electrodes. The main reason is that textile electrodes are susceptible to external interference. In addition, we presented a novel dry disposable electrode prototype. The conductive part is made of carbonized foam (CF). A test protocol focusing on characterizing several important electrical properties of the electrode is designed to investigate its performance when being used to record the surface potential. Experimental results show that the presented CF electrode is capable of acquiring surface potential like ECG with competitive signal quality. Lower powerline interference is observed from the signal acquired by CF electrodes. The issue about biocompatibility and future work about improving the intension of the material and thus the durability of the electrode are also discussed. For respiration, we designed a tensile sensor of graphene composite with the mesh structure. The larger strain range and smaller stress can be obtained by using graphene with the mesh structure. Smaller stresses have less effect on neonatal respiration. we have shown that in a clinical setting the M-PMDS-G sensor in MSP can measure RR, with values showing a clinically relevant agreement with those derived from respiration band in PSG. Compared with the PMDS sensor, the M-PMDS-G sensor has a better deformation capability and wider application scenarios. The subjects in this experiment are adults, and the neonatal RR based on abdominal changes are different from adults'. As a result, it is unclear whether the M-PMDS-G in MSP would detect RR of neonates as well as respiration band in PSG. Further trials are required to demonstrate the practical aspects of device use in different populations.

5.2. Contributions

This Ph.D. research resulted in the following contributions

1. The MSP was designed and developed. This thesis presented the design and development of a set of smart vest embedded with flexible material based non-invasive sensors for neonatal vital signal acquisition and potentially supporting neonatal seizure detection. Different from other neonatal wearable monitoring devices, MSP lays emphasis on the integration and design of multiple sensors, paying attention to the overall comfort and accuracy. Systematic verification about the platform was carried out, involving electrical properties of the new sensing materials, signal quality assessment and comparison with gold standard to validate the feasibility of the system. It is proved by verification experiments that high-quality ECG signals, equivalent to performance to the commercial AgCl adhesive electrodes, can be obtained based on the aforementioned flexible electrode materials and accurate respiration data can be obtained by the new PDMS-Graphene compound based stretching sensor. The proposed platform is expected to ensure comfort during neonatal monitoring.
2. The combination of flexible sensing network and multimodal signal (electrocardiogram, respiratory and motion signals) fusion technology was provided to solve the existing problems in neonatal seizure monitoring and make it comfortable, continuous and efficient. Based on ECG, respiration and acceleration, an algorithm for automatic neonatal seizure detection was explored to evaluate the records of 4 patients with seizures. To estimate the utility of combining ECG, respiration and movement, the performance of three seizure detectors was further compared. The first detector included features from the ECG, respiration and acceleration recordings, the second incorporated respiratory-motion based features from respiration and acceleration recordings, and the third involved ECG-based features only from the ECG recordings. Our research shows the overall performance based on multi-modal features was enhanced with a lower false alarm rate and higher F-measure compared to the detector utilizing single modal features. The proposed algorithm based on multimodal for seizure detection provides a feasible direction in this field.
3. The effects of different textile electrodes on ECG were explored. In the process of comparing the ECG electrodes based on three different textile materials from Shieldex, Ag /CL electrode was used as the gold standard while data were collected under different states. The result presents the textile electrode is promising in ECG

signal acquisition. However, Ag/Cl electrodes and textile electrodes based on RTF (Berlin RS) textile materials showed advantages under the upper body turning state and walking state. The quality of the signals collected by the electrodes based on Medical Fabrics and Technical Fabrics apparently decline under the motion state. The textile electrode made of RTF (Berlin RS) textile material performs better than that made of the other two kinds of textiles. During the motion state, the signal obtained by the RTF material-based electrode is more stable and not easily interfered with by the movement. The electrode based on RTF (Berlin RS) material under motion state has a higher R-wave recognition rate than Ag/CL electrode, but the lower power spectrum ratio value and signal kurtosis (K) value, which signifies the electrode based on RTF (Berlin RS) materials are easily affected by the external environment.

4. A novel dry disposable electrode prototype was developed. The conductive part is made of carbonized foam (CF). The test of its in-vitro impedance rules out the worry about attenuations. And the skin-to-electrode impedance introduced by the proposed electrode is comparable with state-of-art Ag/AgCl electrode. The signal quality obtained through the CF electrode has advantages, especially during motion conditions. Furthermore, the proposed CF electrode works without conductive gel. The conductive part is flexible, which is the possible reason for the CF electrode's higher tolerance on motion artefacts than Ag/AgCl electrode.
5. A novel tensile sensor was presented. To enhance the respiration sensor performance, we designed a tensile sensor of graphene composite with mesh structure (M-PDMS-G) and further compared the properties between M-PDMS-G and PDMS-G. It is found that a larger strain range and smaller stress can be acquired through graphene with the mesh structure. Smaller stresses produce less effect on neonatal respiration. The M-PMDS-G sensor in MSP can measure RR on adults, which presents a clinically accordant value with those derived from respiration band in PSG. All in all, the M-PMDS-G sensor has a better deformation capability and wider application scenarios than the PMDS-G sensor.

5.3. Limitations

This research includes hardware design, software design, algorithm design, clinical validation and so on. It is critical to carry out iterated and constant verification during each step to ensure the feasibility of the system. Due to the lack of neonatal seizure data, the

proposed multimodal fusion seizure detection algorithm has low sensitivity, making the system difficult to be applied in practice. Moreover, the seizure detection algorithm needs to be further optimized. There exist differences between each patient, possibly leading to low sensitivity. In addition, it is necessary to improve data quality, either. During the data collection, infants' crying or motion may cause low data quality and even biased results, so further validation is indispensable.

5.4. Future Work

This thesis has been dedicated to designing a multi-sensor platform for neonatal seizure detection in the past years, but there still exists extensive space to explore in the future. We now address three directions from the future perspective.

5.4.1. Clinical Data Collection and Verifications for MSP

This research only involved small-scale patient data with limited exposure to the system, unable to support the effectiveness of the system for neonatal seizure detection, which means the demand for larger sample sizes and detection outcome measurements. Therefore, data fusion techniques and optimization algorithms will be explored based on larger clinical data in future work. We will compare more seizure detectors to prove that the seizure detection algorithm based on aggregation (full) mode improves the performance of seizure detection. In addition, we can carry out a trial on the clinical effectiveness after ensured the clinical feasibility and safety of the system. The results of clinical real-time seizure detection based on MSP can be compared with traditional EEG-based seizure detection results.

5.4.2. Exploration of Sensors

Researches on MSP have mostly focused on the exploration and integration of new wearable sensor technology, which should be further developed or upgraded for the pursuit of the comfort and stability of MSP. In terms of the proposed CF electrode, the structure of the prototype has been designed to verify the usability and performance of CF as the conductive material, but a new structure for the integration of CF into real-world wearable sensor

systems is still needed and the mechanical intensity of CF should be further enhanced. We, therefore, leave these matters and the assessment of material's biocompatibility as our future work. It is noticeable that the CF electrode is likely to reduce powerline interference, which is serendipity indeed. Shielding measure and driven-leg circuits can be realized under well-structured circumstances but impractical in wearable sensor systems because of its unwieldy medical instruments. There is less demand for high-order digital filters which avoids continuous and intensive computation, conducive to keep low power consumption of the whole system. We, therefore, try to find out its root cause and eliminate the influence of possible irrelevant variables in our further work. Furthermore, the proposed M-PDMS-G sensor still needs further verification due to the difference between adults' and neonatal RR based on abdominal changes. As a result, it is still a mystery whether the M-PMDS-G in MSP would detect neonatal RR as well as respiration band in PSG. Further trials are needed to prove the practical application of the device in different populations. In addition, the development of wearable sensors with different signals for seizure detection, such as the sensors for monitoring mouth movements or eye movements, remains the next important step. These signals, related to seizures, can be integrated into the algorithm to increase the precision of seizure detection in the future.

Reference

- [1] D. R. Nordli, C. W. Bazil, M. L. Scheuer, and T. A. Pedley, ‘Recognition and classification of seizures in infants’, *Epilepsia*, vol. 38, no. 5, pp. 553–560, May 1997, doi: 10.1111/j.1528-1157.1997.tb01140.x.
- [2] R. Jm, ‘Neonatal seizures’, *Eur. J. Pediatr.*, vol. 156, no. 2, pp. 83–87, Feb. 1997, doi: 10.1007/s004310050559.
- [3] R. R. Clancy, ‘Summary proceedings from the neurology group on neonatal seizures’, *Pediatrics*, vol. 117, no. 3 Pt 2, pp. S23-27, Mar. 2006, doi: 10.1542/peds.2005-0620D.
- [4] Dan Chen and Jian Mao, ‘Neonatal seizure’, *Chin. J. Pract. Pediatr.*, no. 1, pp. 77–79, 2010.
- [5] C. Campbell and G. W. and P. Jacob, ‘Seizure-associated brain injury in term newborns with perinatal asphyxia’, Nov. 2020, Accessed: Nov. 12, 2020. [Online]. Available: <https://n.neurology.org/content/seizure-associated-brain-injury-term-newborns-perinatal-asphyxia>.
- [6] B. R. Tharp, ‘Neonatal Seizures and Syndromes’, *Epilepsia*, vol. 43, no. s3, pp. 2–10, 2002, doi: <https://doi.org/10.1046/j.1528-1157.43.s.3.11.x>.
- [7] B. J. Fisch, ‘Current Practice of Clinical Electroencephalography, Third Edition’, *J. Clin. Neurophysiol.*, vol. 20, no. 3, p. 225, Jun. 2003.
- [8] X. Zhu, ‘Clinical analysis of neonatal seizure and its diagnostic value of aEEG’, Fudan University, 2012.
- [9] M. C. Toet and P. M. A. Lemmers, ‘Brain monitoring in neonates’, *Early Hum. Dev.*, vol. 85, no. 2, pp. 77–84, Feb. 2009, doi: 10.1016/j.earlhumdev.2008.11.007.
- [10] B. R. Greene, S. Faul, W. P. Marnane, G. Lightbody, I. Korotchikova, and G. B. Boylan, ‘A comparison of quantitative EEG features for neonatal seizure detection’, *Clin. Neurophysiol.*, vol. 119, no. 6, pp. 1248–1261, Jun. 2008, doi: 10.1016/j.clinph.2008.02.001.
- [11] W. Chen, J. Hu, S. Bouwstra, S. B. Oetomo, and Loe Feijs, ‘Sensor integration for

- perinatology research', *Int. J. Sens. Netw.*, vol. 9, no. 1, pp. 38–49, Dec. 2010, doi: 10.1504/IJSNet.2011.037303.
- [12] S. Bouwstra, W. Chen, S. B. Oetomo, L. M. G. Feijs, and P. J. M. Cluitmans, 'Designing for reliable textile neonatal ECG monitoring using multi-sensor recordings', in *2011 Annual International Conference of the IEEE Engineering in Medicine and Biology Society*, Aug. 2011, pp. 2488–2491, doi: 10.1109/IEMBS.2011.6090690.
- [13] Chen, H. et al., 'A wearable sensor system for neonatal seizure monitoring', May 2017, doi: 10.1109/bsn.2017.7935999.
- [14] G. Fortino, R. Giannantonio, R. Gravina, P. Kuryloski, and R. Jafari, 'Enabling Effective Programming and Flexible Management of Efficient Body Sensor Network Applications', *IEEE Trans. Hum.-Mach. Syst.*, vol. 43, no. 1, pp. 115–133, Jan. 2013, doi: 10.1109/TSMCC.2012.2215852.
- [15] J. van Andel, R. D. Thijs, A. de Weerd, J. Arends, and F. Leijten, 'Non-EEG based ambulatory seizure detection designed for home use: What is available and how will it influence epilepsy care?', *Epilepsy Behav.*, vol. 57, pp. 82–89, Apr. 2016, doi: 10.1016/j.yebeh.2016.01.003.
- [16] A. Van de Vel et al., 'Non-EEG seizure-detection systems and potential SUDEP prevention: State of the art', *Seizure*, vol. 22, no. 5, pp. 345–355, Jun. 2013, doi: 10.1016/j.seizure.2013.02.012.
- [17] H. Chen, M. Xue, Z. Mei, S. Bambang Oetomo, and W. Chen, 'A Review of Wearable Sensor Systems for Monitoring Body Movements of Neonates', *Sensors*, vol. 16, no. 12, Art. no. 12, Dec. 2016, doi: 10.3390/s16122134.
- [18] Z. Zhu, T. Liu, G. Li, T. Li, and Y. Inoue, 'Wearable Sensor Systems for Infants', *Sensors*, vol. 15, no. 2, Art. no. 2, Feb. 2015, doi: 10.3390/s150203721.
- [19] G. Orengo, A. Lagati, and G. Saggio, 'Modeling Wearable Bend Sensor Behavior for Human Motion Capture', *IEEE Sens. J.*, vol. 14, no. 7, pp. 2307–2316, Jul. 2014, doi: 10.1109/JSEN.2014.2309997.
- [20] P. Zhao, N. Deng, X. Li, C. Ren, and Z. Wang, 'Development of highly-sensitive and ultra-thin silicon stress sensor chips for wearable biomedical applications', *Sens. Actuators Phys.*, vol. 216, pp. 158–166, Sep. 2014, doi: 10.1016/j.sna.2014.05.018.
- [21] S. Salman, L. Z. Lee, and J. L. Volakis, 'A Wearable Wrap-Around Sensor for Monitoring Deep Tissue Electric Properties', *IEEE Sens. J.*, vol. 14, no. 8, pp. 2447–2451, Aug. 2014, doi: 10.1109/JSEN.2014.2323896.

- [22] C. Linti, H. Horter, P. Osterreicher, and H. Planck, ‘Sensory baby vest for the monitoring of infants’, in International Workshop on Wearable and Implantable Body Sensor Networks (BSN’06), Apr. 2006, p. 3 pp. – 137, doi: 10.1109/BSN.2006.49.
- [23] W. Chen, S. Dols, S. B. Oetomo, and L. Feijs, ‘Monitoring body temperature of newborn infants at neonatal intensive care units using wearable sensors’, in Proceedings of the Fifth International Conference on Body Area Networks, Corfu, Greece, Sep. 2010, pp. 188–194, doi: 10.1145/2221924.2221960.
- [24] S. Bouwstra, W. Chen, L. Feijs, and S. B. Oetomo, ‘Smart Jacket Design for Neonatal Monitoring with Wearable Sensors’, in 2009 Sixth International Workshop on Wearable and Implantable Body Sensor Networks, Jun. 2009, pp. 162–167, doi: 10.1109/BSN.2009.40.
- [25] Y. Rimet et al., ‘Surveillance of infants at risk of apparent life threatening events (ALTE) with the BBA bootee: a wearable multiparameter monitor’, in 2007 29th Annual International Conference of the IEEE Engineering in Medicine and Biology Society, Aug. 2007, pp. 4997–5000, doi: 10.1109/IEMBS.2007.4353462.
- [26] H. Cao, L. Hsu, T. Ativanichayaphong, J. Sin, and J.- Chiao, ‘A non-invasive and remote infant monitoring system using CO2 sensors’, in 2007 IEEE SENSORS, Oct. 2007, pp. 989–992, doi: 10.1109/ICSENS.2007.4388570.
- [27] I. Murković, M. D. Steinberg, and B. Murković, ‘Sensors in neonatal monitoring: current practice and future trends’, Technol. Health Care Off. J. Eur. Soc. Eng. Med., vol. 11, no. 6, pp. 399–412, 2003.
- [28] E. McAdams et al., ‘Wearable sensor systems: The challenges’, in 2011 Annual International Conference of the IEEE Engineering in Medicine and Biology Society, Aug. 2011, pp. 3648–3651, doi: 10.1109/IEMBS.2011.6090614.
- [29] Yock P G et al., Biodesign: the process of innovating medical technologies. Cambridge University Press. 2015.
- [30] F. S. Silverstein and F. E. Jensen, ‘Neonatal seizures’, Ann. Neurol., vol. 62, no. 2, pp. 112–120, 2007, doi: <https://doi.org/10.1002/ana.21167>.
- [31] ‘Catalogo Biblioteca ELAM - Diagnosis and Management of Neonatal Seizures’. <http://catalogobibliotecaelam.sld.cu/index.php?P=FullRecord&ID=200> (accessed Nov. 29, 2020).
- [32] C. P. Panayiotopoulos, ‘Neonatal epileptic seizures and neonatal epileptic syndromes’, in A Clinical Guide to Epileptic Syndromes and their Treatment, C. P.

- Panayiotopoulos, Ed. London: Springer, 2010, pp. 237–258.
- [33] O. M. Doyle, A. Temko, W. Marnane, G. Lightbody, and G. B. Boylan, ‘Heart rate based automatic seizure detection in the newborn’, *Med. Eng. Phys.*, vol. 32, no. 8, pp. 829–839, Oct. 2010, doi: 10.1016/j.medengphy.2010.05.010.
- [34] C. P. Panayiotopoulos, *A Clinical Guide to Epileptic Syndromes and their Treatment*. Springer, 2010.
- [35] Pressler R M, Cilio M R, Mizrahi E M, et al. The ILAE classification of seizures and the epilepsies: Modification for seizures in the neonate. Position paper by the ILAE Task Force on Neonatal Seizures[J]. *Epilepsia*, 2021, 62(3): 615-628.
- [36] B. Kamalizonouzi, ‘Optimal Inertial Sensor Placement and Motion Detection for Epileptic Seizure Patient Monitoring’, *Electron. Thesis Diss. Repos.*, Dec. 2012, [Online]. Available: <https://ir.lib.uwo.ca/etd/990>.
- [37] W. Chen, S. Bambang Oetomo, L. Feijs, S. Bouwstra, I. Ayoola, and S. Dols, ‘Design of an Integrated Sensor Platform for Vital Sign Monitoring of Newborn Infants at Neonatal Intensive Care Units’, *Journal of Healthcare Engineering*, 2010. <https://www.hindawi.com/journals/jhe/2010/124270/> (accessed Nov. 11, 2020).
- [38] L. Ivonin, H.-M. Chang, M. Diaz, A. Catala, W. Chen, and M. Rauterberg, ‘Traces of Unconscious Mental Processes in Introspective Reports and Physiological Responses’, *PLOS ONE*, vol. 10, no. 4, p. e0124519, Apr. 2015, doi: 10.1371/journal.pone.0124519.
- [39] Chen, W, Augusto, J. C., and Seoane, F, Recent Advances in Ambient Assisted Living - Bridging Assistive Technologies, E-Health and Personalized Health Care. .
- [40] Q. Wang, W. Chen, A. A. A. Timmermans, C. Karachristos, J. B. Martens, and P. Markopoulos, ‘Smart Rehabilitation Garment for posture monitoring’, in 2015 37th Annual International Conference of the IEEE Engineering in Medicine and Biology Society (EMBC), Aug. 2015, pp. 5736–5739, doi: 10.1109/EMBC.2015.7319695.
- [41] K. Frederiks, M. Croes, W. Chen, S. Bambang Oetomo, and P. Sterkenburg, ‘Sense – a biofeedback system to support the interaction between parents and their child with the Prader-Willi syndrome: A pilot study’, *J. Ambient Intell. Smart Environ.*, vol. 7, no. 4, pp. 449–459, Jul. 2015, doi: 10.3233/AIS-150327.
- [42] I. Ayoola, W. Chen, and L. Feijs, ‘Camera on Vessel: A Camera-Based System to Measure Change in Water Volume in a Drinking Glass’, *Sensors*, vol. 15, no. 9, Art. no. 9, Sep. 2015, doi: 10.3390/s150923847.
- [43] X. Shao, *Brain damage of fetuses and newborns*. Shanghai Science and Technology

- Education Publishing House, 2008.
- [44] 埃伯索尔, ‘Modern clinical electroencephalography’, Peoples Med. Publ. HousePMPH, 2009.
- [45] M. BalaKrishnan, P. Colditz, and B. Boashash, ‘A Multi-Channel Fusion Based Newborn Seizure Detection’, J. Biomed. Sci. Eng., vol. 2014, Jun. 2014, doi: 10.4236/jbise.2014.78055.
- [46] B. Boashash, H. Barki, and S. Ouelha, ‘Performance evaluation of time-frequency image feature sets for improved classification and analysis of non-stationary signals: Application to newborn EEG seizure detection’, Knowl.-Based Syst., vol. 132, pp. 188–203, Sep. 2017, doi: 10.1016/j.knosys.2017.06.015.
- [47] D. K. Shah, L. S. de Vries, L. Hellström-Westas, M. C. Toet, and T. E. Inder, ‘Amplitude-Integrated Electroencephalography in the Newborn: A Valuable Tool’, Pediatrics, vol. 122, no. 4, pp. 863–865, Oct. 2008, doi: 10.1542/peds.2008-1000.
- [48] A. Rakshasbhuvankar, S. Paul, L. Nagarajan, S. Ghosh, and S. Rao, ‘Amplitude-integrated EEG for detection of neonatal seizures: a systematic review’, Seizure, vol. 33, pp. 90–98, Dec. 2015, doi: 10.1016/j.seizure.2015.09.014.
- [49] L. Hellström-Westas, ‘Continuous Electroencephalography Monitoring of the Preterm Infant’, Clin. Perinatol., vol. 33, no. 3, pp. 633–647, Sep. 2006, doi: 10.1016/j.clp.2006.06.003.
- [50] M. Qaraqe, M. Ismail, E. Serpedin, and H. Zulfi, ‘Epileptic seizure onset detection based on EEG and ECG data fusion’, Epilepsy Behav., vol. 58, pp. 48–60, May 2016, doi: 10.1016/j.yebeh.2016.02.039.
- [51] A. J. Camm, M. Malik, J. T. Bigger, G. Breithardt, Cerutti, S, and Cohen, R. J, ‘Heart rate variability. Standards of measurement, physiological interpretation, and clinical use’, Ann. Noninvasive Electrocardiol., vol. 1, no. 2, pp. 151–181, 1996, doi: <https://doi.org/10.1111/j.1542-474X.1996.tb00275.x>.
- [52] I. Osorio, ‘Automated seizure detection using ekg’, Int. J. Neural Syst., vol. 24, no. 02, p. 1450001, Sep. 2013, doi: 10.1142/S0129065714500014.
- [53] I. Osorio and B. F. J. Manly, ‘Is seizure detection based on EKG clinically relevant?’, Clin. Neurophysiol., vol. 125, no. 10, pp. 1946–1951, Oct. 2014, doi: 10.1016/j.clinph.2014.01.026.
- [54] E. Kolsal et al., ‘Can heart rate variability in children with epilepsy be used to predict seizures?’, Seizure, vol. 23, no. 5, pp. 357–362, May 2014, doi: 10.1016/j.seizure.2014.01.025.

- [55] M. B. Malarvili, M. Mesbah, and B. Boashash, 'Time-Frequency Analysis of Heart Rate Variability for Neonatal Seizure Detection', *EURASIP J. Adv. Signal Process.*, vol. 2007, no. 1, p. 050396, Dec. 2007, doi: 10.1155/2007/50396.
- [56] K. Fujiwara et al., 'Epileptic Seizure Prediction Based on Multivariate Statistical Process Control of Heart Rate Variability Features', *IEEE Trans. Biomed. Eng.*, vol. 63, no. 6, pp. 1321–1332, Jun. 2016, doi: 10.1109/TBME.2015.2512276.
- [57] I. Conradsen, S. Beniczky, P. Wolf, P. Jennum, and H. B. D. Sorensen, 'Evaluation of novel algorithm embedded in a wearable sEMG device for seizure detection', in *2012 Annual International Conference of the IEEE Engineering in Medicine and Biology Society*, Aug. 2012, pp. 2048–2051, doi: 10.1109/EMBC.2012.6346361.
- [58] M.-Z. Poh et al., 'Convulsive seizure detection using a wrist-worn electrodermal activity and accelerometry biosensor', *Epilepsia*, vol. 53, no. 5, pp. e93–e97, 2012, doi: <https://doi.org/10.1111/j.1528-1167.2012.03444.x>.
- [59] Sharbrough F, 'American Electroencephalographic Society guidelines for standard electrode position nomenclature', *J Clin Neurophysiol*, pp. 200–202, 1991.
- [60] S. Narayanan and P. G. Georgiou, 'Behavioral Signal Processing: Deriving Human Behavioral Informatics From Speech and Language', *Proc. IEEE*, vol. 101, no. 5, pp. 1203–1233, May 2013, doi: 10.1109/JPROC.2012.2236291.
- [61] S. Beniczky, T. Polster, T. W. Kjaer, and H. Hjalgrim, 'Detection of generalized tonic–clonic seizures by a wireless wrist accelerometer: A prospective, multicenter study', *Epilepsia*, vol. 54, no. 4, pp. e58–e61, 2013, doi: <https://doi.org/10.1111/epi.12120>.
- [62] C. R. Baker et al., 'Wireless Sensor Networks for Home Health Care', in *21st International Conference on Advanced Information Networking and Applications Workshops (AINAW'07)*, May 2007, vol. 2, pp. 832–837, doi: 10.1109/AINAW.2007.376.
- [63] Y. Nishida, K. Hiratsuka, and H. Mizoguchi, 'Prototype of Infant Drowning Prevention System at Home with Wireless Accelerometer', in *2007 IEEE SENSORS*, Oct. 2007, pp. 1209–1212, doi: 10.1109/ICSENS.2007.4388626.
- [64] S. Patel, H. Park, P. Bonato, L. Chan, and M. Rodgers, 'A review of wearable sensors and systems with application in rehabilitation', *J. NeuroEngineering Rehabil.*, vol. 9, no. 1, p. 21, Apr. 2012, doi: 10.1186/1743-0003-9-21.
- [65] T. Pola and J. Vanhala, 'Textile Electrodes in ECG Measurement', in *Sensor Networks and Information 2007 3rd International Conference on Intelligent Sensors*,

- Dec. 2007, pp. 635–639, doi: 10.1109/ISSNIP.2007.4496917.
- [66] L. Guo, T. Bashir, E. Bresky, and N.-K. Persson, ‘28 - Electroconductive textiles and textile-based electromechanical sensors—integration in as an approach for smart textiles’, in *Smart Textiles and their Applications*, V. Koncar, Ed. Oxford: Woodhead Publishing, 2016, pp. 657–693.
- [67] Y.-H. Chen et al., ‘Soft, Comfortable Polymer Dry Electrodes for High Quality ECG and EEG Recording’, *Sensors*, vol. 14, no. 12, Art. no. 12, Dec. 2014, doi: 10.3390/s141223758.
- [68] J.-Y. Baek, J.-H. An, J.-M. Choi, K.-S. Park, and S.-H. Lee, ‘Flexible polymeric dry electrodes for the long-term monitoring of ECG’, *Sens. Actuators Phys.*, vol. 143, no. 2, pp. 423–429, May 2008, doi: 10.1016/j.sna.2007.11.019.
- [69] S. Peng, K. Xu, S. Bao, Y. Yuan, C. Dai, and W. Chen, ‘Flexible Electrodes-Based Smart Mattress for Monitoring Physiological Signals of Heart and Autonomic Nerves in a Non-Contact Way’, *IEEE Sens. J.*, vol. 21, no. 1, pp. 6–15, Jan. 2021, doi: 10.1109/JSEN.2020.3012697.
- [70] Z. Wang, C. Chen, L. Tao, X. Zhao, W. Yuan, and W. Chen, ‘An Unconstrained Cardiac Monitoring System With Novel Dual Tripolar Concentric Ring Geometry-Based Flexible Active ECG Electrodes for Sleep Health Surveillance’, *IEEE Access*, vol. 7, pp. 142176–142189, 2019, doi: 10.1109/ACCESS.2019.2943602.
- [71] N. Meziane, J. G. Webster, M. Attari, and A. J. Nimunkar, ‘Dry electrodes for electrocardiography’, *Physiol. Meas.*, vol. 34, no. 9, pp. R47–R69, Aug. 2013, doi: 10.1088/0967-3334/34/9/R47.
- [72] A. Gruetzmänn, S. Hansen, and J. Müller, ‘Novel dry electrodes for ECG monitoring’, *Physiol. Meas.*, vol. 28, no. 11, pp. 1375–1390, Nov. 2007, doi: 10.1088/0967-3334/28/11/005.
- [73] R. Parashkov, E. Becker, T. Riedl, H.-Johannes, and W. Kowalsky, ‘Large Area Electronics Using Printing Methods’, *Proc. IEEE*, vol. 93, no. 7, pp. 1321–1329, Jul. 2005, doi: 10.1109/JPROC.2005.850304.
- [74] F. Q. Al-Khalidi, R. Saatchi, D. Burke, H. Elphick, and S. Tan, ‘Respiration rate monitoring methods: a review’, *Pediatr. Pulmonol.*, vol. 46, no. 6, pp. 523–529, Jun. 2011, doi: 10.1002/ppul.21416.
- [75] T. S. Chadha et al., ‘Validation of Respiratory Inductive Plethysmography Using Different Calibration Procedures’, *Am. Rev. Respir. Dis.*, vol. 125, no. 6, pp. 644–649, Jun. 1982, doi: 10.1164/arrd.1982.125.6.644.

-
- [76] J. Vertens et al., ‘Measuring Respiration and Heart Rate using Two Acceleration Sensors on a Fully Embedded Platform’, Nov. 2015, vol. 2, pp. 15–23, doi: 10.5220/0005604000150023.
- [77] Z. Zhang, W. Wang, B. Wang, H. Wu, H. Liu, and Y. Zhang, ‘A Prototype of Wearable Respiration Biofeedback Platform and Its Preliminary Evaluation on Cardiovascular Variability’, in 2009 3rd International Conference on Bioinformatics and Biomedical Engineering, Jun. 2009, pp. 1–4, doi: 10.1109/ICBBE.2009.5162230.
- [78] H. Cao, L. Hsu, T. Ativanichayaphong, J. Sin, H. E. Stephanou, and J.- Chiao, ‘An Infant Monitoring System Using CO/sub 2/ Sensors’, in 2007 IEEE International Conference on RFID, Mar. 2007, pp. 134–140, doi: 10.1109/RFID.2007.346161.
- [79] C.-H. Hsu and J. C. Chow, ‘Design and clinic monitoring of a newly developed non-attached infant apnea monitor’, Biomed. Eng. Appl. Basis Commun., vol. 17, no. 03, pp. 126–134, Jun. 2005, doi: 10.4015/S1016237205000202.
- [80] Y. Mendelson, R. J. Duckworth, and G. Comtois, ‘A Wearable Reflectance Pulse Oximeter for Remote Physiological Monitoring’, in 2006 International Conference of the IEEE Engineering in Medicine and Biology Society, Aug. 2006, pp. 912–915, doi: 10.1109/IEMBS.2006.260137.
- [81] Y. Mendelson, ‘Pulse Oximetry: Theory and Applications for Noninvasive Monitoring’, Clin. Chem., vol. 38, no. 9, pp. 1601–1607, Sep. 1992, doi: 10.1093/clinchem/38.9.1601.
- [82] S. B. Oetomo, W. Chen, and L. Feijs, ‘Neonatal Monitoring: Current Practice and Future Trends’, Neonatal Monitoring Technologies: Design for Integrated Solutions, 2012. www.igi-global.com/chapter/content/65262 (accessed Nov. 12, 2020).
- [83] Q. Cai, J. Sun, L. Xia, and X. Zhao, ‘Implementation of a wireless pulse oximeter based on wrist band sensor’, in 2010 3rd International Conference on Biomedical Engineering and Informatics, Oct. 2010, vol. 5, pp. 1897–1900, doi: 10.1109/BMEI.2010.5639534.
- [84] O. Abdallah and A. Bolz, ‘Signal Processing by Reflectance Pulse Oximetry for Monitoring the fractional Oxygen Saturation and the Detektion of Anemia’, in World Congress on Medical Physics and Biomedical Engineering 2006, Berlin, Heidelberg, 2007, pp. 1152–1155, doi: 10.1007/978-3-540-36841-0_277.
- [85] M. Maattala, A. Konttila, E. Alasaarela, and W. Chung, ‘Optimum Place for Measuring Pulse Oximeter Signal in Wireless Sensor-Belt or Wrist-Band’, in 2007

- International Conference on Convergence Information Technology (ICCIT 2007), Nov. 2007, pp. 1856–1861, doi: 10.1109/ICCIT.2007.63.
- [86] J. Sola et al., ‘SpO2 Sensor Embedded in a Finger Ring: design and implementation’, in 2006 International Conference of the IEEE Engineering in Medicine and Biology Society, Aug. 2006, pp. 4295–4298, doi: 10.1109/IEMBS.2006.260820.
- [87] W. Chen, I. Ayoola, S. B. Oetomo, and L. Feijs, ‘Non-invasive blood oxygen saturation monitoring for neonates using reflectance pulse oximeter’, in 2010 Design, Automation Test in Europe Conference Exhibition (DATE 2010), Mar. 2010, pp. 1530–1535, doi: 10.1109/DATE.2010.5457054.
- [88] A. J. Spittle, L. W. Doyle, and R. N. Boyd, ‘A systematic review of the clinimetric properties of neuromotor assessments for preterm infants during the first year of life’, *Dev. Med. Child Neurol.*, vol. 50, no. 4, pp. 254–266, 2008, doi: <https://doi.org/10.1111/j.1469-8749.2008.02025.x>.
- [89] E. C. Cameron, V. Maehle, and J. Reid, ‘The effects of an early physical therapy intervention for very preterm, very low birth weight infants: a randomized controlled clinical trial’, *Pediatr. Phys. Ther. Off. Publ. Sect. Pediatr. Am. Phys. Ther. Assoc.*, vol. 17, no. 2, pp. 107–119, 2005, doi: 10.1097/01.pep.0000163073.50852.58.
- [90] P. H. Casey, R. H. Bradley, L. Whiteside-Mansell, K. Barrett, J. M. Gossett, and P. M. Simpson, ‘Effect of Early Intervention on 8-Year Growth Status of Low-Birth-Weight Preterm Infants’, *Arch. Pediatr. Adolesc. Med.*, vol. 163, no. 11, Nov. 2009, doi: 10.1001/archpediatrics.2009.192.
- [91] A. F. Bos, ‘Differential effects of brain lesions and systemic disease on the quality of general movements: a preliminary report’, *Early Hum. Dev.*, vol. 34, no. 1, pp. 39–45, Sep. 1993, doi: 10.1016/0378-3782(93)90039-W.
- [92] E. Lee, ‘Baby by the numbers [Resources Tools]’, *IEEE Spectr.*, vol. 6, no. 52, p. 24, 2015, doi: 10.1109/MSPEC.2015.7115553.
- [93] A. Rihar, M. Mihelj, J. Pašič, J. Kolar, and M. Munih, ‘Infant trunk posture and arm movement assessment using pressure mattress, inertial and magnetic measurement units (IMUs)’, *J. NeuroEngineering Rehabil.*, vol. 11, no. 1, p. 133, Sep. 2014, doi: 10.1186/1743-0003-11-133.
- [94] F. Taffoni, V. Focaroli, D. Formica, E. Gugliemelli, F. Keller, and J. M. Iverson, ‘Sensor-based technology in the study of motor skills in infants at risk for ASD’, in 2012 4th IEEE RAS EMBS International Conference on Biomedical

- Robotics and Biomechanics (BioRob), Jun. 2012, pp. 1879–1883, doi: 10.1109/BioRob.2012.6290922.
- [95] B. A. Smith, I. A. Trujillo-Priego, C. J. Lane, J. M. Finley, and F. B. Horak, ‘Daily Quantity of Infant Leg Movement: Wearable Sensor Algorithm and Relationship to Walking Onset’, *Sensors*, vol. 15, no. 8, Art. no. 8, Aug. 2015, doi: 10.3390/s150819006.
- [96] M. Singh and D. J. Patterson, ‘Involuntary gesture recognition for predicting cerebral palsy in high-risk infants’, in *International Symposium on Wearable Computers (ISWC) 2010*, Oct. 2010, pp. 1–8, doi: 10.1109/ISWC.2010.5665873.
- [97] E. Saadatian et al., ‘Low cost infant monitoring and communication system’, in *2011 IEEE Colloquium on Humanities, Science and Engineering*, Dec. 2011, pp. 503–508, doi: 10.1109/CHUSER.2011.6163782.
- [98] F. Heinze, K. Hesels, N. Breitbach-Faller, T. Schmitz-Rode, and C. Disselhorst-Klug, ‘Movement analysis by accelerometry of newborns and infants for the early detection of movement disorders due to infantile cerebral palsy’, *Med. Biol. Eng. Comput.*, vol. 48, no. 8, pp. 765–772, Aug. 2010, doi: 10.1007/s11517-010-0624-z.
- [99] H. Gima, S. Ohgi, S. Morita, H. Karasuno, T. Fujiwara, and K. Abe, ‘A Dynamical System Analysis of the Development of Spontaneous Lower Extremity Movements in Newborn and Young Infants’, *J. Physiol. Anthropol.*, vol. 30, no. 5, pp. 179–186, 2011, doi: 10.2114/jpa2.30.179.
- [100] S. Boughorbel, F. Bruekers, and J. Breebaart, ‘Baby-Posture Classification from Pressure-Sensor Data’, in *2010 20th International Conference on Pattern Recognition*, Aug. 2010, pp. 556–559, doi: 10.1109/ICPR.2010.141.
- [101] M. Fan, D. Gravem, D. M. Cooper, and D. J. Patterson, ‘Augmenting gesture recognition with erlang-cox models to identify neurological disorders in premature babies’, in *Proceedings of the 2012 ACM Conference on Ubiquitous Computing*, Pittsburgh, Pennsylvania, Sep. 2012, pp. 411–420, doi: 10.1145/2370216.2370278.
- [102] S. Waldmeier et al., ‘Correlation properties of spontaneous motor activity in healthy infants: a new computer-assisted method to evaluate neurological maturation’, *Exp. Brain Res.*, vol. 227, no. 4, pp. 433–446, Jun. 2013, doi: 10.1007/s00221-013-3504-6.
- [103] D. Gravem et al., ‘Assessment of Infant Movement With a Compact Wireless Accelerometer System’, *J. Med. Devices*, vol. 6, no. 2, Jun. 2012, doi: 10.1115/1.4006129.

- [104] D. H. Abney, A. S. Warlaumont, A. Haussman, J. M. Ross, and S. Wallot, 'Using nonlinear methods to quantify changes in infant limb movements and vocalizations', *Front. Psychol.*, vol. 5, 2014, doi: 10.3389/fpsyg.2014.00771.
- [105] Wei Lin, R. Zhang, J. Brittelli, and C. Lehmann, 'Wireless Infant Monitoring Device for the prevention of sudden infant death syndrome', in 2014 11th International Conference Expo on Emerging Technologies for a Smarter World (CEWIT), Oct. 2014, pp. 1–4, doi: 10.1109/CEWIT.2014.7021146.
- [106] E. Department and R. Singh, *Infant Monitoring and Fall Avoidance System using Tri-Axial Accelerometer and ARM7 Microcontroller* Aryan Kaushik Student. .
- [107] G. R. Hayes, D. J. Patterson, M. Singh, D. Gravem, J. Rich, and D. Cooper, 'Supporting the transition from hospital to home for premature infants using integrated mobile computing and sensor support', *Pers. Ubiquitous Comput.*, vol. 15, no. 8, pp. 871–885, Dec. 2011, doi: 10.1007/s00779-011-0402-4.
- [108] P. Jourand, H. De Clercq, and R. Puers, 'Robust monitoring of vital signs integrated in textile', *Sens. Actuators Phys.*, vol. 161, no. 1, pp. 288–296, Jun. 2010, doi: 10.1016/j.sna.2010.05.002.
- [109] G. López, M. López, and L. A. Guerrero, 'An Augmented Object Prototype for Helping to Prevent the Sudden Infant Death Syndrome', in *Ambient Assisted Living and Active Aging*, Cham, 2013, pp. 132–135, doi: 10.1007/978-3-319-03092-0_20.
- [110] H. De Clercq, P. Jourand, and R. Puers, 'Textile Integrated Monitoring System for Breathing Rhythm of Infants', in *XII Mediterranean Conference on Medical and Biological Engineering and Computing 2010*, Berlin, Heidelberg, 2010, pp. 525–528, doi: 10.1007/978-3-642-13039-7_132.
- [111] M. Donati, F. Cecchi, F. Bonaccorso, M. Branciforte, P. Dario, and N. Vitiello, 'A Modular Sensorized Mat for Monitoring Infant Posture', *Sensors*, vol. 14, no. 1, Art. no. 1, Jan. 2014, doi: 10.3390/s140100510.
- [112] A. G. Ferreira et al., 'A smart wearable system for sudden infant death syndrome monitoring', in 2016 IEEE International Conference on Industrial Technology (ICIT), Mar. 2016, pp. 1920–1925, doi: 10.1109/ICIT.2016.7475060.
- [113] M. Leier and G. Jervan, 'Sleep apnea pre-screening on neonates and children with shoe integrated sensors', in 2013 NORCHIP, Nov. 2013, pp. 1–4, doi: 10.1109/NORCHIP.2013.6702029.
- [114] M. Farooq, P. C. Chandler-Laney, M. Hernandez-Reif, and E. Sazonov, 'Monitoring of Infant Feeding Behavior Using a Jaw Motion Sensor', *Journal of Healthcare*

- Engineering, 2015. <https://www.hindawi.com/journals/jhe/2015/610243/> (accessed Nov. 22, 2020).
- [115] H. Vu et al., ‘Detection of Activities During Newborn Resuscitation Based on Short-Time Energy of Acceleration Signal’, in *Image and Signal Processing*, Cham, 2016, pp. 262–270, doi: 10.1007/978-3-319-33618-3_27.
- [116] A. Rihar et al., ‘CareToy: Stimulation and Assessment of Preterm Infant’s Activity Using a Novel Sensorized System’, *Ann. Biomed. Eng.*, vol. 44, no. 12, pp. 3593–3605, Dec. 2016, doi: 10.1007/s10439-016-1669-4.
- [117] E. Koch and A. Dietzel, ‘Skin attachable flexible sensor array for respiratory monitoring’, *Sens. Actuators Phys.*, vol. 250, pp. 138–144, Oct. 2016, doi: 10.1016/j.sna.2016.09.020.
- [118] B. C. Galland, G. J. Kennedy, E. A. Mitchell, and B. J. Taylor, ‘Algorithms for using an activity-based accelerometer for identification of infant sleep–wake states during nap studies’, *Sleep Med.*, vol. 13, no. 6, pp. 743–751, Jun. 2012, doi: 10.1016/j.sleep.2012.01.018.
- [119] E. Rogers, P. Polygerinos, C. Walsh, and E. Goldfield, ‘Smart and Connected Actuated Mobile and Sensing Suit to Encourage Motion in Developmentally Delayed Infants’, *J. Med. Devices*, vol. 9, no. 3, Sep. 2015, doi: 10.1115/1.4030550.
- [120] D. Karch et al., ‘Kinematic assessment of stereotypy in spontaneous movements in infants’, *Gait Posture*, vol. 36, no. 2, pp. 307–311, Jun. 2012, doi: 10.1016/j.gaitpost.2012.03.017.
- [121] T. Seel, J. Raisch, and T. Schauer, ‘IMU-Based Joint Angle Measurement for Gait Analysis’, *Sensors*, vol. 14, no. 4, Art. no. 4, Apr. 2014, doi: 10.3390/s140406891.
- [122] N. Yazdi, F. Ayazi, and K. Najafi, ‘Micromachined inertial sensors’, *Proc. IEEE*, vol. 86, no. 8, pp. 1640–1659, Aug. 1998, doi: 10.1109/5.704269.
- [123] S. Yang and Q. Li, ‘Inertial Sensor-Based Methods in Walking Speed Estimation: A Systematic Review’, *Sensors*, vol. 12, no. 5, Art. no. 5, May 2012, doi: 10.3390/s120506102.
- [124] P. S. Pandian et al., ‘Smart Vest: Wearable multi-parameter remote physiological monitoring system’, *Med. Eng. Phys.*, vol. 30, no. 4, pp. 466–477, May 2008, doi: 10.1016/j.medengphy.2007.05.014.
- [125] J. Coosemans, B. Hermans, and R. Puers, ‘Integrating wireless ECG monitoring in textiles’, *Sens. Actuators Phys.*, vol. 130–131, pp. 48–53, Aug. 2006, doi: 10.1016/j.sna.2005.10.052.

- [126] S. G. Mallat, *A wavelet tour of signal processing: the sparse way*, 3rd ed. Amsterdam ; Boston: Elsevier/Academic Press, 2009.
- [127] J. Gotman and P. Gloor, 'Automatic recognition and quantification of interictal epileptic activity in the human scalp EEG', *Electroencephalogr. Clin. Neurophysiol.*, vol. 41, no. 5, pp. 513–529, Nov. 1976, doi: 10.1016/0013-4694(76)90063-8.
- [128] J. Gotman, 'Automatic recognition of epileptic seizures in the EEG', *Electroencephalogr. Clin. Neurophysiol.*, vol. 54, no. 5, pp. 530–540, Nov. 1982, doi: 10.1016/0013-4694(82)90038-4.
- [129] R. Yadav, R. Agarwal, and M. N. S. Swamy, 'STFT-Based Segmentation in Model-Based Seizure Detection', 2007, pp. 729–732, doi: 10.1109/CCECE.2007.187.
- [130] K. Samiee, P. Kovacs, and M. Gabbouj, 'Epileptic Seizure Classification of EEG Time-Series Using Rational Discrete Short-Time Fourier Transform', *IEEE Trans. Biomed. Eng.*, vol. 62, no. 2, pp. 541–552, Feb. 2015, doi: 10.1109/TBME.2014.2360101.
- [131] M. K. Islam, A. Rastegarnia, and Z. Yang, 'A Wavelet-Based Artifact Reduction From Scalp EEG for Epileptic Seizure Detection', *IEEE J. Biomed. Health Inform.*, vol. 20, no. 5, pp. 1321–1332, Sep. 2016, doi: 10.1109/JBHI.2015.2457093.
- [132] H. Ocak, 'Automatic detection of epileptic seizures in EEG using discrete wavelet transform and approximate entropy', *Expert Syst. Appl.*, vol. 36, no. 2, pp. 2027–2036, Mar. 2009, doi: 10.1016/j.eswa.2007.12.065.
- [133] A. Subasi and E. Erçelebi, 'Classification of EEG signals using neural network and logistic regression', *Comput. Methods Programs Biomed.*, vol. 78, no. 2, pp. 87–99, May 2005, doi: 10.1016/j.cmpb.2004.10.009.
- [134] H. Adeli, S. Ghosh-Dastidar, and N. Dadmehr, 'A Wavelet-Chaos Methodology for Analysis of EEGs and EEG Subbands to Detect Seizure and Epilepsy', *IEEE Trans. Biomed. Eng.*, vol. 54, no. 2, pp. 205–211, Feb. 2007, doi: 10.1109/TBME.2006.886855.
- [135] A. T. Tzallas, M. G. Tsipouras, and D. I. Fotiadis, 'Epileptic Seizure Detection in EEGs Using Time-Frequency Analysis', *IEEE Trans. Inf. Technol. Biomed.*, vol. 13, no. 5, pp. 703–710, Sep. 2009, doi: 10.1109/TITB.2009.2017939.
- [136] B. Boashash and S. Ouelha, 'Automatic signal abnormality detection using time-frequency features and machine learning: A newborn EEG seizure case study', *Knowl.-Based Syst.*, vol. 106, pp. 38–50, Aug. 2016, doi: 10.1016/j.knosys.2016.05.027.

- [137] P. Celka and P. Colditz, 'A computer-aided detection of EEG seizures in infants: a singular-spectrum approach and performance comparison', *IEEE Trans. Biomed. Eng.*, vol. 49, no. 5, pp. 455–462, May 2002, doi: 10.1109/10.995684.
- [138] S. M. S. Alam and M. I. H. Bhuiyan, 'Detection of Seizure and Epilepsy Using Higher Order Statistics in the EMD Domain', *IEEE J. Biomed. Health Inform.*, vol. 17, no. 2, pp. 312–318, Mar. 2013, doi: 10.1109/JBHI.2012.2237409.
- [139] B. R. Greene, P. de Chazal, G. B. Boylan, S. Connolly, and R. B. Reilly, 'Electrocardiogram Based Neonatal Seizure Detection', *IEEE Trans. Biomed. Eng.*, vol. 54, no. 4, pp. 673–682, Apr. 2007, doi: 10.1109/TBME.2006.890137.
- [140] M. Qaraqe, M. Ismail, E. Serpedin, and H. Zulfı, 'Epileptic seizure onset detection based on EEG and ECG data fusion', *Epilepsy Behav.*, vol. 58, pp. 48–60, May 2016, doi: 10.1016/j.yebeh.2016.02.039.
- [141] P. Thodoroff, J. Pineau, and A. Lim, 'Learning Robust Features using Deep Learning for Automatic Seizure Detection', [Online]. Available: <https://ru.arxiv.org/abs/1608.00220>.
- [142] U. R. Acharya, S. L. Oh, Y. Hagiwara, J. H. Tan, and H. Adeli, 'Deep convolutional neural network for the automated detection and diagnosis of seizure using EEG signals', *Comput. Biol. Med.*, Sep. 2017, doi: 10.1016/j.compbimed.2017.09.017.
- [143] I. Kiral-Kornek et al., 'Epileptic Seizure Prediction Using Big Data and Deep Learning: Toward a Mobile System', *EBioMedicine*, vol. 27, pp. 103–111, Jan. 2018, doi: 10.1016/j.ebiom.2017.11.032.
- [144] Y. Yuan, G. Xun, K. Jia, and A. Zhang, 'A Multi-view Deep Learning Method for Epileptic Seizure Detection using Short-time Fourier Transform', 2017, pp. 213–222, doi: 10.1145/3107411.3107419.
- [145] J. R. M. Joshua S Richman, 'Physiological time-series analysis using approximate entropy and sample entropy', *Am. J. Physiol.-Heart Circ. Physiol.*, vol. 278, no. 6, 2000.
- [146] W. Sweldens, 'Lifting scheme: a new philosophy in biorthogonal wavelet constructions', Sep. 1995, pp. 68–79, doi: 10.1117/12.217619.
- [147] C. E. Shannon, 'A mathematical theory of communication', *ACM SIGMOBILE Mob. Comput. Commun. Rev.*, vol. 5, no. 1, p. 3, Jan. 2001, doi: 10.1145/584091.584093.
- [148] A. N. Kolmogorov, 'A new metric invariant of transient dynamical systems and automorphisms in Lebesgue spaces', *Dokl.Akad.Nauk,SSSR*, vol. 119, pp. 861–

- 864, 1958.
- [149] S. M. Pincus, ‘Approximate entropy as a measure of system complexity.’, *Proc. Natl. Acad. Sci.*, vol. 88, no. 6, pp. 2297–2301, Mar. 1991, doi: 10.1073/pnas.88.6.2297.
 - [150] M. Costa, A. L. Goldberger, and C.-K. Peng, ‘Multiscale Entropy Analysis of Complex Physiologic Time Series’, *Phys. Rev. Lett.*, vol. 89, no. 6, Jul. 2002, doi: 10.1103/PhysRevLett.89.068102.
 - [151] P. Li, C. Karmakar, C. Yan, M. Palaniswami, and C. Liu, ‘Classification of 5-S Epileptic EEG Recordings Using Distribution Entropy and Sample Entropy’, *Front. Physiol.*, vol. 7, Apr. 2016, doi: 10.3389/fphys.2016.00136.
 - [152] L. Guo, D. Rivero, and A. Pazos, ‘Epileptic seizure detection using multiwavelet transform based approximate entropy and artificial neural networks’, *J. Neurosci. Methods*, vol. 193, no. 1, pp. 156–163, Oct. 2010, doi: 10.1016/j.jneumeth.2010.08.030.
 - [153] S.-F. Liang, H.-C. Wang, and W.-L. Chang, ‘Combination of EEG Complexity and Spectral Analysis for Epilepsy Diagnosis and Seizure Detection’, *EURASIP J. Adv. Signal Process.*, vol. 2010, no. 1, p. 853434, 2010, doi: 10.1155/2010/853434.
 - [154] D. Labate, I. Palamara, N. Mammone, G. Morabito, F. L. Foresta, and F. C. Morabito, ‘SVM classification of epileptic EEG recordings through multiscale permutation entropy’, *Aug. 2013*, pp. 1–5, doi: 10.1109/IJCNN.2013.6706869.
 - [155] N. Kannathal, M. L. Choo, U. R. Acharya, and P. K. Sadasivan, ‘Entropies for detection of epilepsy in EEG’, *Comput. Methods Programs Biomed.*, vol. 80, no. 3, pp. 187–194, Dec. 2005, doi: 10.1016/j.cmpb.2005.06.012.
 - [156] G. E. Polychronaki et al., ‘Comparison of fractal dimension estimation algorithms for epileptic seizure onset detection’, *J. Neural Eng.*, vol. 7, no. 4, p. 046007, Aug. 2010, doi: 10.1088/1741-2560/7/4/046007.
 - [157] R. Albert and A.-L. Barabási, ‘Statistical mechanics of complex networks’, *Rev. Mod. Phys.*, vol. 74, no. 1, pp. 47–97, Jan. 2002, doi: 10.1103/RevModPhys.74.47.
 - [158] G. J. Ortega, R. G. Sola, and J. Pastor, ‘Complex network analysis of human ECoG data’, *Neurosci. Lett.*, vol. 447, no. 2–3, pp. 129–133, Dec. 2008, doi: 10.1016/j.neulet.2008.09.080.
 - [159] S. C. Ponten, F. Bartolomei, and C. J. Stam, ‘Small-world networks and epilepsy: Graph theoretical analysis of intracerebrally recorded mesial temporal lobe seizures’, *Clin. Neurophysiol.*, vol. 118, no. 4, pp. 918–927, Apr. 2007, doi:

- 10.1016/j.clinph.2006.12.002.
- [160] J. Zhang and M. Small, ‘Complex Network from Pseudoperiodic Time Series: Topology versus Dynamics’, *Phys. Rev. Lett.*, vol. 96, no. 23, Jun. 2006, doi: 10.1103/PhysRevLett.96.238701.
- [161] L. Lacasa, B. Luque, F. Ballesteros, J. Luque, and J. C. Nuno, ‘From time series to complex networks: The visibility graph’, *Proc. Natl. Acad. Sci.*, vol. 105, no. 13, pp. 4972–4975, Apr. 2008, doi: 10.1073/pnas.0709247105.
- [162] G. Zhu, Y. Li, and P. (Paul) Wen, ‘Epileptic seizure detection in EEGs signals using a fast weighted horizontal visibility algorithm’, *Comput. Methods Programs Biomed.*, vol. 115, no. 2, pp. 64–75, Jul. 2014, doi: 10.1016/j.cmpb.2014.04.001.
- [163] B. Wang and L. Meng, ‘Functional brain network alterations in epilepsy: A magnetoencephalography study’, *Epilepsy Res.*, vol. 126, pp. 62–69, Oct. 2016, doi: 10.1016/j.eplesyres.2016.06.014.
- [164] M. Diych, Y. Li, and P. Wen, ‘Classify epileptic EEG signals using weighted complex networks based community structure detection’, *Expert Syst. Appl.*, vol. 90, pp. 87–100, Dec. 2017, doi: 10.1016/j.eswa.2017.08.012.
- [165] L. Wang, X. Long, J. B. A. M. Arends, and R. M. Aarts, ‘EEG analysis of seizure patterns using visibility graphs for detection of generalized seizures’, *J. Neurosci. Methods*, vol. 290, pp. 85–94, Oct. 2017, doi: 10.1016/j.jneumeth.2017.07.013.
- [166] K. Cuppens, L. Lagae, and B. Vanrumste, ‘Towards automatic detection of movement during sleep in pediatric patients with epilepsy by means of video recordings and the optical flow algorithm’, in *4th European Conference of the International Federation for Medical and Biological Engineering*, Berlin, Heidelberg, 2009, pp. 784–789, doi: 10.1007/978-3-540-89208-3_188.
- [167] M. Stoppa and A. Chiolerio, ‘Wearable Electronics and Smart Textiles: A Critical Review’, *Sensors*, vol. 14, no. 7, Art. no. 7, Jul. 2014, doi: 10.3390/s140711957.
- [168] G. Paul, R. Torah, S. Beeby, and J. Tudor, ‘The development of screen printed conductive networks on textiles for biopotential monitoring applications’, *Sens. Actuators Phys.*, vol. 206, pp. 35–41, Feb. 2014, doi: 10.1016/j.sna.2013.11.026.
- [169] D. C. Mack, J. T. Patrie, P. M. Suratt, R. A. Felder, and M. Alwan, ‘Development and Preliminary Validation of Heart Rate and Breathing Rate Detection Using a Passive, Ballistocardiography-Based Sleep Monitoring System’, *IEEE Trans. Inf. Technol. Biomed.*, vol. 13, no. 1, pp. 111–120, Jan. 2009, doi: 10.1109/TITB.2008.2007194.

- [170] P. Huang, C. Hsieh, M. Liang, C. Tsou, and S. Lee, 'ECG monitoring and emotion stabilization system with a physiological information platform for drivers', in 2015 International Symposium on Bioelectronics and Bioinformatics (ISBB), Oct. 2015, pp. 180–183, doi: 10.1109/ISBB.2015.7344953.
- [171] F. Q. AL-Khalidi, R. Saatchi, D. Burke, H. Elphick, and S. Tan, 'Respiration rate monitoring methods: A review', *Pediatr. Pulmonol.*, vol. 46, no. 6, pp. 523–529, Jun. 2011, doi: 10.1002/ppul.21416.
- [172] H. Chen, M. Xue, Z. Mei, S. Bambang Oetomo, and W. Chen, 'A Review of Wearable Sensor Systems for Monitoring Body Movements of Neonates', *Sensors*, vol. 16, no. 12, p. 2134, Dec. 2016, doi: 10.3390/s16122134.
- [173] S. Bouwstra, W. Chen, L. Feijs, and S. B. Oetomo, 'Smart Jacket Design for Neonatal Monitoring with Wearable Sensors', in 2009 Sixth International Workshop on Wearable and Implantable Body Sensor Networks, Jun. 2009, pp. 162–167, doi: 10.1109/BSN.2009.40.
- [174] Toshiyo Tamura, *Seamless Healthcare Monitoring*. Springer Nature, 2018.
- [175] H. Cho and J. H. Lee, 'A Study on the Optimal Positions of ECG Electrodes in a Garment for the Design of ECG-Monitoring Clothing for Male', *J. Med. Syst.*, vol. 39, no. 9, p. 95, Aug. 2015, doi: 10.1007/s10916-015-0279-2.
- [176] YIN, L, 'Design of Screen-Printed Electrodes on Infant Garment for Electrocardiogram Measurement', 2017.
- [177] 'Wearable Sensor Technology | Wireless IMU | ECG | EMG | GSR'. <http://www.shimmersensing.com/> (accessed Jul. 02, 2019).
- [178] J. Lee, K. Jeong, J. Yoon, and M. Lee, 'A simple real-time QRS detection algorithm', in *Proceedings of 18th Annual International Conference of the IEEE Engineering in Medicine and Biology Society*, Oct. 1996, vol. 4, pp. 1396–1398 vol.4, doi: 10.1109/IEMBS.1996.647473.
- [179] A. J. Camm et al., 'Heart rate variability: standards of measurement, physiological interpretation and clinical use. Task Force of the European Society of Cardiology and the North American Society of Pacing and Electrophysiology', vol. 93, no. 5, pp. 1043–1065, 1996, doi: 10.1161/01.CIR.93.5.1043.
- [180] J. Pan and W. J. Tompkins, 'A Real-Time QRS Detection Algorithm', *IEEE Trans. Biomed. Eng.*, vol. BME-32, no. 3, pp. 230–236, Mar. 1985, doi: 10.1109/TBME.1985.325532.
- [181] P. S. Hamilton and W. J. Tompkins, 'Quantitative Investigation of QRS Detection

- Rules Using the MIT/BIH Arrhythmia Database', IEEE Trans. Biomed. Eng., vol. BME-33, no. 12, pp. 1157–1165, Dec. 1986, doi: 10.1109/TBME.1986.325695.
- [182] D. P. Golden, R. A. Wolthuis, and G. W. Hoffler, 'A Spectral Analysis of the Normal Resting Electrocardiogram', IEEE Trans. Biomed. Eng., vol. BME-20, no. 5, pp. 366–372, Sep. 1973, doi: 10.1109/TBME.1973.324231.
- [183] O. Y. D. Vel, 'R-Wave Detection in the Presence of Muscle Artifacts', IEEE Trans. Biomed. Eng., vol. BME-31, no. 11, pp. 715–717, Nov. 1984, doi: 10.1109/TBME.1984.325395.
- [184] G. M. Friesen, T. C. Jannett, M. A. Jadallah, S. L. Yates, S. R. Quint, and H. T. Nagle, 'A comparison of the noise sensitivity of nine QRS detection algorithms', IEEE Trans. Biomed. Eng., vol. 37, no. 1, pp. 85–98, Jan. 1990, doi: 10.1109/10.43620.
- [185] M. Merri, D. C. Farden, J. G. Mottley, and E. L. Titlebaum, 'Sampling frequency of the electrocardiogram for spectral analysis of the heart rate variability', IEEE Trans. Biomed. Eng., vol. 37, no. 1, pp. 99–106, Jan. 1990, doi: 10.1109/10.43621.
- [186] A. R. Antony, S. P. Preejith, V. S. Raja, J. Joseph, and M. Sivaprakasam, 'Clinical Validation of a Wearable Respiratory Rate Device for Neonatal Monitoring.', Conf. Proc. Annu. Int. Conf. IEEE Eng. Med. Biol. Soc. IEEE Eng. Med. Biol. Soc. Annu. Conf., vol. 2018, pp. 1628–1631, Jul. 2018, doi: 10.1109/EMBC.2018.8512548.
- [187] G.-Z. Liu, Y.-W. Guo, Q.-S. Zhu, B.-Y. Huang, and L. Wang, 'Estimation of Respiration Rate from Three-Dimensional Acceleration Data Based on Body Sensor Network', Telemed. E-Health, vol. 17, no. 9, pp. 705–711, Oct. 2011, doi: 10.1089/tmj.2011.0022.
- [188] K. Cuppens et al., 'Accelerometry-Based Home Monitoring for Detection of Nocturnal Hypermotor Seizures Based on Novelty Detection', IEEE J. Biomed. Health Inform., vol. 18, no. 3, pp. 1026–1033, May 2014, doi: 10.1109/JBHI.2013.2285015.
- [189] M. Malik, 'Heart Rate Variability', Ann. Noninvasive Electrocardiol., vol. 1, no. 2, pp. 151–181, 1996, doi: <https://doi.org/10.1111/j.1542-474X.1996.tb00275.x>.
- [190] A. Boardman, F. S. Schlindwein, A. P. Rocha, and A. Leite, 'A study on the optimum order of autoregressive models for heart rate variability', Physiol. Meas., vol. 23, no. 2, pp. 325–336, Mar. 2002, doi: 10.1088/0967-3334/23/2/308.
- [191] M. B. Malarvili and M. Mesbah, 'Newborn Seizure Detection Based on Heart Rate Variability', IEEE Trans. Biomed. Eng., vol. 56, no. 11, pp. 2594–2603, Nov. 2009,

- doi: 10.1109/TBME.2009.2026908.
- [192] D. M. Goldenholz et al., ‘Long-term monitoring of cardiorespiratory patterns in drug-resistant epilepsy’, *Epilepsia*, vol. 58, no. 1, pp. 77–84, 2017, doi: <https://doi.org/10.1111/epi.13606>.
- [193] M. Sun and J. O. Hill, ‘A method for measuring mechanical work and work efficiency during human activities’, *J. Biomech.*, vol. 26, no. 3, pp. 229–241, Mar. 1993, doi: 10.1016/0021-9290(93)90361-H.
- [194] M. P. S. Brown et al., ‘Knowledge-based analysis of microarray gene expression data by using support vector machines’, *Proc. Natl. Acad. Sci.*, vol. 97, no. 1, pp. 262–267, Jan. 2000, doi: 10.1073/pnas.97.1.262.
- [195] M. Brown, H. G. Lewis, and S. R. Gunn, ‘Linear spectral mixture models and support vector machines for remote sensing’, *IEEE Trans. Geosci. Remote Sens.*, vol. 38, no. 5, pp. 2346–2360, Sep. 2000, doi: 10.1109/36.868891.
- [196] I. Guyon, J. Weston, S. Barnhill, and V. Vapnik, ‘Gene Selection for Cancer Classification using Support Vector Machines’, *Mach. Learn.*, vol. 46, no. 1, pp. 389–422, Jan. 2002, doi: 10.1023/A:1012487302797.
- [197] W. S. Noble, ‘What is a support vector machine?’, *Nat. Biotechnol.*, vol. 24, no. 12, Art. no. 12, Dec. 2006, doi: 10.1038/nbt1206-1565.
- [198] V. Vapnik and O. Chapelle, ‘Bounds on Error Expectation for Support Vector Machines’, *Neural Comput.*, vol. 12, no. 9, pp. 2013–2036, Sep. 2000, doi: 10.1162/089976600300015042.
- [199] R. Akbani, S. Kwek, and N. Japkowicz, ‘Applying Support Vector Machines to Imbalanced Datasets’, in *Machine Learning: ECML 2004*, Berlin, Heidelberg, 2004, pp. 39–50, doi: 10.1007/978-3-540-30115-8_7.
- [200] P. Schwartz, ‘Guidelines for the interpretation of the neonatal electrocardiogram’, *Eur. Heart J.*, vol. 23, no. 17, pp. 1329–1344, Sep. 2002, doi: 10.1053/ehhj.2002.3274.
- [201] P. Davey, ‘ECG’, *Medicine (Baltimore)*, vol. 34, no. 4, pp. 128–135, Apr. 2006, doi: 10.1383/medc.2006.34.4.128.
- [202] Bioelectromagnetism. .
- [203] Karilainen A, Hansen S, and Müller J, ‘Dry and capacitive electrodes for long-term ECG-monitoring’, 8th Annu. Workshop Semicond. Adv., 2005.
- [204] T. Lin, L. Wang, X. Wang, and A. Kaynak, ‘Polymerising pyrrole on polyester textiles and controlling the conductivity through coating thickness’, *Thin Solid*

- Films, vol. 479, no. 1, pp. 77–82, May 2005, doi: 10.1016/j.tsf.2004.11.146.
- [205] H. Chen et al., ‘A wearable sensor system for neonatal seizure monitoring’, May 2017, pp. 27–30, doi: 10.1109/BSN.2017.7935999.
- [206] G.-Z. Yang, Ed., *Body Sensor Networks*. London: Springer London, 2014.
- [207] L. Beckmann et al., ‘Characterization of textile electrodes and conductors using standardized measurement setups’, *Physiol. Meas.*, vol. 31, no. 2, pp. 233–247, Feb. 2010, doi: 10.1088/0967-3334/31/2/009.
- [208] W. Einthoven, ‘Ein neues Galvanometer’, *Ann. Phys.*, vol. 317, no. 13, pp. 1059–1071, 1903, doi: 10.1002/andp.19033171308.
- [209] B.-Y. Chang and S.-M. Park, ‘Electrochemical Impedance Spectroscopy’, *Annu. Rev. Anal. Chem.*, vol. 3, no. 1, pp. 207–229, Jun. 2010, doi: 10.1146/annurev.anchem.012809.102211.
- [210] M. A. Yokus and J. S. Jur, ‘Fabric-Based Wearable Dry Electrodes for Body Surface Biopotential Recording’, *IEEE Trans. Biomed. Eng.*, vol. 63, no. 2, pp. 423–430, Feb. 2016, doi: 10.1109/TBME.2015.2462312.
- [211] C. Pang, C. Lee, and K.-Y. Suh, ‘Recent advances in flexible sensors for wearable and implantable devices: Review’, *J. Appl. Polym. Sci.*, vol. 130, no. 3, pp. 1429–1441, Nov. 2013, doi: 10.1002/app.39461.
- [212] L. A. Geddes, ‘Historical evolution of circuit models for the electrode-electrolyte interface’, *Ann. Biomed. Eng.*, vol. 25, no. 1, p. 1, Jan. 1997, doi: 10.1007/BF02738534.
- [213] M. A. Yokus and J. S. Jur, ‘Fabric-Based Wearable Dry Electrodes for Body Surface Biopotential Recording’, *IEEE Trans. Biomed. Eng.*, vol. 63, no. 2, pp. 423–430, Feb. 2016, doi: 10.1109/TBME.2015.2462312.
- [214] S. Fleming et al., ‘Normal ranges of heart rate and respiratory rate in children from birth to 18 years of age: a systematic review of observational studies’, *The Lancet*, vol. 377, no. 9770, pp. 1011–1018, Mar. 2011, doi: 10.1016/S0140-6736(10)62226-X.
- [215] S. Reuter, C. Moser, and M. Baack, ‘Respiratory Distress in the Newborn’, *Pediatr. Rev.*, vol. 35, no. 10, pp. 417–429, Oct. 2014.
- [216] M. O. Edwards, S. J. Kotecha, and S. Kotecha, ‘Respiratory distress of the term newborn infant’, *Paediatr. Respir. Rev.*, vol. 14, no. 1, pp. 29–36; quiz 36–37, Mar. 2013, doi: 10.1016/j.prrv.2012.02.002.
- [217] J. B. Warren and J. M. Anderson, ‘Newborn respiratory disorders’, *Pediatr. Rev.*,

- vol. 31, no. 12, pp. 487–495; quiz 496, Dec. 2010, doi: 10.1542/pir.31-12-487.
- [218] P. D. Hung, S. Bonnet, R. Guillemaud, E. Castelli, and P. T. N. Yen, ‘Estimation of respiratory waveform using an accelerometer’, in 2008 5th IEEE International Symposium on Biomedical Imaging: From Nano to Macro, May 2008, pp. 1493–1496, doi: 10.1109/ISBI.2008.4541291.
- [219] G.-Z. Liu, Y.-W. Guo, Q.-S. Zhu, B.-Y. Huang, and L. Wang, ‘Estimation of Respiration Rate from Three-Dimensional Acceleration Data Based on Body Sensor Network’, *Telemed. E-Health*, vol. 17, no. 9, pp. 705–711, Oct. 2011, doi: 10.1089/tmj.2011.0022.
- [220] A. Cesareo, Y. Previtali, E. Biffi, and A. Aliverti, ‘Assessment of Breathing Parameters Using an Inertial Measurement Unit (IMU)-Based System’, *Sensors*, vol. 19, no. 1, Art. no. 1, Jan. 2019, doi: 10.3390/s19010088.
- [221] A. Rasheed et al., ‘An Active Self-Driven Piezoelectric Sensor Enabling Real-Time Respiration Monitoring’, *Sensors*, vol. 19, no. 14, Art. no. 14, Jan. 2019, doi: 10.3390/s19143241.
- [222] N. Yi et al., ‘Fully Water-Soluble, High-Performance Transient Sensors on a Versatile Galactomannan Substrate Derived from the Endosperm’, *ACS Appl. Mater. Interfaces*, vol. 10, no. 43, pp. 36664–36674, Oct. 2018, doi: 10.1021/acsami.8b11682.
- [223] M. D. Ho et al., ‘Percolating Network of Ultrathin Gold Nanowires and Silver Nanowires toward “Invisible” Wearable Sensors for Detecting Emotional Expression and Apexcardiogram’, *Adv. Funct. Mater.*, vol. 27, no. 25, p. 1700845, 2017, doi: <https://doi.org/10.1002/adfm.201700845>.
- [224] J.-W. Jeong et al., ‘Capacitive Epidermal Electronics for Electrically Safe, Long-Term Electrophysiological Measurements’, *Adv. Healthc. Mater.*, vol. 3, no. 5, pp. 642–648, 2014, doi: <https://doi.org/10.1002/adhm.201300334>.
- [225] H. Chen, Y. Zhao, Z. Mei, Y. Mei, S. B. Oetomo, and W. Chen, ‘Characterization of a novel carbonized foam electrode for wearable bio-potential recording’, in 2018 IEEE 15th International Conference on Wearable and Implantable Body Sensor Networks (BSN), Mar. 2018, pp. 173–176, doi: 10.1109/BSN.2018.8329686.
- [226] Y. Wang et al., ‘Flexible electrically resistive-type strain sensors based on reduced graphene oxide-decorated electrospun polymer fibrous mats for human motion monitoring’, *Carbon*, vol. 126, pp. 360–371, Jan. 2018, doi: 10.1016/j.carbon.2017.10.034.

- [227] X. Liao et al., ‘Flexible and Highly Sensitive Strain Sensors Fabricated by Pencil Drawn for Wearable Monitor’, *Adv. Funct. Mater.*, vol. 25, no. 16, pp. 2395–2401, 2015, doi: <https://doi.org/10.1002/adfm.201500094>.
- [228] P. J. Lee, ‘Clinical evaluation of a novel respiratory rate monitor’, *J. Clin. Monit. Comput.*, vol. 30, no. 2, pp. 175–183, Apr. 2016, doi: 10.1007/s10877-015-9697-4.

Publication

1. **Chen, H.**, Xue, M., Mei, Z., Bambang Oetomo, S., & Chen, W. (2016). A review of wearable sensor systems for monitoring body movements of neonates. *Sensors*, 16(12), 2134.
2. **Chen, H.**, Xue, M., Oetomo, S. B., & Chen, W. (2016). Neonatal Seizure Detection with Wearable Sensor System. In *Intelligent Environments (Workshops)* (pp. 560-569).
3. **Chen, H.**, Gu, X., Mei, Z., Xu, K., Yan, K., Lu, C., ... & Chen, W. (2017, May). A wearable sensor system for neonatal seizure monitoring. In *2017 IEEE 14th International Conference on Wearable and Implantable Body Sensor Networks (BSN)* (pp. 27-30). IEEE.
4. **Chen, H.**, Zhao, Y., Mei, Z., Mei, Y., Oetomo, S. B., & Chen, W. (2018, March). Characterization of a novel carbonized foam electrode for wearable bio-potential recording. In *2018 IEEE 15th International Conference on Wearable and Implantable Body Sensor Networks (BSN)* (pp. 173-176). IEEE.
5. Chen, C., Wang, Z., Li, W., **Chen, H.**, Mei, Z., Yuan, W., ... & Chen, W. (2018). Novel flexible material-based unobtrusive and wearable body sensor networks for vital sign monitoring. *IEEE Sensors Journal*, 19(19), 8502-8513.
6. Mei, Z., Zhao, X., **Chen, H.**, & Chen, W. (2018). Bio-signal complexity analysis in epileptic seizure monitoring: A topic review. *Sensors*, 18(6), 1720.
7. Mei, Z., Gu, X., **Chen, H.**, & Chen, W. (2018). Automatic atrial fibrillation detection based on heart rate variability and spectral features. *IEEE Access*, 6, 53566-53575.
8. Bao, S., Yin, S., **Chen, H.**, & Chen, W. (2018, May). A wearable multimode system with

soft sensors for lower limb activity evaluation and rehabilitation. In 2018 IEEE International Instrumentation and Measurement Technology Conference (I2MTC) (pp. 1-6). IEEE.

9. Mei, Z., Zhao, X., **Chen, H.**, & Chen, W. (2018, July). A distributed descriptor characterizing structural irregularity of EEG time series for epileptic seizure detection. In 2018 40th Annual International Conference of the IEEE Engineering in Medicine and Biology Society (EMBC) (pp. 3386-3389). IEEE.

10. **Chen, H.**, Bao, S., Ma, J., Wang, P., Lu, H., Oetomo, S. B., & Chen, W. (2019, July). A wearable daily respiration monitoring system using pdms-graphene compound tensile sensor for adult. In 2019 41st Annual International Conference of the IEEE Engineering in Medicine and Biology Society (EMBC) (pp. 1269-1273). IEEE.

11. Ma, J., Wang, P., **Chen, H.**, Bao, S., Chen, W., & Lu, H. (2019). Highly sensitive and large-range strain sensor with a self-compensated two-order structure for human motion detection. *ACS applied materials & interfaces*, 11(8), 8527-8536.

12. **Chen, H.**, Bao, S., Lu, C., Wang, L., Ma, J., Wang, P., ... & Chen, W. (2020). Design of an integrated wearable multi-sensor platform based on flexible materials for neonatal monitoring. *IEEE Access*, 8, 23732-23747.

Award

Geneva inventions salon international des inventions: Silver medal

National Undergraduate Biomedical Engineering Innovation Design Competition: The first prize

China service robot competition: The first prize

Acknowledgements


This dissertation would not have been possible without the help of my supervisors, colleagues, co-workers, friends and family. Firstly, I would like to express my appreciation to my promotors prof. Sidarto Bambang Oetomo and prof. Wei Chen. Throughout the PhD project you have kindly provided me with your guidance, knowledge, advice and understanding support. Thank you, Sidarto. It is your rigorous attitude that fills me with awe for scientific research, and it is also you that initiated my road of scientific research. Thank you, Wei. I feel grateful to your support all along. You inspired me the possible directions, you guided me the detailed tasks, you answered me all my questions, you indicated the lessons I learnt and you encouraged me. Thank you, prof. Laisuan Wang and Cunmei Lu. You are the experts who gave me so many tips and hands-on techniques of neonatal wearable. Also many thanks to all the people who supported me. Especially Kai Yan, I admired a lot your profession on studies. Xiao Gu, you're a young talent that I feel so luckily to work with you. Zhenning Mei, I've benefitted so much by our numerous discussions.

Furthermore, I would like to thank Shenjie Bao, XianZhao, etc. They have helped me and encouraged me a lot in my writing. Without them, my Ph.D. life will lose much happiness. Then, I am deeply indebted to my beloved wife, who always supported me, willingly discussed with me, and offered valuable insights. Her help and support have accompanied me through the difficult course of the thesis and moments of my life.

Ultimately, thanks go to my parents who are my mentor and guardian from the very beginning in primary school. Without their refined education and care, I could never grow up in such a joyous and cozy environment nor have the courage to confront any obstacles on my way to success.

Curriculum Vitae

Hongyu Chen was born on the 20th of May 1988 in Jiangxi, China. In 2012, he received his bachelor's degree in Industrial Design from NanChang University where he was recommended for admission to his master's study in Zhejiang University. He obtained his master's degree in 2015 with great interests in the field of Human-Computer Interaction. Subsequently, he was awarded a scholarship from the Chinese Scholarship Council (CSC) for her Ph.D. research in the Industrial Design Department in Eindhoven University of Technology (Tu/e) in the Netherlands. He is fascinated by the combination of design, technology and medicine and therefore enjoys designing innovative medical products. This thesis is the result of his research topic of “Design of a wearable sensor system for neonatal seizure monitoring”. He won multiple awards including Red Dot Award, IF Award and Silver medal of Ge-neva inventions salon international des inventions. During his doctoral education, he also founded Magikare Medical Technology Co., Ltd. which transformed scientific research achievements.

The background of the slide is a dark blue color with a complex, light blue circuit board pattern. The pattern consists of numerous thin, interconnected lines and dots, resembling a microchip or a network of sensors. The lines are more prominent in the upper right and lower right areas, while the lower left area is relatively clearer.

Design of a wearable sensor system for neonatal seizure monitoring